

Aggregation of α -synuclein monomers and engineered oligomers in solution

by

Xi Li

A thesis submitted in partial fulfillment of the requirements for the degree of

Master of Science

Department of Chemistry

University of Alberta

© Xi Li, 2015

Abstract

α -Synuclein is a protein that has been found as fibrillar aggregates in Lewy bodies in the brain of Parkinson's disease patients. Though the cause of the Parkinson's disease is unknown, previous research suggest that there is a close association between the disease and the toxicity of the intermediary α -synuclein oligomers in human neurons. Therefore, it is important to investigate the aggregation behaviour of intermediary oligomers. To do this we investigate aggregation of protein constructs that are monomers (Snca1), or engineered dimers (Snca2), tetramers (Snca4), and octamers (Snca8) of α -synuclein with a C terminal cysteine. Single-molecule fluorescence methods were used to study the molecular interactions between pairs of these oligomers under "physiological" aggregation conditions (10 mM PBS at pH = 7.4 at 37 °C). To be specific, we applied dual-color fluorescence cross correlation spectroscopy (dual-color FCCS) to study the self-aggregation (aggregation of one kind of α -synuclein) and the cross-aggregation (aggregation between the monomeric and oligomeric α -synuclein) of α -synuclein. The engineered α -synuclein monomers, dimers, tetramers and octamers were labelled with either Oregon Green 488 maleimide (green dye) or Cy5-tetrazine (red dye). A green dye labelled protein was incubated with a red dye labelled protein at micromolar concentrations with continuous shaking at 250 rpm and diluted aliquots of the aggregation mixture was measured by dual-color FCCS at nanomolar concentrations after different incubation times. The experimental results indicate that the engineered α -synuclein octamers aggregate faster and to a greater extent than monomers and dimers, with the tetramers being intermediate.

The engineered oligomers preferred to incorporate themselves rather than the monomer into aggregates. Therefore, these oligomer constructs do not appear to seed the aggregation of monomers.

Acknowledgements

I would first like to express my gratitude to my supervisor, Prof. Nils Petersen for his continuous encouragement, wise guidance and inspiration. Without his support, I would have never finished my degree. Throughout the two and half years in the lab, I have learned invaluable lessons from Dr. Petersen on how to be professional, positive, curious and passionate about research and life in general. I would also like to thank the project leader, Prof. Michael Woodside, for giving me the opportunity to work on this project in his lab and for continuously providing beneficial feedback. Then, I would like to thank Prof. Charles Lucy and Prof. Julianne Gibbs-Davis for offering me great insights for my career and into my research.

There are many exceptional colleagues that have to be thanked for helping me through this stage of my life, they are Meijing Wang, Lindsay Shearer, Chunhua Dong, Nick Smisdom, Daniel Foster, Derek Dee, Craig Garen, Supratik Sen Mojumdar, Marion Becker, Armin Hoffmann, Allison Solanki, Angela Brigley I really appreciate that I had a chance to work with these professional, caring and very interesting researchers to produce some high-quality results.

In the end, my deepest thanks and love are given to my grandparents, my parents, my cousins, and my partner, Lei, who have been of great support and motivation for me throughout these years. Without them, I would never make it this far in my studies. I am so thankful and blessed to have them in my life.

TABLE OF CONTENTS

ABSTRACT.....	II
ACKNOWLEDGEMENTS	IV
LIST OF FIGURES	VIII
LIST OF TABLES	XIII
LIST OF SYMBOLS, NOMENCLATURE OR ABBREVIATIONS.....	XV
CHAPTER 1: INTRODUCTION AND LITERATURE REVIEW.....	1
1.1 OVERVIEW OF NEURODEGENERATIVE DISEASES	1
1.2 STUDIES OF THE AGGREGATION-PRONE PROTEINS	4
1.2.1 Protein sequence alignment and comparison.....	4
1.2.2 Protein hydrodynamic size measurement	5
1.2.3 Protein three-dimensional (3D) structure estimation.....	5
1.2.4 Monitoring protein aggregation in vitro and in vivo	7
1.3 α -SYNUCLEIN.....	8
1.3.1 Research about α -synucleins (1997-2008).....	8
1.3.2 Recent research into α -synuclein (2009-2014)	12
1.4 MY RESEARCH OBJECTIVES	15
CHAPTER 2: METHODOLOGY AND THEORY.....	17
2.1 TECHNIQUES USED IN PROTEIN AGGREGATION STUDIES	17
2.1.1 Sodium dodecyl sulfate-polyacrylamide gel electrophoresis (SDS-PAGE)	17
2.1.2 Size-exclusion chromatography.....	18
2.1.3 Dynamic light scattering (DLS).....	20
2.2 FLUORESCENCE SPECTROSCOPY.....	22
2.2.1 Structure of a fluorescence microscope	22
2.2.2 Fluorescence correlation spectroscopy (FCS)	24

The principle of FCS.....	25
Physical meaning of the important parameters in FCS.....	27
Two-component FCS fitting equation	29
Other fitting factors needed to be considered	30
2.2.3 Dual-color fluorescence cross-correlation spectroscopy (FCCS).....	32
The principle of dual-color FCCS.....	32
Other general factors need to be considered	35
CHAPTER 3: MATERIALS AND METHODS	38
3.1 LABELLING.....	38
3.2 PURIFICATION AND LABELLING EFFICIENCY	44
3.2.1 Fast protein liquid chromatography (FPLC).....	44
3.2.1 Centrifuges, centrifuge, and UV/Vis spectroscopy.....	45
3.2.3 HPLC-ESI-MS/MS	47
3.3 QUANTUM YIELDS OF LABELLED α -SYNUCLEINS	49
3.4 DLS	50
3.5 FCS AND DUAL-COLOR FCCS	51
3.5.1 Calibration measurements.....	51
3.5.2 Hydrodynamic diameters of α -synucleins by FCS	67
3.5.3 Aggregation tests by FCS	67
3.5.4 Aggregation tests by dual-color FCCS.	69
CHAPTER 4: RESULTS AND DISCUSSIONS	74
4.1 PURIFICATION AND LABELLING EFFICIENCY	74
4.1.1 Distinguishing non-specific binding from covalent labelling.....	74
4.1.2 High labelling efficiency demonstrated by centrifugal purification	80
4.1.3 HPLC-MS confirms covalent labelling at high efficiency	84

4.1.4 HPLC-MS confirms coupling of TPM with α -synuclein.....	85
4.2 QUANTUM YIELDS OF OREGON GREEN 488 IS AFFECTED BY CONJUGATION TO α -SYNUCLEINS.....	88
4.3 DETERMINATION OF HYDRODYNAMIC SIZE OF LABELLED A-SYNUCLEINS	91
4.3.1 Hydrodynamic diameters of α -synucleins by DLS.....	91
4.3.2 Hydrodynamic diameters of α -synucleins by FCS	94
4.3.3 Hydrodynamic diameters of α -synucleins are independent of the protein concentration.	96
4.3.4 Overall Discussion.....	97
4.4 AGGREGATION OF LABELLED α -SYNUCLEINS	99
4.4.1 Aggregation tests by FCS	99
4.4.2 Aggregation tests by dual-color FCCS.....	101
CHAPTER 5: CONCLUSION.....	113
5.1 RESEARCH SUMMARY AND CONTRIBUTIONS.....	113
5.2 FUTURE WORKS	114
BIBLIOGRAPHY	115

List of Figures

Figure 1: Recap of the toxic protein aggregation process (Adapted from reference). ⁶	2
Figure 2: Primary structure of α -synuclein labelled with seven KTKEGV motifs and three mutation sites associated with familial Parkinson's diseases (Adapted from reference). ⁶⁸	9
Figure 3: Formation of oligomers or fibrils with different morphology (Adapted from reference). ⁸⁰	11
Figure 4: Principle of SEC (Adapted from reference). ⁹⁷	19
Figure 5: Principle of DLS.....	20
Figure 6: A simplified diagram of confocal microscope with two detectors.....	24
Figure 7: Principle of FCS (Adapted from reference). ¹⁰⁷	26
Figure 8: (a) Autocorrelation function of two component translational fluctuations; (b) Autocorrelation function for one component translational fluctuation with triplet and rotational diffusion.	31
Figure 9: Principle of dual-color FCCS.....	33
Figure 10: Three common protein-dye labelling reactions.....	41
Figure 11: Autocorrelation function and corresponding fitting curves (dashed lines) of Cy5 excited by 488 nm (green) and 633 nm (red), respectively.....	52

Figure 12: Autocorrelation functions and cross-correlation function of Rhodamine 6G. Red line is the fitting curve of data obtained by the red detector, Green line is from the green detector, Black line is data calculated based on the cross correlation function.	55
Figure 13: Count rate is a function of laser powers at different concentrations of Alexa Fluor® 488 C5-maleimide. Black is at 1312 nM, Red is at 656 nM, Green is at 328 nM, Purple is at 164 nM and Blue is at 82 nM.	56
Figure 14: Observed number of fluorescent particles in a confocal volume, N , as a function of the concentrations of Alexa Fluor 488.	61
Figure 15: Viscosity of 10% ethanol as a function of temperature.	65
Figure 16: Scheme of the aggregation tests by using FCS.	68
Figure 17: Scheme of the aggregation tests using dual-color FCCS.	69
Figure 18: Comparison of FPLC elution profiles for Alexa Fluor® 488 C5-Maleimide and Snca1. (a) Alexa Fluor® 488 at pH 7.40, (b) Snca1 at pH 7.40, (c) Non-reacted the dye and Snca 1 at pH 7.40, (d) Non-reacted dye and Snca 1 at pH 4.68 and (e) Snca1_alex Fluor® 488 C5-Maleimide	75
Figure 19: Comparison of FPLC elution profiles for CF TM 488A Dye and α -synuclein. (a) CF TM 488A Dye, and (b) Snca1 mixed with CF TM 488A Dye without labelling reaction.	76
Figure 20: Comparison of FPLC elution profiles for Oregon Green® 488 Carboxylic Acid Succinimidyl Ester, 6-isomer dye and α -synuclein. (a) Oregon	

Green® 488 Carboxylic Acid Dye, (b) The mixture of Snca8 and the dye, and (c) Snca8_ORNH488. 77

Figure 21: Comparison of FPLC elution profiles for Oregon Green® 488 Maleimide and α -synuclein. (a) Snca4_ORM488 using sulfhydryl maleimide labelling Method One. (b) Snca4_ORM488 using sulfhydryl maleimide labelling Method Two. 79

Figure 22: (a) Spectra of TCO-PEG3-Maleimides (TPM) (yellow), the first filtrate volume (black) and the second filtrate volume (blue) from centrifugation of the Snca4 labelled with large amounts of TPM. (b) Spectra of Snca4_TPM (green), spectra of Cy5 tetrazine (red) and spectra of Snca4_TPM_Cy5 (purple). 81

Figure 23: Spectra of Oregon Green 488 maleimide (green), Snca4 before labelling (yellow) and 5 μ L of Snca4_ORM488 diluted by 20 times (purple). 83

Figure 24: MS spectra for labelled and unlabelled monomeric α -synuclein. 85

Figure 25: MS spectrum for Snca1_Cys_TPM. 87

Figure 26: MS spectrum for Snca2_Cys_TPM. 87

Figure 27: Fluorescence as a function of emission wavelengths for Cy5 tetrazine (Blue) and the mixture of Snca1_Cys and Cy5 tetrazine (Red). Dashed line indicated the starting point (656 nm) of all integrated emission. 88

Figure 28: Fluorescence as a function of emission wavelength for Oregon Green 488 maleimide (Blue) and the mixture of Snca1_Cys and the dye (Red). 89

Figure 29: Intensity particle size distributions of Snca1, 2, 4 and 8_Cys_TCM. . 93

Figure 30: Weighted-volume particle size distributions of Snca1, 2, 4 and 8_Cys_TPM. 93

Figure 31: Fitted correlograms of Snca1, 2, 4, and 8_Cys_TPM. 94

Figure 32: (a) Distribution of the diffusion time of Snca1_Cys_Dye with Snca1_Cys at different incubation times. (b) Distribution of the diffusion time of Snca4_Cys_Dye with Snca4_Cys at different incubation times..... 100

Figure 33: Distribution of the diffusion time of Snca4_Cys_Dye incubated with Snca1_Cys at different times. 101

Figure 34: (a) Autocorrelation functions and cross-correlation function of a mixture of Snca8_ORM488 and Snca8_Cy5 at t = 0 hour. (b) Autocorrelation functions and cross-correlation function of a mixture of Snca8_ORM488 and Snca8_Cy5 at t = 6 hours. Red dashed line is the fitting curve of data obtained by the red detector, Green dashed line is from the green detector and Black dashed is data calculated based on the cross correlation. 103

Figure 35: (a) **nrgnr** as a function of incubation time; (b) **nrgng** as a function of incubation time for FCCS 11 (red), FCCS 22 (black), FCCS 44 (blue) and FCCS 88 (purple)..... 104

Figure 36: (a) **nrgnr** as a function of incubation time for FCCS 12, 14 and 18; (b) **nrgng** as a function of incubation time for for FCCS 12, 14 and 18; (c) **nrgnr** as a function of incubation time for FCCS 21, 41 and 81; (d) **nrgng** as a

function of incubation time for FCCS 21, 41 and 81. Black for sample contained dimeric α -synuclein, blue for tetramers and purple for octamers. 107

Figure 37: (a) and (b) are **nrgnr** as a function of incubation time for FCCS 88 with and without continuous shaking, respectively. (c) and (d) are **nrgng** as a function of incubation time for FCCS 88 with and without continuous shaking, respectively. 112

List of Tables

Table 1: Common neurodegenerative diseases associated toxic protein structure in aqueous condition and the protein deposits in vivo.	3
Table 2: The producer and name for each dye used in the research.	39
Table 3: Selection of the Amicon® Ultra filters for Sncal, 2, 4 and 8.	46
Table 4: The buffer gradient for α -synucleins.	48
Table 5: Molar absorptivities of Sncal, 2, 4 and 8.	50
Table 6: $G(0)$, N and τ_D of Rhodamine 6G measured by FCCS.	54
Table 7: Count Rates of Oregon Green® 488 maleimide and Cy5 Tetrazine in FCCS.	57
Table 8: Fitting results of Oregon Green 488 maleimide in PBS at pH=7.40 in FCS.	58
Table 9: Fitting results of Cy5 tetrazine in 10% of Ethanol in FCS.	59
Table 10: Fitting results of Alexa Fluor® 488 C5-maleimide at different concentration in PBS at pH=7.40 at 298.15 K in FCS.	60
Table 11: t-Tests for comparing two independent values.	63
Table 12: Viscosity of 10% ethanol (by weight) at different temperature ¹¹⁵	64
Table 13: Viscosity of water, 10 mM PBS and 10% of Ethanol at 298.15 K.	65
Table 14: Calculated diffusion coefficients (D) and diffusion times (τ_D) of different dyes in water, 10 mM PBS and 10% Ethanol at 298.15 K.	66
Table 15: Codes and repeated times of all dual-color FCCS experiments.	70
Table 16: Expected mass and experimental result of Sncax_Cys_TPM.	86
Table 17: Summary of relative quantum yields for Cy5 tetrazine alone, in mixture with proteins and conjugated to proteins.	89
Table 18: Summary of relative quantum yields for Oregon Green 488 C5 maleimide alone, in mixture with proteins and conjugated to proteins.	90
Table 19: Weighted-volume particle size distributions for α -synucleins.	94
Table 20: Fitting results of labelled Sncal, 2, 4 and 8 in PBS at pH = 7.40 and comparison of the hydrodynamic diameters obtained from FCS and DLS.	95

Table 21: Fitting results of labelled Snca4 with different concentration of unlabelled Snca4 in PBS at pH=7.40.....	97
Table 22: Comparison of the estimated hydrodynamic diameters of Snca1, 2, 4, and 8 with DLS and FCS results.....	98
Table 23: Summary of fitting amplitude of FCCS self-aggregation tests.	105
Table 24: Summary of fitting amplitude of FCCS cross-aggregation tests.	108
Table 25: Another format of summary the fitting amplitudes of all FCCS tests.	109
Table 26: Detailed information of fitting k values for all FCCS tests.	111

List of Symbols, Nomenclature or Abbreviations

Alexa 488	Alexa Fluor® 488 C5-maleimide
ATR-FTIR	Attenuated total reflectance-Fourier transform infrared
Cy5	Cy5 Tetrazine
Cys	Cysteine
DLS	Dynamic light scattering
DMSO	Dimethylsulfoxide
EM	Electron microscopy
ESI	Electrospray ionization
FCCS	Fluorescence cross-correlation spectroscopy
FCS	Fluorescence correlation spectroscopy
FPLC	Fast protein liquid chromatography
FRET	Forster resonance energy transfer
HFT	Main dichroic beam splitter
HPLC-MS	High performance liquid chromatography-mass spectrometry
ICS	Image correlation spectroscopy
MS	Mass spectrometry
NFT	Secondary dichroic beam splitter
NMR	Nuclear magnetic resonance
ORM488	Oregon Green® 488 maleimide
PBS	Phosphate-buffered saline (137 mM NaCl, 2.7 mM KCl, 10 mM Na ₂ HPO ₄ and 1.8 mM KH ₂ PO ₄)
SDS	Sodium dodecyl sulfate
SH group	Thiol group
smFS	Single-molecule force spectroscopy
SDS-PAGE	Sodium dodecyl sulfate-polyacrylamide gel electrophoresis
TCEP-HCl	Tris-(2-carboxyethyl) phosphine hydrochloride
TCO	Trans-Cyclooctene group
TEM	Transmission electron microscopy
ThT	Thioflavin-T
TPM	Trans-Cyclooctene-PEG ₃ -Maleimide
$A(\dots \text{ nm })$	Absorbance at a specific wavelength
$G(0)$	Amplitude of a correlation function of fluorescence fluctuation
$G_g(0)$	Amplitude of a correlation function of green fluorescence fluctuation
$G_r(0)$	Amplitude of a correlation function of red fluorescence fluctuation
$G_{rg}(0)$	Amplitude of a cross correlation function
$G_g(\tau)$	Autocorrelation function of green fluorescence fluctuation
$G_r(\tau)$	Autocorrelation function of red fluorescence fluctuation
$\langle \dots \rangle$	Average
N_A	Avogadro constant
k	Boltzmann constant
c	Concentration
CF	Correction factor
$G(\tau)$	Correlation function
$G_{rg}(\tau)$	Cross-correlation function
τ_D	Diffusion time

τ_{D_1}	Diffusion time of component 1
τ_{D_2}	Diffusion time of component 2
$\tau_{D_{rg}}$	Diffusion time of protein aggregates emitted green and red fluorescence
V_{eff}	Effective confocal volume
V_{eff_green}	Effective confocal volume of a green detector
V_{eff_red}	Effective confocal volume of a red detector
E	Emission
w_{xy}	Equatorial radii of a confocal volume
w_{xy_green}	Equatorial radii of a confocal volume of a green detector
w_{xy_red}	Equatorial radii of a confocal volume of a red detector
$\epsilon(\dots)$	Molar absorptivity
δ	Fluctuations around the mean
$t_{1/2}$	Half time
R	Hydrodynamic radius
R_{rg}	Hydrodynamic radius of the aggregate emitted both green and red fluorescence
$F(t)$	Intensity of fluorescence intensity
$I(t)$	Intensity of Rayleigh scattering
t_d	Lag time
μ	Mean
N	Number of amino acids
N	Observed number of fluorescent particles in a confocal volume
N_g	Observed number of fluorescent particles in a green confocal
N_r	Observed number of fluorescent particles in a red confocal volume
N_{rg}	Observed number of fluorescent particles in a cross confocal volume
n_g	Observed number of fluorescent particles per unit green volume
n_r	Observed number of fluorescent particles per unit red volume
n_{rg}	N_{rg} divided by V_{eff_Cross}
V_{eff_Cross}	Overlapped effective confocal volume of the green and red detector
w_z	Polar radii of the confocal volume
w_{z_green}	Polar radii of the confocal volume of a green detector
w_{z_red}	Polar radii of the confocal volume of a red detector
s_m	Standard error of the mean
T	Temperature
D	Translational diffusion coefficient
D_{rg}	Translational diffusion coefficient of aggregates emitted green and red light
σ^2	Variance
η	Viscosity

Chapter 1: Introduction and Literature Review

1.1 Overview of neurodegenerative diseases

A variety of diseases that primarily damage neurons in the brain and spinal cord are termed neurodegenerative diseases. The dramatic impact of these diseases arises because the neurons in an adult's brain and spinal cord are terminally differentiated and they cannot be repaired or replaced once they are injured. As the general population ages, neurodegenerative diseases such as dementias, with most cases occurring at ages 65 and over, have become one of the leading burdens that threaten the health of modern society. According to Statistics Canada's Canadian Community Health Survey, there are more than 3 million Canadians suffering from the neurodegenerative diseases in 2010-2011. Of these, there were 112,245 cases of Alzheimer's disease, 93,535 cases of Multiple sclerosis, 54,897 cases of Parkinson's disease, 4,067 cases of Amyotrophic lateral sclerosis and 2,911 cases of Huntington's disease. Since the pathogenesis of these diseases remains unclear, very few of them are curable.

Simple cellular behaviours, such as cell proliferation, cell differentiation and cell apoptosis, are regulated in different levels in vivo, such as: (i) extracellular signals; (ii) membrane protein interactions; (iii) intracellular mechanisms; (iv) nuclear import and; (v) gene expression. In case one or more of the above aspects malfunctions, a cell's viability can be impaired, which consequently leads to diseases. For many neurodegenerative diseases, they are initiated by irregular

gene expression and impaired intracellular protein-degradation pathways. One of the common examples is polyglutamine disorders, which include Huntington's disease and spinocerebellar ataxia 1. The polyglutamine disorders are caused by mutated genes, which possess extra repeated CAG nucleotide triplets.¹ These mutated genes then encode toxic proteins. The accumulated toxic proteins then impair the intracellular protein-degradation pathways so that there is a very low proteasome activity to clear the toxic proteins, leading to injured organelles in eukaryotic cells.^{2,3} For example, evidence has shown that the proteasome activity and levels of 20/26S proteasome are much lower in the cells which are affected by Huntington's disease than healthy cells.^{4,5} According to Rubinsztein, drugs that enhance intracellular protein-degradation pathway could provide a solution for curing associated neurodegenerative diseases including Parkinson's diseases and Alzheimer's diseases.²

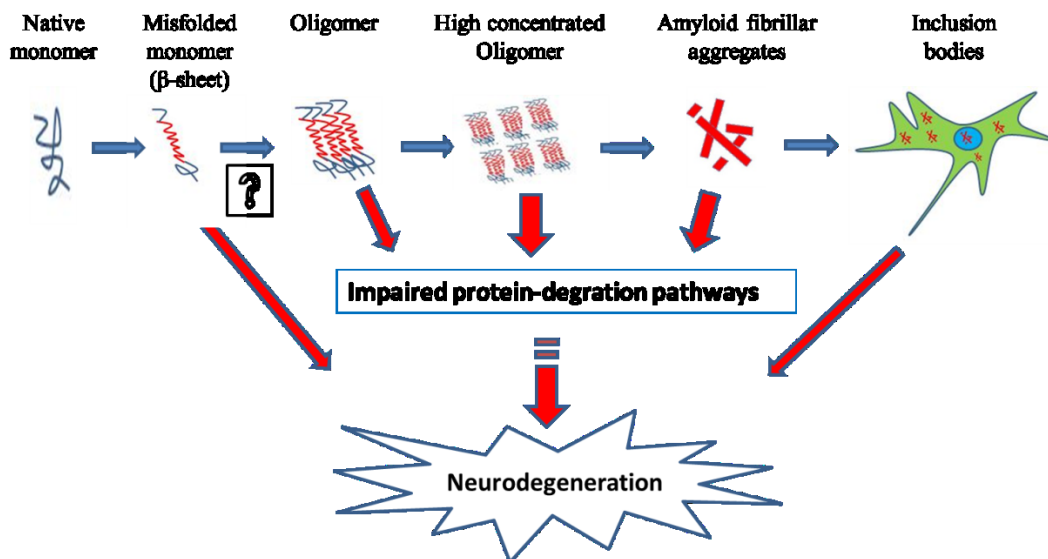


Figure 1: Recap of the toxic protein aggregation process (Adapted from reference).⁶

Table 1: Common neurodegenerative diseases associated toxic protein structure in aqueous condition and the protein deposits in vivo (Adapted from reference).³

Disease	Toxic Protein³	3D structure in solution	Protein deposits in vivo³
Alzheimer's disease	beta Amyloid (A β)	Has significant secondary and tertiary structure ^{12,13}	Extracellular plaques
	tau Protein	Intrinsically disordered ⁹	Intracellular tangles, Lewy bodies
Parkinson's disease	α -Synuclein	Intrinsically disordered ⁸	Lewy bodies
Prion disease	PrP ^{Sc}	Has significant secondary structure with high proportion of β -sheet ¹⁴	Prion plaque
Amyotrophic lateral sclerosis	Superoxide dismutase (SOD1)	Intrinsically disordered ¹⁰	Bunina bodies
Polyglutamine disease	Mutant proteins contains polyglutamine	-	Inclusion bodies

In general, a conspicuous characteristic of neurodegenerative diseases is the protein aggregates found in the contaminated eukaryotic cells. There are similarities and differences between these aggregation-prone proteins. First, most of these proteins are intrinsically disordered in solution. Although they lack a stable 3D structure in solution, they can form a regular tertiary structure after binding to oneself or to a target.⁷⁻¹¹ However, the other proteins have a partially folded structure in aqueous conditions;¹²⁻¹⁴ Second, all misfolded forms of the proteins are disposed to aggregation and to be accumulated as protein inclusions inside and outside of neurons as shown in Figure 1, but the protein inclusions of different diseases are found deposited in diverse compartments of a cell (See Table 1); Third, it is believed that many neurodegenerative diseases are eventually

triggered by the aggregation products as shown in Figure 1, but it is not clear, at the micron-level, which toxic agent(s) actually cause the neurodegenerative diseases. Gadad et al. suggested that the toxic agents causing Parkinson's diseases are oligomers.^{15,16} On the other hand, some researchers believe that oligomer itself is not sufficient to cause human disease.^{1,17}

1.2 Studies of aggregation-prone proteins

Protein misfolding and aggregation are the upstream events of the neurodegenerative cascade; therefore, it is vital to understand the molecular mechanisms of both processes in order to develop rational and effective treatments of the neurodegenerative diseases. To address these challenges, previous efforts studied the aggregation-prone proteins from the following aspects: (i) protein sequence alignment and comparison; (ii) protein hydrodynamic size measurement; (iii) protein three-dimensional (3D) structure estimation; and (iv) monitoring protein aggregation in vitro and in vivo.

1.2.1 Protein sequence alignment and comparison

Matching the amino-acid sequences of the toxic proteins with those of normal proteins provides invaluable information to predict the subcellular locations, the interacting regions and even the three-dimensional structure of the toxic protein.¹⁸

Take α -synuclein protein and β -synuclein protein for example. They almost have the same amino acid sequence except that α -synuclein has 11 more amino acids than the latter. However, α -synuclein is identified as the chief "culprit" for Parkinson's diseases, while β -synuclein shows no direct relation to the diseases.¹⁹

By sequence alignments, it is found that the extra 11 amino acids locate in a

region of α -synuclein from residues 61 to 95, named NAC 35. Most interestingly, NAC 35 demonstrated extreme hydrophobicity and rapid self-aggregation both in vitro and in vivo.²⁰

1.2.2 Protein hydrodynamic size measurement

Empirical relations between the number of amino acids in a protein (N) and the measured hydrodynamic radius (R_h) of the protein have been found for both native folded protein and highly denatured protein ($R_h = 4.75N^{0.29}\text{\AA}$ for native folded protein and $R_h = 2.21N^{0.57}\text{\AA}$ for unfolded protein).²¹ Therefore, the hydrodynamic radius measurement of proteins with known residue numbers can be used as a method to predict whether proteins are folded or unfolded under variable conditions. The widely used techniques to determine the hydrodynamic radius of a protein are dynamic light scattering (DLS),²² size-exclusion filtration,²³ sedimentation and gel filtration,²⁴ Electron Microscopy (EM),²⁴ Fluorescence Correlation Spectroscopy (FCS)²³ and Pulse Field Gradient Nuclear Magnetic Resonance (NMR).²¹ For instance, the hydrodynamic radius of A β (40 amino acids) is $9 \pm 1 \text{\AA}$ based on FCS, DLS and size-exclusion filtration measurements.²³ By comparing the experimental results with those calculated from the empirical equations, it also suggests that A β is more likely to be a natively folded protein.

1.2.3 Protein three-dimensional (3D) structure estimation

Transmission electron microscopy (TEM) is used to study the morphology of aggregates,³ while circular dichroism spectroscopy and Fourier transfer infrared spectroscopy are commonly used to estimate protein secondary structure.²⁵⁻²⁷ X-

ray crystallography²⁸ and NMR²⁹ are accepted techniques to determine protein tertiary and quaternary structures in crystal and in solution, respectively. The 3D structure of a protein, which includes secondary, tertiary and quaternary structures, defines its function. For example, the α -helix and the β -sheet are the most common secondary structures of a protein. While the α -helix plays a significant role in DNA binding,³⁰ membrane crossing³¹ and resistance towards axial tensile deformation,³² the β -sheet is usually adopted by many immunoregulatory proteins, including Interleukin-8 (IL-8)^{33,34} and Glycosylation-inhibiting factor (GIF).³⁵

Recent research further indicates that oligomers rich in β -sheets are accumulated in protein aggregates corresponding to many neurodegenerative diseases.³⁶ Another well-known example is the sickle hemoglobin which aggregates once the protein side chains have changed their hydrophobicity and thus, the 3D structures of the protein³⁷ on the whole. A further example is the A β residues regions of 15-23 and 31-35, which based on recent studies are transmembrane helices in membrane-mimicking environments.^{38,39} These helix sequences are very similar to those of the prion protein helices, which involve a conformational change from an α -helix to a β -sheet when the prion protein becomes pathogenic.³⁹⁻⁴¹ Last but not least, it is found that micelle- or membrane-bound α -synucleins have α -helical domains,⁴²⁻⁴⁴ but α -synuclein is known to be intrinsically disordered in solution at neutral pH.^{8,45}

1.2.4 Monitoring protein aggregation in vitro and in vivo

Research monitoring protein aggregation in vitro and in vivo can reveal optimized environments for protein aggregation/disaggregation and the molecular mechanisms of protein misfolding and aggregation processes. A variety of techniques have been utilized in this area: FCS,⁴⁶ image correlation spectroscopy (ICS),⁴⁷ and molecular probes such as thioflavin-T (ThT) and 8-anilino-1-naphthalene-sulfonate, which can non-specifically bind to fibrillar aggregates.⁴⁸ For instance, by using ThT assays, scientists reveal that the aggregation of A β , PrP^{Sc} and α -synuclein in vitro and in vivo evolve according to the nucleation-dependent polymerization models,^{49–51} which indicates that both the initial monomer concentration and the nucleus size determine the lag time (t_d) and half time ($t_{1/2}$) of the aggregation process.⁵² Subsequently, FCS experiments demonstrate that A β multimerization is a concentration-dependent⁵³ reaction and 0.2% sodium dodecyl sulfate (SDS) can be used to prevent prion protein from aggregating.⁵⁴ In 1998, Pitschke et al. proposed using FCS to detect A β aggregates in the cerebrospinal fluid of Alzheimer's patients, which became a pillar for future medical applications.⁵⁵ Other than the techniques mentioned above, numerous approaches are also utilized in aggregation-prone protein studies, such as mass spectrometry (MS), FRET and single-molecule force spectroscopy (smFS).

1.3 α -Synuclein

1.3.1 Research about α -synucleins (1997-2008)

α -Synuclein was first discovered in 1988, quickly followed by the identification of specific mutations of α -synuclein as the chief “culprits” for Parkinson’s diseases in 1997.⁵⁶ Thenceforth, our understanding of α -synuclein greatly improved over the ten years that followed. Most information can be summarized below into four aspects: (i) the native function of α -synuclein in cells; (ii) the primary structure of α -synuclein; (iii) the factors that can induce or inhibit α -synuclein aggregation; and (iv) the identification of the toxic species in the aggregation process.

The native α -synucleins are abundantly found in the terminal of neurons in the brain and the spinal cord, and their original functions are thought to be one of support of the plasticity of synaptic membranes,⁵⁷ to mediate the synaptic function of neurons, such as vesicular releasing and recycling,^{58,59} to participate in the regulation of neuronal apoptosis, including protecting neurons from neuronal apoptotic stimuli,⁶⁰ and to act as a molecular chaperone.⁶¹ However, the α -synucleins arising from gene mutation are found to cause neuron death, thus leading to Parkinson’s disease. For example, scientists have found that 85% of patients whose neurons expressed α -synuclein A53T mutants (the alanine located at residue 53 of native α -synuclein are substituted by threonine) gained symptoms of Parkinson’s disease.⁶² The other two human α -synuclein gene mutations related to familial Parkinson’s diseases are A30P and E46K.⁶³

The primary structure of a wild-type α -synuclein is well known; its monomer has 140 residues, which consists of a positive charged N-terminus, a negative charged

C-terminus and a hydrophobic central range with residues 61-95, known as NAC35 (See Figure 2). The N-terminus of α -synuclein, which can form α -helices for lipid-binding, has four and half KTKEGV motifs and three common mutation sites associated with familial Parkinson's diseases as mentioned above.⁵⁶ Similarly for the E46K mutation, replacing any glutamic acid (E) residue within the KTKEGV motif with lysine (K) will promote the conformational transition of α -synuclein from unfolded to partially folded protein, and eventually induces α -synuclein aggregation.⁶⁴ The C-terminus of the protein adopts a disordered conformation, even for lipid-bound α -synuclein. It is thought to act as an intramolecular chaperone to prevent the protein from aggregating,⁵⁶ because the cells that expressed C-terminal truncated α -synuclein are more easily damaged by oxidative stress^{56,65} and that NAC35 peptide alone can readily forms fibrils in vitro.⁶⁶ Therefore, the central hydrophobic NAC35 range is believed to play the most important role in the α -synuclein multimerization.²⁰ Another two and half non-conserved KTKEGV motifs are located in the central NAC35 region (Figure 2). Experiments illustrate that mutations of the last two non-conserved motifs to the precise hexameric sequence KTKEGV can significantly inhibit α -synuclein aggregation.⁶⁷



Figure 2: Primary structure of α -synuclein labelled with seven KTKEGV motifs and three mutation sites associated with familial Parkinson's diseases (Adapted from reference).⁶⁸

Abundant artificial circumstances induce α -synuclein aggregation in vitro. These circumstances include but are not limited to: (i) low pH (pH = 2.0 ~ 5.5);^{69,70} (ii) the presence of organic solvents;⁷¹ (iii) high temperature (T = 37 °C ~ 57 °C);⁶⁹ (iv) high protein concentration (above 8 mg/mL);⁵⁶ (v) the presence of small α -synuclein fibrils;⁵⁰ (vi) the addition of metal ions, such as, Al³⁺, Fe³⁺, Cu²⁺ and Co³⁺ into the protein solution;^{56,72,73} (vii) the presence of lipids or of a membrane;^{42,74} (viii) the introduction of mutations at specific sites;⁷⁵ and (ix) spontaneous dimerization by prolonged incubation time (more than 2 weeks).⁵⁶ On the other hand, some molecules are found to inhibit α -synuclein aggregation in vivo, such as chaperones and dopamine.⁵⁶ In addition, scientists discovered that Baicalein (a flavone), dopamine and catecholamines (a monoamine) are helpful in treatments for Parkinson' disease by inhibiting aggregation and dissolving the preformed fibrils in vitro.^{76,77} High pH (pH = 8.3 or higher) can also be used to dissolve the preformed fibrils in vitro.^{70,78}

While different factors that cause the α -synuclein aggregation have been discovered, a large number of α -synuclein aggregated forms have been observed, such as torroid-shaped oligomers, twisted-ribbon oligomers, straight oligomers, amorphous aggregates and fibrils.⁵⁶ Even electron micrographs of α -synuclein fibrils under a variable range of pH (2.0~ 7.0) and salt concentration (0.2 M NaCl or 10 mM MgCl₂) have shown different morphologies.^{69,79} The different morphologies of fibrils are believed to be due to the diversity of the partially folded conformations and differences in the molecular packing in α -synuclein monomers and oligomers (See Figure 3).⁵⁶

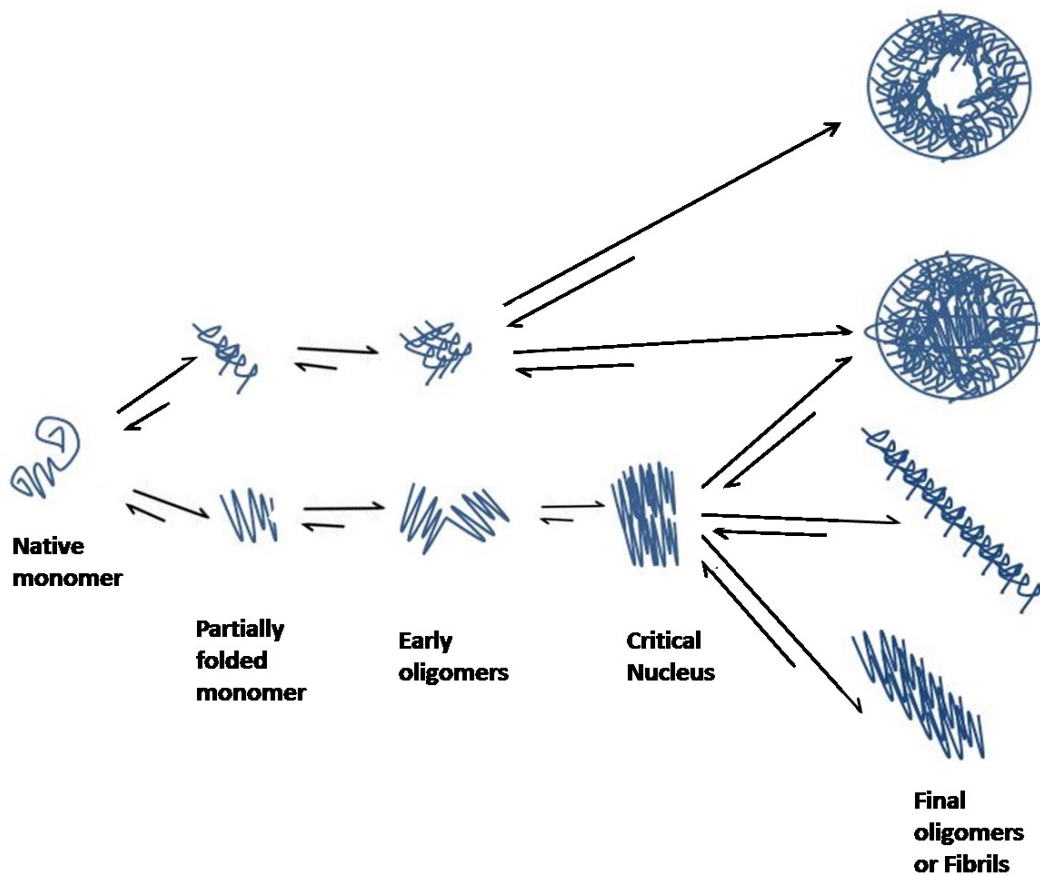


Figure 3: Formation of oligomers or fibrils with different morphology (Adapted from reference).⁸⁰

The question of what kind of small α -synuclein oligomers are neurotoxic has been raised. Although α -synuclein has been found fibrillarly aggregated into Lewy bodies in the brains of Parkinson patients, there is much evidence to indicate that Lewy bodies are neuroprotective⁸¹ and the soluble species are neurotoxic, namely the oligomers. For instance, the doughnut-shaped oligomers of α -synuclein from the brain of the Parkinson patients damage the neurons by forming pores that leak nutrients from the cell plasma.⁸²⁻⁸⁴ In addition, neuron deaths develop ahead of

the formation of detectable fibrils in vitro, which further demonstrate that soluble media may be more neurotoxic.⁸⁵

1.3.2 Recent research into α -synuclein (2009-2014)

Based on the above findings, the emphasis of α -synuclein-related research from 2009 to 2014 has shifted to the molecular basis of α -synuclein oligomerization. To be more specific, studies on the process of the α -synuclein misfolding and oligomerization from the molecular perspective can be categorized as the followings: (i) to identify the important conformational transitions and to determine the transition rate under “physiological” conditions (10 mM PBS at neutral pH) and; (ii) to perceive the effects of aggregation-induced factors on the intermediate molecular structures and the transition rates throughout the misfolding and oligomerization process; and (iii) to elucidate the misfolding and oligomerization pathways at the molecular level. Single-molecule assays including FCS, ICS, FRET and smFS have become invaluable techniques to study the aggregation-prone single protein molecules.

Firstly, several α -synuclein conformational transitions, of which the majority occurred in the N-terminal and NAC35 region, have been seen under “physiological” conditions. In 2012, Cremades et al. discovered there was a conformational change between newly formed oligomers and oligomers that were proteinase-K-resistant under “physiological” conditions by using smFRET, and its transition rate was $\sim 5 \times 10^{-6} \text{s}^{-1}$ (5×10^{-6} moles of oligomers A convert to oligomers B per second).⁷⁸ In the same year, Raussens et al. used attenuated total reflectance – Fourier-transform infrared (ATR – FTIR) spectroscopy to detect the

secondary structures in both α -synuclein oligomers and fibrils formed by spontaneous aggregation over prolonged incubation times. Structures rich in antiparallel β -sheet were found in the α -synuclein oligomers, while parallel β -sheets ranging from residues 38-95 were detected in its final fibrilisation.⁶⁸ In 2014, by using smFS, Neupane et al. discovered ~ 5 metastable transition states for the α -synuclein monomer, ~ 15 for the dimer and $\sim 20-25$ for the tetramer. Those metastable structures lasted for $\sim 10^{-1\pm 0.5}$ s before the protein unfolded again, which further demonstrated that α -synuclein is intrinsically disordered.⁸⁶

Secondly, numerous experiments have explored the effects of aggregation-inducing factors on the intermediate molecular structures. For example, two antiparallel α -helices of α -synuclein can be assembled to “grab” the micelle of a fatty acid found in neurons of the brain.^{44,87} In 2010, Trexler et al. discovered that the α -synuclein monomer was globular, because, while the distances between its residue 130 and residues 9, 33, 54, 72, 92 were almost the same at the neutral pH, all the distances were shortened when the pH is lowered to 3.0, with the exception of the distance between residues 9 and 130. By using smFRET, the C-terminal of α -synuclein was shown to fold toward its NAC35 region at pH = 3.0. Trexler et al. explained that low pH greatly changed the charge distributions of the C-terminus and destroyed its original interactions, which may be helpful to shield the NAC35 region from aggregation. Therefore, the closer proximity of each hydrophobic NAC35 region driven by C-terminus folding leads to faster α -synuclein oligomerization at pH = 3.⁸⁸ Many other researchers agreed with the idea that aggregation-induced factors can destroy α -synucleins’ original features including

long-range interactions, electrostatic interactions, low hydrophobicity and high net charge, all of which help to shield the protein from aggregation.^{43,81,89} Uversky gives a further explanation: the normal α -synuclein is a natively unfolded protein, so it can possess unstable secondary and tertiary structures as needs dictate for its dynamic functions. However, the aggregation-inducing factors trap the natively unfolded α -synuclein into a specific secondary structure, this causes the native function of unfolded α -synuclein to be lost.⁵⁶ Furthermore, partially folded α -synuclein proteins with specific secondary structures have the potential to act as a tightly packed nucleus that largely reduces the lag time of the aggregation phenomenon.⁹⁰ Consistent with this hypothesis, more partially folded α -synucleins were found to populate under the environments mentioned above which are able to induce neurotoxic fibrillation, such as low pH⁶⁹, high temperature,⁶⁹ the presence of metal ions,⁷³ the presence of SDS⁴⁴ and so forth.

Lastly, nucleation-dependent polymerization is thought to be a good model to describe α -synuclein misfolding and the oligomerization process at the molecular level. The nucleation-polymerization model indicates that the initial step of the α -synuclein aggregation process, being the addition of monomers, is thermodynamically unfavourable and the final step of forming fibrils is based on a critical nucleus which is thermodynamically favourable.⁹¹ Therefore, the critical nucleus is transient but its formation becomes the rate-limiting step of the whole polymerization process. These critical nuclei are believed to be highly associated with the cytotoxic oligomers. More and more research has then shifted towards the study of the structure, cytotoxicity of α -synuclein oligomers and their ability to

act as a critical nucleus. Recent studies identified several oligomeric structures and recognized their cellular toxicity. For example, donut-shaped oligomers were discovered when α -synuclein monomer concentration were above a specific concentration (8 mg/mL), where they then are potential cytotoxic by permeabilization of the membrane.⁹² Annular and spherical oligomers of Ca^{2+} -binding α -synuclein were discovered to increase the aggregation rate of the protein.⁹³ Smaller spherical oligomers of Fe^{3+} -binding α -synuclein in the presence of ethanol are SDS-resistant but they can form ion-permeable pores in a lipid bilayer.⁹⁴ Although the majority of α -synuclein oligomers are cytotoxic and able to accelerate fibril formation, nontoxic oligomers have also been discovered, some of which are even able to inhibit fibril formations! For instance, the globular α -synucleins oligomers stabilized by the flavonoid baicalein are able to greatly slow down the fibrillation and found to show mild effect on the membrane surface.⁹⁰ Moreover, α -synucleins oligomers oxidized by methionine completely inhibit the fibrillation of non-oxidized α -synuclein at neutral pH.⁹⁵

1.4 My research objectives

Knowledge of the structure and the cell cytotoxicity of small α -synuclein oligomers, together with the molecular mechanisms of their formation and the molecular mechanism of how they shorten the aggregation lag time are still sparse. As the critical nucleus is transient and difficult to separate from cell in vitro, an engineered α -synuclein dimer, tetramer and octamer were made in the lab by tandem linking a repeated monomer with three-amino-acid peptide linker (GSG).⁸⁶ To understand whether these engineered α -synuclein oligomers can act

as or convert to a critical nucleus in vitro, I aimed to monitor the aggregation processes of all engineered α -synuclein oligomers constructs in solution. To achieve this goal, the following research objectives were completed: *(i)* to characterize the sizes of α -synuclein monomers and the engineered oligomers by measuring their hydrodynamic diameters under phosphate-buffered saline (PBS) at pH = 7.4; *(ii)* to study the effects of the engineered α -synuclein oligomers on the monomer fibrillations (acceleration or inhibition); and *(iii)* to compare and contrast the kinetics between the self-aggregation (aggregations of the same construct of α -synuclein) and the cross-aggregation (aggregation of the monomeric and oligomeric α -synucleins). In general, there are two ways to experimentally observe proteins aggregation. One is to monitor the increase of the hydrodynamic sizes of the targeted proteins over time. The other is to detect the fractions of the proteins that are used to form aggregates as a function of incubation time. The latter one will be applied in my research.

Chapter 2: Methodology and Theory

2.1 Techniques used in protein aggregation studies

The techniques that have been used to monitor protein aggregation in solution include but are not limited to: (i) SDS-PAGE and Western blot analysis with chemiluminescence detection; (ii) Size-exclusion chromatography; (iii) Dynamic light scattering; (iv) ThT assay; (v) In-line Raman spectroscopy; and (vi) Fluorescence spectroscopy. In this Chapter, the fundamental of some common techniques will be reviewed, and their pros and cons in protein aggregates studies will be discussed.

2.1.1 SDS-PAGE

SDS-PAGE refers to sodium dodecyl sulfate-polyacrylamide gel electrophoresis. SDS is commonly used to denature the 3D structure of a protein so that the protein becomes one linear amino acid chain with the same negative charges per unit mass. SDS-PAGE is a technique that is widely used to separate proteins based on differences in molecular mass. An electric field is used in SDS-PAGE to pull the charged amino acid chains through the gel and the protein with larger molecular mass moves slower. Once the diverse proteins are separated from each other, all protein bands are transferred from the gel to a nitrocellulose membrane and a specific dye is used to stain the band of interest in the membrane. This method enables us to quickly distinguish the α -synuclein monomer and oligomers in a small amount of clinical sample. For example, Baba et al. utilized this method

to prove the existence of full-length α -synuclein, truncated α -synuclein and insoluble aggregates in the Lewy bodies purified from the brain of patients with Parkinson's disease. The anti-synuclein antibodies MAb, LB509 and antiserum 259 were used to specifically bind to the purified human α -synuclein.⁹⁶ There are several disadvantages of this method. First of all, the results are non-quantified and have limited reproducibility. Second, the dynamic process of α -synuclein aggregation cannot be captured early using this method.

2.1.2 Size-exclusion chromatography

Size-exclusion chromatography (SEC) is a technique used to separate molecules in solution based on their different hydrodynamic volumes. Figure 4 demonstrates the basic theory behind the separation: the aqueous protein sample is pumped through a column that consists of small porous and tightly packed particles; smaller proteins of the sample will elute later than the larger proteins. Because smaller proteins will diffuse in and out of the solvent inside of the pores of the packed particles, which takes more time for them to be eluted from the column. In the combination of a detector, such as UV-Vis, light scattering or MS, SEC is able to determine the concentration, the approximate hydrodynamic size and molar mass of samples in each eluted band. Here is an example of applying SEC to study α -synuclein aggregations. By using quantitative SEC with a Superdex 75 10/300 column (GE Healthcare), Cremades et al. observed that an increasing amount of α -synuclein oligomers and large fragments formed from 1 mg/mL α -synuclein monomer under "physiological" conditions (Tris 25 mM, pH 7.4, 0.1M NaCl and 0.01% NaN₃) at 37 °C under constant shaking at 200 rpm within

15~150 hours.⁷⁸ However, one major drawback of SEC prevents us from studying α -synuclein aggregation: the size exclusion column has a comparatively narrow working range and all α -synuclein oligomers elute as one band. Therefore, it is impossible to figure out if different kinds of α -synuclein oligomers are formed during the incubation. Moreover, dramatic protein loss is observed during each experiment. In my research work, size-exclusion chromatography is only used to remove excess free dye from the labelled α -synuclein by using Sephadex G-25 desalting column.

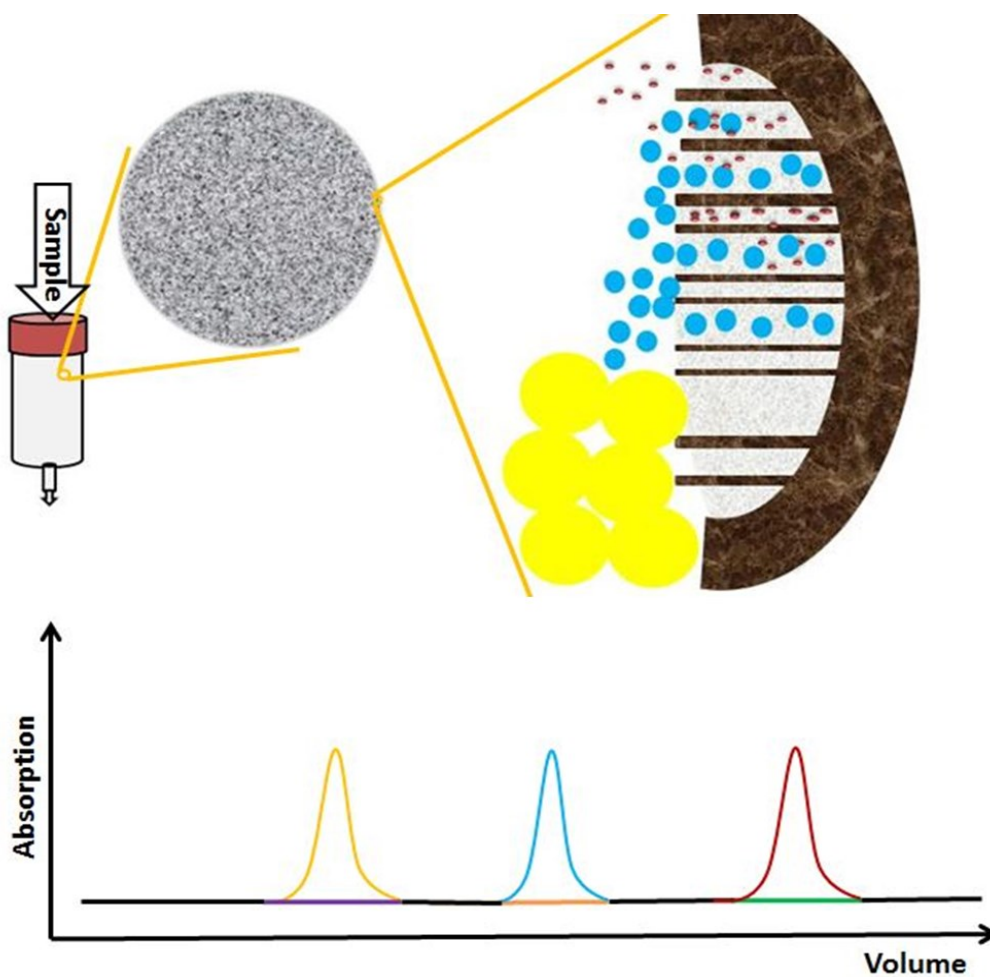


Figure 4: Principle of SEC (Adapted from reference).⁹⁷

2.1.3 Dynamic light scattering (DLS)

DLS is widely used to determine the hydrodynamic radius of a particle ranging from 0.3 nm to 10.0 μm in a monodisperse solution. As shown in Figure 5, monochromatic and coherent light hits the moving particles with the same size and the scattered lights at certain angle are detected to generate a spectrum of the fluctuations of scattering light intensity over time.

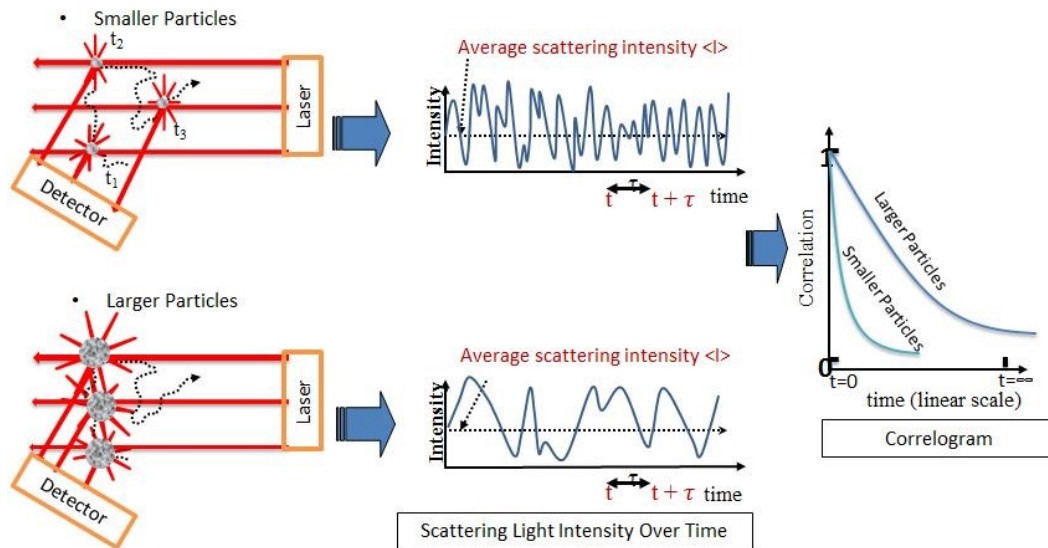


Figure 5: Principle of DLS.

With the assumption that all particles in a sample move by Brownian motion, the smaller particles move faster and thus their scattering light fluctuate faster compared with those of larger particles. The correlation function of DLS can be defined as⁹⁸

$$G(\tau) = \int_0^{\infty} I(t)I(t + \tau)dt \quad (1)$$

where $I(t)$ is the scattered light intensity, and a plot of $G(t)$ as a function of time can be drawn. This plot is also called a correlogram. Equation (2) demonstrates that the decay rate of the correlogram is related to the diffusion coefficient (D) of the measured particle.

$$\int_0^{\infty} I(t)I(t + \tau)dt = B + Ae^{-2q^2D\tau} \quad (2)$$

In Equation (2), B and A are the baseline and the amplitude of the correlogram, respectively. The parameter, q , is the scattering vector which is affected by the solvent refractive index, laser wavelength and the scattering angle, and D is the diffusion coefficient of the particle of interest. Once D is known, the hydrodynamic radius of the particle can be calculated based on the Stokes-Einstein equation (More details in Section 2.2.3).²² Previous research has used DLS to monitor the formation of α -synuclein oligomers. For instance, Fink et al. obtained the hydrodynamic radius of the mutated α -synuclein monomer Y39W (3.1 ± 0.2 nm) by DLS and observed the formation of its oligomeric species with the hydrodynamic radius equal to 22 ± 2 nm after 3 hours of incubation (20 mM phosphate buffer containing 150 mM NaCl at 37 °C and pH 7.4)⁹⁹. They also showed that the concentration of the oligomeric species increased to 15% of the total protein concentration after 18 hours of incubation and then decreased.⁹⁹

Compared with the techniques mentioned above, DLS is easy to use and its results are highly reproducible. However, the drawback of using DLS in protein aggregation study is that the heavily aggregated protein solution being incubated for a very long time becomes too polydisperse to be accurately interpreted. In my

research work, DLS is used to measure the hydrodynamic diameters of the native α -synuclein monomer, as well as the engineered α -synuclein dimer, tetramer and octamer. Then, the DLS data are used to validate those obtained from FCS.

2.2 Fluorescence Spectroscopy

Fluorescence Spectroscopy is a technique which has noticeable advantages in the protein aggregation studies compared with the other techniques summarized above. First of all, it allows us to monitor the protein misfolding and aggregation process both in vitro and vivo at very low sample concentration (\sim nM) with small volume (\sim several 100 μ L). Second, a variety of information including the concentration of a fluorescent sample, the averaged hydrodynamic radius of the fluorescent particles in the sample and even the averaged molar fraction of a specific component in the fluorescent particles can be obtained. Because of its high sensitivity, high precision and multifunction, fluorescence spectroscopy can not only be used to detect the changes of the hydrodynamic sizes of α -synuclein within a long incubation time, it can also be used to monitor the dynamic changes in the fractions of α -synuclein monomers contributed in the aggregation over long incubation time. Therefore, fluorescence spectroscopy is the main technique used to study the self-aggregation and cross-aggregation between α -synuclein monomer and the engineered oligomers in solution in our work.

2.2.1 Structure of a fluorescence microscope

A fluorescence microscope can “see” fluorescent molecules in solution. Experiments can be performed with one excitation only or with both excitations simultaneously. A simplified fluorescence microscope with specific excitation

wavelengths and dichroic mirrors used in my research is shown in Figure 6. The filtered excitation light of 488 nm and 633 nm is first expanded by a beam expander, and then is reflected along the optical axis to the edges of the objective lens by hitting a dichroic mirror (HFT 488/633) at 45 degrees. Next, the objective lens focuses the excitation light onto a sample solution to form a specific detection volume. The fluorescent species of interest diffuse in the detection volume are excited and emit the fluorescence light as well as the scattered and reflected light along the optical axis to hit back onto the dichroic mirror (HFT 488/633). However, only the emitted fluorescence light can pass through the dichroic mirror and the scattered and reflected light from the sample will be reflected by 90°. Then another dichroic mirror (NFT 635) allows wavelengths above 635 nm to pass through and the rest of wavelengths are reflected 90 degrees. The pass-through light passes through a high pass filter (LP 650 nm) and hits a detector, which is the “red detector”. Another band pass filter (BP 505 nm ~ 550 nm) is also set before the other detector, which refers to the “green detector”, so that only wavelength at 505 nm ~ 550 nm hits the detector.

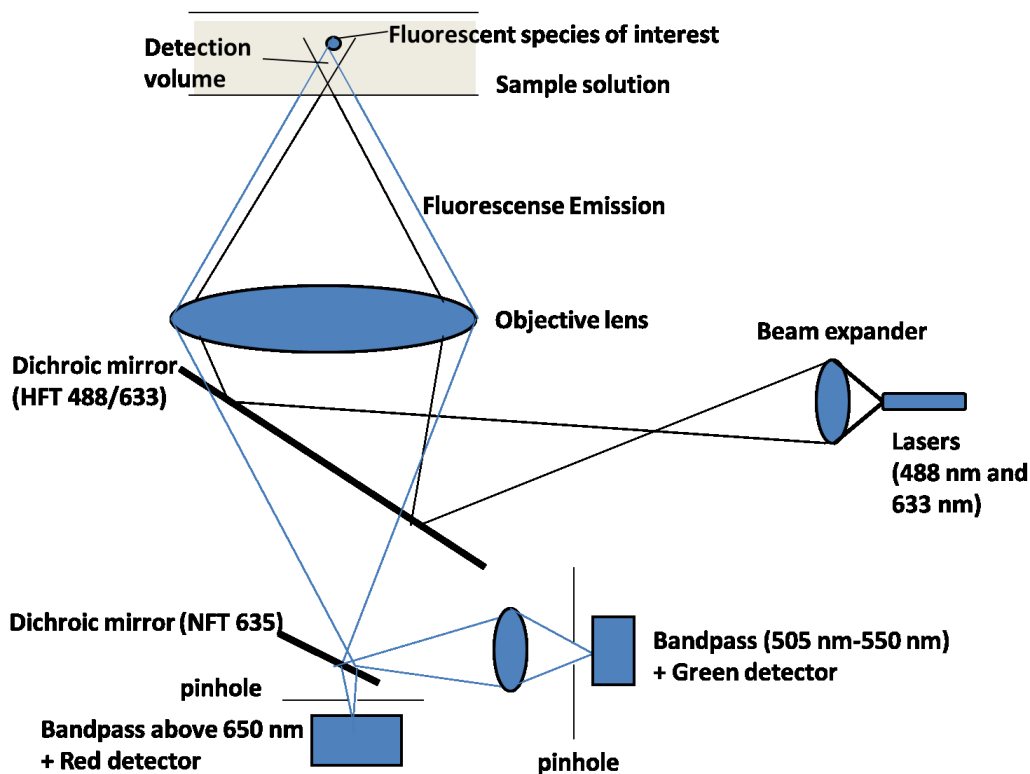


Figure 6: A simplified diagram of confocal microscope with two detectors.

2.2.2 Fluorescence Correlation Spectroscopy (FCS)

FCS was first defined in the 1970s by Magde, Elson and Webb in four classic papers.¹⁰⁰⁻¹⁰³ But it was not widely used for single molecule detection late until 1994.¹⁰⁴ Nowadays, it has become a powerful technique that can be used for the measurement of hydrodynamic size and reaction kinetics. It is even used as a diagnostic tool for Alzheimer's disease.¹⁰⁵ In this section, the principle of FCS and dual-color fluorescence cross-correlation spectroscopy (dual-color FCCS) is introduced. A better way of presenting dual-color FCCS data to decrease sample to sample variability caused by diluted sample preparation is proposed in the end of the section.

The principle of FCS

Fluorescence autocorrelation spectroscopy is a correlation analysis method for the study of fluorescence intensity fluctuation within a detection volume (similar in principle to DLS). The best sample for fluorescence autocorrelation spectroscopy contains only one fluorescent species or two independent fluorescent species with at least 10 fold differences in their molecular weights. This method can be ultimately used to determine the concentration of the fluorescent sample, as well as the hydrodynamic radius of a fluorescent particle in the sample.

The theory of FCS is based on two assumptions.¹⁰⁶ First, the fluorescent molecules of the FCS sample are in Brownian motion and can freely diffuse through the detection volume. Second, quantities of fluorescent molecules that diffuse through the detection volume follow a Poisson distribution,

$$P(k; \mu) = \frac{\mu^k \times e^{-\mu}}{k!} \quad (3)$$

where $P(k; \mu)$ refers to the probability of the cases for exactly k fluorescent molecules occurring in the detection volume, when μ of fluorescent molecules detected in average in the same region. The most important characteristic of a Poisson experiment is that the variance of the successes (σ^2) is equal to its mean:

$$\sigma^2 = \mu \quad (4)$$

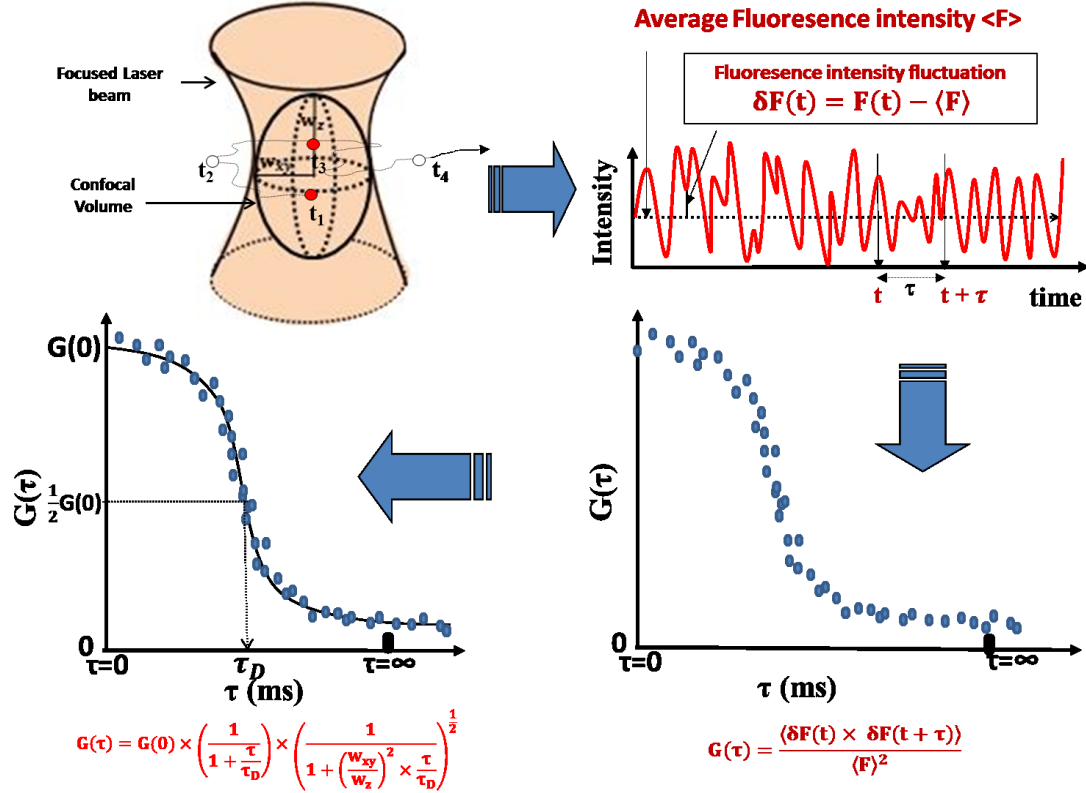


Figure 7: Principle of FCS (Adapted from reference).¹⁰⁷

As shown in Figure 7, the excitation and detection volume of FCS performance is a very small ellipsoid ($\sim 10^{-15}$ liters) along the focused laser beam. It is also called the confocal volume. With the consideration of the above two assumptions, the fluorescent molecules freely diffuse through the confocal volume, and the total fluorescence intensity within the confocal volume fluctuates with time. The fluorescence intensity shown in the figure is denoted as $F(t)$, the mean fluorescence intensity of the overall measurements is denoted as $\langle F \rangle$ and $\delta F(t)$ refers to the fluctuations around the mean fluorescence intensity. The autocorrelation function of the fluorescence fluctuations is defined as^{105,106}

$$G(\tau) = \frac{\langle \delta F(t) \times \delta F(t + \tau) \rangle}{\langle F \rangle^2} \quad (5)$$

where t is the actual measured time when $\delta F(t)$ is obtained, and τ is the time difference between one measurement and the other measurement, usually range from 0.01 ms to 0.1 s. $\langle \delta F(t) \times \delta F(t + \tau) \rangle$ refer to the average value of the $\delta F(t) \times \delta F(t + \tau)$ throughout the overall data accumulation time.

Once the autocorrelation function of the fluorescence fluctuation is obtained, a specific equation is used to fit the autocorrelation function as shown in the last plot of Figure 7. For the case that only one fluorescent species translationally diffuses in a 3D detection volume, the following fitting equation is used^{105,106}

$$G(\tau) = G(0) \times \left(\frac{1}{1 + \frac{\tau}{\tau_D}} \right) \times \left(\frac{1}{1 + \left(\frac{w_{xy}}{w_z} \right)^2 \times \frac{\tau}{\tau_D}} \right)^{\frac{1}{2}} \quad (6)$$

where τ and $G(\tau)$ are variables obtained from the experiments, $G(0)$ and τ_D are the important parameters generated by fitting, their physical meanings are described below in detail. The parameter, w_{xy} , can also be found in Figure 7; it refers to the equatorial radius of the confocal volume. The parameter, w_z , is the polar radius of the confocal volume which is along the direction of propagation of the focused laser beam. Both w_{xy} and w_z are independent of the sample, and they only change when different excitation wavelengths are used. Therefore, the ratio of w_{xy} and w_z is a constant during the measurements.

Physical meaning of the important parameters in FCS

Two important parameters can be generated from the fitting of the autocorrelation function: $G(0)$ and τ_D . $G(0)$ can be used to deduce the actual concentration of a

fluorescent species in the sample and τ_D can be used to calculate the hydrodynamic radius of the species.

$G(0)$ is the amplitude of a correlation function when τ is equal to zero. In practice, $G(0)$ is equal to the reciprocal of average observed number of fluorophores within a confocal volume as shown in Equation (7)¹⁰⁶

$$G(0) = \frac{1}{\langle N \rangle} \quad (7)$$

Once $\langle N \rangle$ is known, the mean concentration of a FCS sample can be calculated by

$$\langle c \rangle = \frac{\langle N \rangle}{V_{eff} \cdot N_A} \quad (8)$$

where N_A is the Avogadro constant. V_{eff} is the effective confocal volume which is calculated based on the the equatorial radius (w_{xy}) and the polar radius (w_z) of the confocal volume by¹⁰⁶

$$V_{eff} = \pi^{\frac{3}{2}} w_{xy}^2 w_z \quad (9)$$

There are two important requirements for a reliable FCS measurement. First, a FCS sample has to be measured at the nanomolar scale to ensure only a few of fluorophores are detected in the confocal volume throughout the overall data accumulation time. Second, the effective confocal volume has to be minimized to the femtoliter range ($\sim 1 fL$). Only by following these requirements, the fluorescence fluctuation caused by a single fluorophore translationally diffusing in/out of the confocal volume is significant relative to the noise.

Another important fitting parameter is the diffusion time (τ_D), which is equal to the time needed when $G(\tau) = \frac{1}{2}G(0)$, as shown in Figure 7. The translational diffusion coefficient (D) of a fluorescent molecule can be calculated based on its measured diffusion time as below

$$D = \frac{w_{xy}^2}{4 \times \tau_D} \quad (10)$$

Moreover, the relationship between the hydrodynamic radius (R) of a fluorescent molecule and its translational diffusion coefficient (D) is known as Stokes-Einstein equation, Equation (11)

$$R = \frac{kT}{6\pi\eta D} \quad (11)$$

where $k = 1.38 \times 10^{-23} \frac{\text{m}^2\text{kg}}{\text{s}^2\text{K}}$ is the Boltzmann constant. T is the temperature during a FCS measurement, and η is the viscosity of the buffer used in the measurement. To sum up, FCS is a technique to obtain the concentration of one kind of fluorescent species as well as its average hydrodynamic diameter in a sample solution.

Two-component FCS fitting equation

For the case that two independent fluorescent species laterally diffusing in the sample, the equation described autocorrelation function of total fluorescence fluctuations is the same, but a new fitting equation is used.¹⁰⁶ The mathematic equation is shown in Equation (12)

$$\frac{G(\tau)}{G(0)} = \frac{N_1}{N} D_1(\tau) + \frac{N_2}{N} D_2(\tau) \quad (12)$$

$$D_i(\tau) = \left(\frac{1}{1 + \frac{\tau}{\tau_{D_i}}} \right) \times \left(\frac{1}{1 + \left(\frac{w_{xy}}{w_z} \right)^2 \times \frac{\tau}{\tau_{D_i}}} \right)^{\frac{1}{2}} \quad (13)$$

where $D_1(\tau)$ and $D_2(\tau)$ as defined in Equation (13), are a part of the correlation function that contains information about the diffusion time of the two fluorescent species. The parameters, N_1 and N_2 correspond to the number of the fluorescent species 1 and 2 observed in the confocal volume. N is the sum of N_1 and N_2 . Consequently, $\frac{N_1}{N}$ refers to the mole fraction of species 1. In my research, two-component correlation fitting equation is often used, because the free dye (the dye without binding to any protein) cannot be completely removed from the labelled protein solution. Therefore, the fluorescent species 1 refers to the free dye and the fluorescent species 2 refers to the labelled protein. Combined with Equations (8), (9), (10) and (11), the concentration and the hydrodynamic radius of a labelled protein are still able to be obtained by a FCS experiment.

Other fitting factors needed to be considered

In a real FCS experiment, many other factors are taken into consideration to properly fit a FCS curve. These include the rotational diffusion of a fluorophore and its dynamic fluorescence property. Their influences on the correlation function of the fluorescence fluctuations are discussed here and are shown in Figure 8 (b).

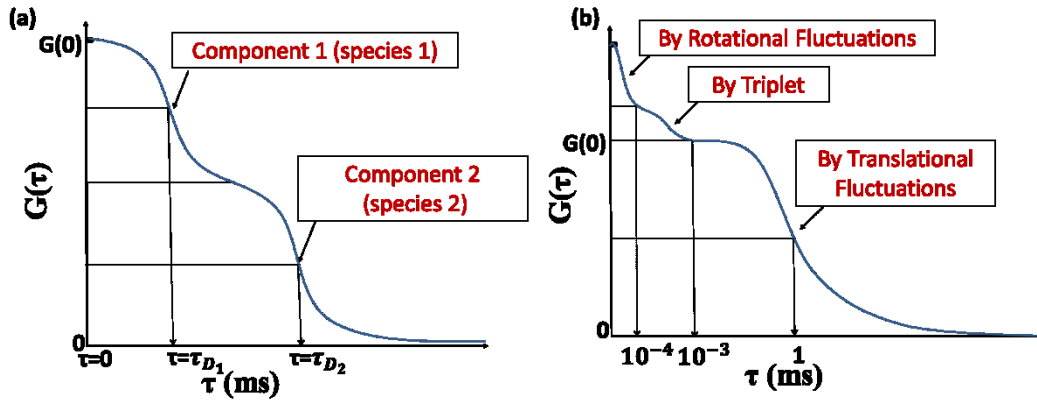


Figure 8: (a) Autocorrelation function of two component translational fluctuations; (b) Autocorrelation function for one component translational fluctuation with triplet and rotational diffusion.

First, an unobvious decay is usually found in an autocorrelation function around $\tau = 10^{-8} \sim 10^{-7} s$. This decay is formed when the measured fluorophores rotate while they cross the confocal volume. This is because laser is polarized and it is only be detected if detector is polarized. Therefore, the rotation of fluorophores can usually be neglected. Moreover, the rotational correlation time is much shorter than the diffusional correlation time. Second, a triplet shoulder is commonly observed in an autocorrelation function around $\tau = 10^{-7} \sim 10^{-6} s$. This phenomenon is caused by the forbidden transition of the fluorophores to the triplet state. In other words, a few of fluorophores, which are excited to the triplet state, are dark while they laterally pass through the confocal volume.¹⁰⁸ In order to avoid these problems which may cause an improper fitting, FCS curves in my research are usually fitted starting at $\tau = 10^{-6} s$.

2.2.3 Dual-color FCCS

Dual-color fluorescence cross-correlation spectroscopy (Dual-color FCCS) is an advanced correlation analysis method for the translational diffusions of multiple components in a system. The main advantage of dual-color FCCS is that it allows us to distinguish any of two species even if there is only a small molecular weight difference between the two species.¹⁰⁹

The principle of dual-color FCCS

As shown in Figure 9, the sample for dual-color FCCS usually contains two independent fluorescent species which are able to form conjugates over time.¹⁰⁸ For an FCCS experiment, two laser beams at different excitation wavelengths (488 and 633 nm are the most common excited wavelengths used in dual-color FCCS experiments) are overlapped to form a confocal volume. Then, the fluorescence fluctuations of green and red emissions are captured by a green detector and a red detector, respectively. Then, the two fluorescence fluctuations of emission are overlapped to find out the spots that two types of fluorescence are captured at the same time point. Based on the result, a cross-correlation function is generated.

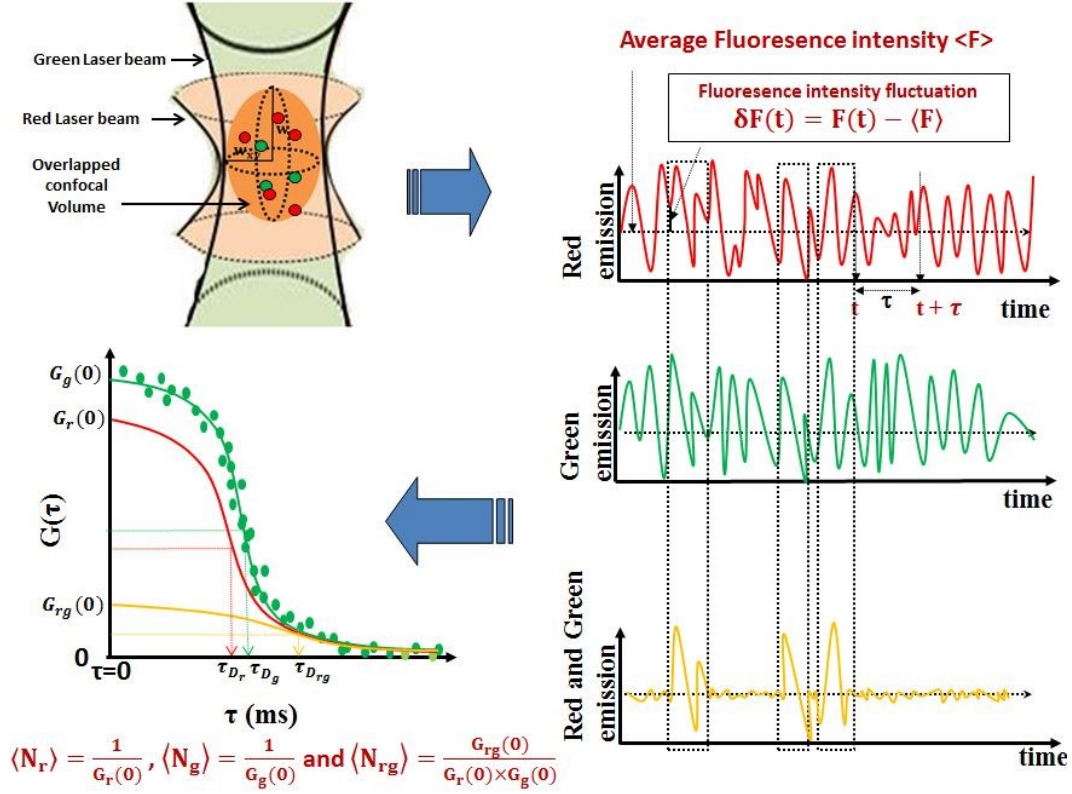


Figure 9: Principle of dual-color FCCS.

The same as the autocorrelation functions, the cross-correlation function reveals important information of the sample solution, such as the concentration and the hydrodynamic size of the conjugates, percentage of each species used in the formation of a conjugate and the kinetics of the overall conjugation process. The cross-correlation function of fluorescence fluctuation is defined below¹⁰⁶

$$G_{rg}(\tau) = \frac{\langle \delta F_r(t) \times \delta F_g(t+\tau) \rangle}{\langle F_r \rangle \times \langle F_g \rangle} \quad (14)$$

Its fitting function is similar as that of the autocorrelation function,¹⁰⁶

$$G_{rg}(\tau) = G_{rg}(0) \times \left(\frac{1}{1 + \frac{\tau}{\tau_{Drg}}} \right) \times \left(\frac{1}{1 + \left(\frac{w_{xy}}{w_z} \right)^2 \times \frac{\tau}{\tau_{Drg}}} \right)^{\frac{1}{2}} \quad (15)$$

The amplitude of the cross-correlation function equals:

$$\mathbf{G}_{rg}(\mathbf{0}) = \frac{\langle \delta F_r(t) \times \delta F_g(t) \rangle}{\langle F_r \rangle \times \langle F_g \rangle} = \frac{\langle N_{rg} \rangle}{\langle N_r \rangle \times \langle N_g \rangle} \quad (16)$$

To rearrange Equation (16):

$$N_{rg} = \frac{G_{rg}(\mathbf{0})}{G_r(\mathbf{0}) \times G_g(\mathbf{0})} \quad (17)$$

where $\langle N_{rg} \rangle$ is the average number of conjugates that can emit both red and green fluorescence within the overlapped confocal volume, and $\langle N_r \rangle$ is the average number of species that emit red fluorescence, which includes the red fluorescent species and all conjugates. Similarly, $\langle N_g \rangle$ includes the green fluorescent species and all conjugates. Once $\langle N_{rg} \rangle$ is known, the mean concentration of the conjugates can be calculated based on Equation (8). One difference is that the V_{eff_Cross} now refers to the overlapped effective confocal volume of two laser beams, which is defined as¹⁰⁶

$$V_{eff_Cross} = \left(\frac{\pi}{2}\right)^{\frac{3}{2}} (w_{xy_red}^2 + w_{xy_green}^2)(w_{z_red}^2 + w_{z_green}^2)^{\frac{1}{2}} \quad (18)$$

where w_{xy_red} , as shown in Figure 9, is the equatorial radius and w_{z_red} , is the polar radius of the confocal volume which along the focused red laser beam. w_{xy_green} and w_{z_green} refer to the corresponding radius of the focused green laser beam. Another difference is that the translational diffusion coefficient of the combined species (D_{rg}) is calculated as¹⁰⁶

$$D_{rg} = \frac{w_{xy_red}^2 + w_{xy_green}^2}{8 \times \tau_{D_rg}} \quad (19)$$

where $\tau_{D_{rg}}$ refers to the translational diffusion time of the aggregate. The Stokes-Einstein equation, the Equation (11), can also be used here to calculate the hydrodynamic radius (R_{rg}) of the aggregate from its translational diffusion coefficient (D_{rg}).

Other general factors that need to be considered

In theory, three correlation functions, the last diagram in Figure 9, are exactly the same if there are only red-green aggregates presenting in the sample. However, even then, the three correlation functions are rarely the same in reality. There are two reasons. First, the two laser beams or their detection volumes do not exactly overlap. Second, the effect of green dye to red channel is not negligible.

To solve the former issue, a calibration for FCCS experiments is required.¹⁰⁹ To ensure the overlap of detection volumes, a FCCS test can be done by exciting Rhodamine 6G with a 488 nm laser beam and receiving its emission by both Green and Red detection. By comparing the two amplitudes of the autocorrelation functions with the amplitude of the cross correlation function, it is known whether the two detections “see” the same spot. To ensure the overlap of lasers, a FCCS test can be done by exciting a red dye with a 633 nm laser beam and then exciting the same dye with a 488 nm laser beam. If the two autocorrelation functions have the same amplitude and diffusion time, it means that two lasers overlap.¹⁰⁹ Usually, the width of a laser beam is proportional to its wavelength,¹¹⁰ which will eventually cause a larger red laser beam and detection volume. In this case, instead of using $\langle N_r \rangle$, $\langle N_g \rangle$ and $\langle N_{rg} \rangle$ for the further calculation of the aggregation

process, $\langle n_r \rangle$, $\langle n_g \rangle$ and $\langle n_{rg} \rangle$ will be applied. $\langle n_{rg} \rangle$ is the concentration of the conjugated fluorescent species observed in the effective cross detection volume, which is defined as

$$\langle n_{rg} \rangle = \frac{\langle N_{rg} \rangle}{V_{effrg}} = \frac{\langle N_{rg} \rangle}{\left(\frac{\pi}{2}\right)^{\frac{3}{2}} (w_{xy_red}^2 + w_{xy_green}^2) (w_{z_red}^2 + w_{z_green}^2)^{\frac{1}{2}}} \quad (20)$$

The same for $\langle n_r \rangle$ and $\langle n_g \rangle$,

$$\langle n_r \rangle = \frac{\langle N_r \rangle}{V_{effr}} = \frac{\langle N_r \rangle}{\left(\frac{\pi}{2}\right)^{\frac{3}{2}} \cdot w_{xy_red}^2 \cdot w_{z_red}} \quad (21)$$

$$\langle n_g \rangle = \frac{\langle N_g \rangle}{V_{effg}} = \frac{\langle N_g \rangle}{\left(\frac{\pi}{2}\right)^{\frac{3}{2}} \cdot w_{xy_green}^2 \cdot w_{z_green}} \quad (22)$$

The issue that the cross talk of green dye to red channel may not be negligible is solved when a proper dye system is chosen. the cross talk of green dye to red channel is negligible when the following condition is fulfilled¹⁰⁹

$$\frac{E_{GGG}}{E_{RRR}} \approx \mathbf{1} \quad (23)$$

$$\frac{E_{GGG}}{E_{RGG}} \approx \mathbf{20} \quad (24)$$

$$\frac{E_{RRR}}{E_{RRG}} \approx \mathbf{8} \quad (25)$$

$$\frac{E_{RGG} + E_{RRG} + E_{RRR}}{E_{RGG}} \approx \mathbf{20} \quad (26)$$

where E_{GGG} refers to the green emission of green dye excited by green laser, E_{RRR} refers to the red emission of red dye excited by red laser, E_{RGG} refers to the red

emission of green dye excited by green laser and E_{RRG} refers to the red emission of red dye excited by green laser.

Chapter 3: Materials and Methods

3.1 Labelling

α -Synuclein preparation. During the experiments, the engineered α -synuclein dimer, tetramer and octamer are made by tandem linking repeated monomer with three-amino-acid peptide linker (GSG). In order to specifically label each α -synuclein with a fluorescence dye, one cysteine was inserted to the C terminal of each construct. Overall, the α -synuclein monomer and these engineered dimer, tetramer and octamer with one C-terminal cysteine are my study objects. My coworker, Meijing Wang, synthesized them by the following procedures. First, the native monomeric, dimeric tetrameric and octameric α -synuclein expression constructs were obtained from B-Bridge International. Second, the Site-Directed Mutagenesis Kit from Agilent Technologies was used to add one cysteine on the C-terminal of each α -synuclein construct. Once the DNA sequence and the amino acid sequence of the mutated α -synulcein were confirmed, the plasmid containing the α -synuclein of interest were inserted into the Rosetta™ 2 (DE3) Competent Cells from EMD Millipore for over expression. Then, osmotic shock was used to break the cell and release all proteins from the cell. Finally, Ion exchange chromatography with Q Sepharose medium was used to purify the α -synuclein of interest from all other proteins and 90% ammonia sulfate were used to precipitate the purified α -synuclein for labelling or storage at -80 °C. In the following research, the α -synuclein monomer and its engineered dimer, tetramer and

octamer with one C-terminal cysteine are represented as Snca1, Snca2, Snca4 and Snca8, respectively.

A variety of dyes. The fluorescent dyes tested and used in my research can be categorized into two groups; one has maximum absorbance around 492 nm (the green dye) and the other has maximum absorbance above 540 nm (the red dye). The producers and names for all dyes are summarized in Table 2.

Table 2: The producer and name for each dye used in the research.

Company Names	Names of dyes max. abs at 492 nm	Company Names	Names of dyes max. abs above 540 nm
Life Technologies	Alexa Fluor® 488 C5-maleimide (Catalog Number: A-10254)	Life Technologies	Alex Fluor 546 C5-maleimide (Catalog Number: A-10258)
	Oregon Green® 488 Carboxylic Acid, Succinimidyl Ester, 6-isomer (Catalog Number: O-6149)		Alex Fluor 633 C5-maleimide (Catalog Number: A-20342)
	Oregon Green® 488 maleimide (Catalog Number: O-6034)	Bioconjugate Technology Company	Cy5 Tetrazine (Catalog Number: 1019)
Biotium	CF™488A Dye		

Other materials. Other materials used in the labelling experiments include: 10 mM phosphate-buffered saline (PBS, includes 137 mM NaCl, 2.7 mM KCl, 10 mM Na₂HPO₄ and 1.8 mM KH₂PO₄) at pH = 7.0 or 7.4, 1 M of sodium bicarbonate buffer at pH = 9.0, dimethylsulfoxide (DMSO) from Life Technologies, tris-(2-carboxyethyl) phosphine hydrochloride (TCEP-HCl) from

Pierce Protein Biology Products, trans-cyclooctene-PEG₃-Maleimide (TCO-PEG₃-Maleimide, TPM) from Bioconjugate Technology Company, HiTrap Desalting Columns from GE Healthcare and Amicon[®] Ultra Centrifugal Filters with regenerated cellulose at 3K, 10K and 50K nominal molecular weight limit (NMWL) from Merck Millipore Ltd.

Methods. Three labelling reactions were applied in my research: (i) the reaction of a primary amine with a succinimidyl ester; (ii) the reaction of a sulfhydryl with a maleimide; and (iii) the Diels-Alder cycloaddition reaction of trans-cyclooctenes (TCO) with tetrazines. Their reaction schemes are summarized in Figure 10. Among these reactions, the last one is a click chemistry reaction, which has extremely fast kinetics ($k > 800M^{-1}s^{-1}$) to produce protein-dye conjugates at lower protein concentration (e.g. $5\mu M$) with shorter reaction time (e.g. 30 min).^{111,112}

Filter with appropriate cutoff was used to remove any leftover ammonium ion and to concentrate the protein solution to 7~8 mg/mL. Third, 0.1 mL of 1 M of sodium bicarbonate buffer at pH 9.0 was added for each mL of protein solution. Fourth, 20 moles of the succinimidyl-ester dye were added for each mole of protein solution. Finally, the protein-dye solution was incubated at 4 °C with continuous stirring overnight. Because there are fifteen Lysines in the sequence of monomeric α -synuclein, multiple dyes are theoretically able to form covalent bonds with each monomeric α -synuclein in this method.

Sulfhydryl Maleimide Reaction. There are two ways to label the C-terminal Cysteine of α -synucleins with dyes containing a maleimide group. The first approach is similar to that described in the labelling probes of Life Technologies¹¹⁴ with the following modifications. First, the frozen α -synuclein with C-terminal Cysteine was dissolved with 10 mM PBS at pH 7.0 to ensure protein concentration is 1.75 ~ 2 mg/mL. To reduce the disulfide bonds of α -synuclein, 0.067 M of TCEP-HCl solution at pH 7.0 (TCEP-HCl solution is titrated with NaOH solution to pH 7.0) were added into the protein solution to ensure approximately 10-20 moles of TCEP-HCl for each mole of protein. After 45 minutes of incubation at room temperature, 20-30 moles of the maleimide dye were added for each mole of protein. Last, the protein-dye solution was incubated at 4 °C with continuous stirring overnight. However, according to Kim¹¹⁵, large amounts of TCEP-HCl will interfere with the sulfhydryl maleimide reaction. In this case, the first labelling method requires large amounts of dye to compromise the effects of interference, which complicate the purification steps.

To solve this problem, a second labelling approach was proposed and applied. First of all, one modification was added in the last step of α -synuclein synthesis: while 90% ammonia sulfate were used to precipitate the purified α -synuclein for labelling or storage at $-80\text{ }^{\circ}\text{C}$, 10 mM TCEP-HCl was added into the 90% ammonia sulfate to produce the reduced solid α -synucleins. By doing this, the unreacted excess amounts of TCEP-HCl would stay in the solution while the protein precipitated. Moreover, the reduced solid proteins were not easily oxidized to form disulfide bonds since movement of the solid proteins was restricted. Next, the reduced solid α -synuclein was washed with 90% ammonia sulfate twice to remove leftover TCEP-HCl on the surface of the solid protein. Then, only 5~10 moles of dye solution were added for each mole of protein. Finally, 10 mM PBS at pH 7.0 was used to dissolve the mixture of the protein and the dye, so that the final protein concentration was around 2 mg/mL. Then, the protein-dye solution was incubated at $4\text{ }^{\circ}\text{C}$ with continuous stirring overnight.

To distinguish these two different sulfhydryl maleimide labelling methods, the former one was called sulfhydryl maleimide labelling Method One and the latter was sulfhydryl maleimide labelling Method Two.

Trans-cyclooctenes (TCO) Tetrazine Reaction. The mutated C-terminal Cysteine α -synucleins have no TCO group. Therefore, TPM were used to conjugate with the mutated α -synuclein based on the sulfhydryl maleimide labelling protocol. Then, an Amicon[®] Ultra Centrifugal Filter with appropriate cutoff was used to remove excess TPM. Last, only 1~1.1 moles of the tetrazine

dye were added for each mole of the TPM-modified α -synuclein and the protein-dye solution was incubated at 4 °C with continuous stirring for 4 hours.

3.2 Purification and labelling efficiency

In my research, two different approaches were applied to remove the excess dye after labelling. They are fast protein liquid chromatography (FPLC) and centrifugation with specific centrifugal filters. The detailed instrumentation, materials and methods are discussed below. Then, high performance liquid chromatography - mass spectrometry (HPLC-MS) was applied to ensure the labelling efficiency calculation and to validate the labelling protocols based on the sulfhydryl maleimide reaction.

3.2.1 Fast protein liquid chromatography (FPLC)

Instrumentation. All FPLC elution profiles and purified protein-dye conjugates were obtained using an ÄKTA FPLC system, which consists of a ÄKTAmicro and a Fraction Collector Frac-950. The ÄKTAmicro is a chromatography system including a Pump P-905, a Monitor pH/C-900, and a Monitor UV-900. In combination with two GE Healthcare HiTrap desalting columns (5mL for each), the whole system allows me to purify at most 1.5 mL of labelled α -synuclein solution at each sample run and to automatically collect all fraction volumes in microliterscale. Moreover, the whole experiment process is operated by UNICORN 5 control software. For each sample run, a FPLC chromatogram, a plot of absorption of eluted solution vs. the elution volume, is generated. Therefore, the fraction volume that contains purified labelled α -synucleins can be easily determined based on their absorption and expected elution time.

Materials and methods. Materials of this experiment include: Two HiTrap desalting columns (5×5 mL, Product Code: 71-1408-01) from GH Healthcare Life Sciences, 20% Ethanol solution from Sigma-Aldrich, 10 mM PBS at pH = 7.4, fluorescent dye labelled α -synuclein solution (100 μ L, protein concentration is less than 3 mg/mL), original fluorescent dye dissolved in PBS ($\sim 3 \mu$ M). Theoretically, the protein and dye concentration does not affect the FPLC separation as long as the viscosity of total protein and dye solution is similar to the viscosity of the PBS buffer. However, α -synuclein sample concentration used by FPLC purification was no more than 3 mg/mL. There are two reasons: α -synuclein aggregates quickly at high protein concentration (~ 8 mg/mL); and excess dye and the protein are not able to be completely separated when sample protein concentration is too high. The FPLC purification procedure is the same as that described in the ÄKTA FPLC system online standard operating procedure.¹¹⁶ The injection volume of sample is 1 mL, flow rate of separating the protein and dye is set at 3 mL/min and the column pressure during the separation is usually below 0.67 MPa. Before each separation experiment, 40 mL ddH₂O, and then 40 mL 1 \times PBS will be used to wash the column and the line. After each separation, 50 mL ddH₂O are used to wash the column. Finally the column is stored at 25% ethanol.

3.2.1 Centrifugation, centrifuge, and UV/Vis spectroscopy

Instrumentation and materials. The instruments used in this section were an Allegra™ 25R Centrifuge from Beckman Coulter and an Agilent Cary 60 UV/Vis spectrophotometer. The necessary materials are several Amicon® Ultra

Centrifugal Filters with regenerated cellulose at 3K, 10K and 50K molecular weight cutoff (MWCO) from Merck Millipore Ltd., 10 mM PBS at pH = 7.4 used as dispersant and exchange buffer, fluorescent dye dissolved in PBS ($\sim 3 \mu\text{M}$) and fluorescent dye labelled α -synuclein solution ($4\sim 15 \text{ mL}$, protein concentration is less than 3 mg/mL). Table 3 summarizes the molecular weights of the engineered α -synuclein monomer and oligomers in Dalton as well as the types of Amicon[®] Ultra Centrifugal Filters with suitable MWCO for each α -synuclein construct.

Table 3: Selection of the Amicon[®] Ultra filters for Snca1, 2, 4 and 8.

	Snca1	Snca2	Snca4	Snca8
Molecular Weight (Da)	14,460	29,103	58,390	116,963
Molecular Weight Cut off	3 K	10 K	10 K	50 K

Method. Purification using a centrifuge with swinging bucket rotor was performed at 4 degrees and 5100 g for 10 ~ 30 minutes. Normally, the purification was repeated one or two more times after filling the Centrifugal Filters with 10 mM PBS at pH = 7.4. Then, both filtrate volumes and diluted aliquots of the final purified solution were measured using the Agilent Cary 60 UV/Vis spectrophotometer to ensure complete removal of free dyes and high protein recovery.

Data analysis. A good purification result with high protein recovery is characterized by a high labelling efficiency. For instance, Alexa Fluor[®] 488 C5 Maleimide has its maximum absorption at 493 nm. The labelling efficiency for a purified protein sample labelled with Alexa Fluor[®] 488 C5 Maleimide is defined in Equation (27).

$$\frac{\text{Concentration of dye}}{\text{Concentration of protein}} = \frac{A(492 \text{ nm})/\varepsilon(\text{alexa 488})}{[A(280 \text{ nm})-A(492 \text{ nm})\times CF]/\varepsilon(\text{Protein})} \quad (27)$$

where $A(493 \text{ nm})$ refers to the absorption at wavelength 493 nm, $\varepsilon(\text{Alexa 488})$ is the molar absorptivity of Alexa Fluor[®] 488 C5 Maleimide ($7.0000 \times 10^4 \text{ M}^{-1}\text{cm}^{-1}$) and CF is the correction factor¹¹³, which is equal to $\frac{A(280 \text{ nm})}{A(493 \text{ nm})}$ of a sample only contained Alexa Fluor[®] 488 C5 Maleimide. Normally, CF of a specific dye was given by the manufacturer, for example, CF of that Alexa Fluor[®] 488 C5 Maleimide is 0.11, CF of Oregon Green 488 maleimide is 0.12 and CF of Cy5 tetrazine is 0.08.

3.2.3 HPLC-ESI- α TOF

High performance liquid chromatography with an orthogonal acceleration time-of-flight mass spectrometer (HPLC-ESI- α TOF) was used: (i) as an innovative method to confirm the calculation of the labelling efficiency; and (ii) to ensure a successful labelling between TPM and α -synuclein.

Instrumentation. The instruments used in this section were Agilent 1200 SL HPLC system and an α TOF mass spectrometer. Electrospray ionization (ESI) was used to generate the ion source for the α TOF mass spectrometer. A 75×0.5

mm, 5 μ m particle size, C8 poroshell column from Agilent Technologies with Opti-pak trap cartridge kit, 5 μ L BED, C8, thermostated at 65°C was used in the HPLC system. The buffer gradient consists of 0.1% formic acid in double-distilled water (ddH₂O) (v/v) as solvent A and 0.1% formic acid (v/v) in acetonitrile as solvent B. The most suitable buffer gradient for α -synuclein was summarized in Table 4. The flow rate was 0.15 mL/min and the first five minutes flow-through went to the waste.

Table 4: The buffer gradient for α -synucleins.

Time (mins)	0	10	25	55	65	70	75	80	85
% B	5	30	35	45	65	75	85	98	98

Method and sample preparation. The experimental procedure of using HPLC-ESI- α TOF was followed the University of Alberta Mass Spectrometry Facility protocol¹¹⁷. The sample used for confirming the labelling efficiency calculation was a fraction of monomeric α -synulcein labelled with Alexa Fluor 488 which is then purified by FPLC. The samples used for the confirmation of the coupling of TPM with α -synucleins were the α -synuclein monomer and the engineered dimer with their C-terminal Cysteine labelled with TPM. These samples were purified by the specific Amicon[®] Ultra-15 Centrifugal Filters and ddH₂O was used as the exchange buffer during the purification to ensure no salt existed in the final solution for HPLC- α TOF measurement. Then each sample was dissolved in ddH₂O. The Agilent Cary 60 UV/Vis spectrophotometer was used to ensure the

protein concentration was approximately 30 μM . Then 2 μL of the sample was diluted with 12 μL of 0.1% formic acid in (ddH₂O) (v/v), and 2 μL of the diluted sample was injected.

3.3 Quantum yields of labelled α -synucleins

This experiment aimed to find out whether the quantum yield of Oregon Green 488 Maleimide or Cy5 tetrazine changed or not when they were mixed with or were conjugated to the monomeric, dimeric, tetrameric and octameric α -synucleins.

Instrumentation. The instrument used in this section was a PTI Fluorescence QuantaMasterTM Fluorescence Spectrofluorometer. The accompanying software was FelixGX 4.1.2. A wavelength of 492 nm was used to excite Oregon Green 488 Maleimide and its labelled protein. The fluorescence of the dye from 493 nm to 600 nm was detected at 90°. Similarly, a wavelength of 650 nm was used to excite Cy5 tetrazine and its labelled protein, the fluorescence of the dye from 651 nm to 750 nm was detected at 90°. For all measurements, the entrance and exits sides of both the excitation and emission monochromators were set to 1 nm. A clean, 1 cm, quartz cuvette was used.

Method and sample preparation. The α -synuclein monomer, dimer, tetramer and octamer with their C-terminal Cysteine labelled with either Oregon Green 488 maleimide or Cy5 tetrazine, together with the pure dyes and 10 mM PBS buffer were measured using the PTI Fluorescence Spectrofluorometer. Each sample was dissolved in the 10 mM PBS at pH 7.4 and the protein concentration was

measured by an Agilent Cary 60 UV/Vis spectrophotometer at 280 nm. The molar absorptivity of α -synuclein monomer and oligomers at 280 nm are summarized in Table 5. The protein concentration of α -synuclein solution is controlled around 0.5 mg/mL by the UV/Vis spectrophotometer, and then it was diluted for 10 times for fluorescence measurements. The reason is that a concentrated fluorescent protein sample will experience inner filter effects. Each sample was measured using the fluorescence spectrofluorometer three times. For each measurement, all emission counts within the detection range were summed after the background counts were deducted. The background counts were the emission counts at the corresponding wavelength of 10 mM PBS upon excitation the same wavelength as that of the protein solution.

Table 5: Molar absorptivities of Snca1, 2, 4 and 8.

	Snca1	Snca2	Snca4	Snca8
$\epsilon(\lambda = 280\text{nm})$ in $\text{M}^{-1}\cdot\text{cm}^{-1}$	5960	11920	23840	47680
$\epsilon(\lambda = 280\text{nm})$ in $(\text{mg/mL})^{-1}\cdot\text{cm}^{-1}$	0.4122	0.4096	0.4083	0.4076

3.4 Dynamic Light Scattering (DLS)

The aims of DLS experiments were to measure the hydrodynamic diameter distributions of α -synuclein monomers as well as that of its engineered dimers, tetramers and octamers.

Instrumentation and method. The instrument used in this experiment was a Zetasizer Nano ZS. It used an excitation wavelength of 633 nm and detected the scattering light at 173°. The accompanied software for the Zetasizer Nano ZS is Malvern Software (version 7.02). For all measurements, the suggested Standard Operating Procedures (SOP) was used. The SOP includes that the refractive index and the absorption of the measured protein were set at 1.450 and 0.001, respectively, 10 mM PBS was used as dispersant, and its viscosity and refractive index at the measurement temperature (22.0 °C) were set at 1.05 cP and 1.334, respectively. Disposable DTS0012 cuvettes were used. To improve the signal-to-noise ratio, each sample was measured three times and each measurement contained 13 runs.

Sample Preparation. The α -synuclein monomer, dimer, tetramer and octamer with their C-terminal Cysteine labelled with TPM were measured by DLS. Each sample was dissolved in 10 mM PBS at pH 7.4 and with a protein concentration of approximately 1.4 mg/mL. An Agilent Cary 60 UV/Vis spectrophotometer was used to measure the protein concentration at 280 nm. To remove dust and large protein aggregates, Whatman Anotop 10 Syringe Filters with 100 nm pore size were used to filter 1.5 mL of each protein sample directly into new disposable DTS0012 cuvettes for measurements.

3.5 FCS and dual-color FCCS

3.5.1 Calibration measurements

Laser-scanning microscope LSM 510/ConfoCor 2 (CarlZeiss, Jena, Germany) was used for all FCS measurements and a C-Apochromat 40X/NA 1.2 water

objective was used. Before all FCS experiments, several things were done to ensure that the instrument was well calibrated: (i) to show that red and green laser beams were well overlapped; (ii) to show that red and green detection volumes were well overlapped; (iii) to choose the proper laser power; (iv) to show a proper dye system is chosen so that the cross talk of green dye to red channel is negligible; (v) to measure the diffusion times of the dyes used in my research; and (vi) to determine the equatorial radius and the confocal volumes of both green laser beam and red laser beam, together with the estimated cross confocal volume.

Calibration Measurement One.

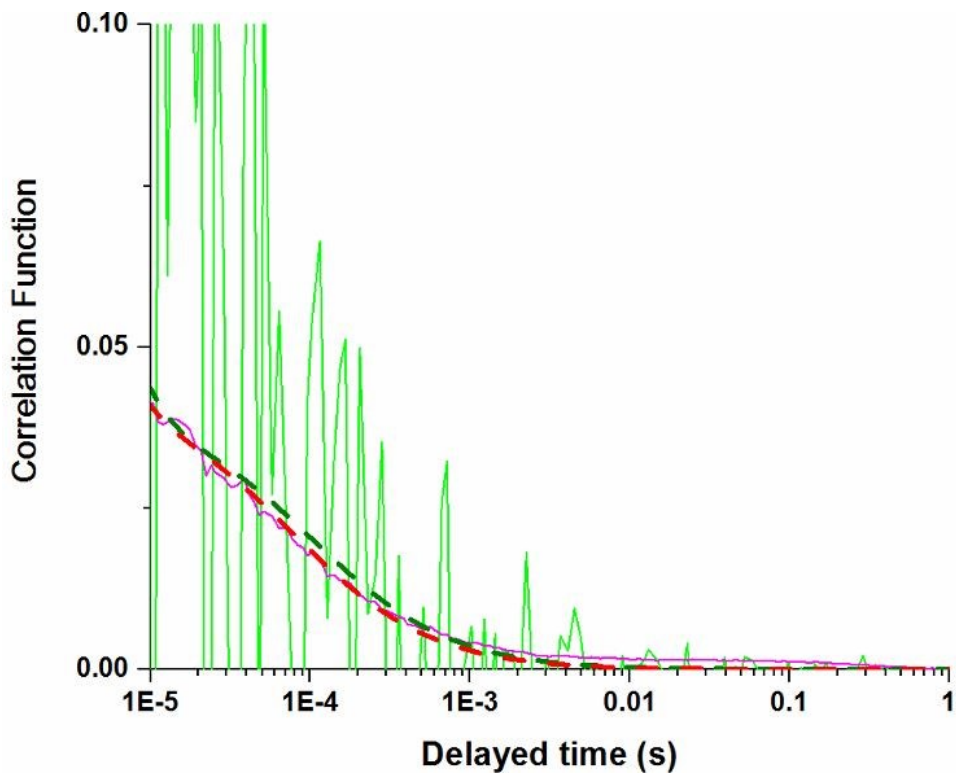


Figure 11: Autocorrelation function and corresponding fitting curves (dashed lines) of Cy5 excited by 488 nm (green) and 633 nm (red), respectively.

To check whether the red and green laser beams used in my research overlapped, 100 nM Cy5 in water (provided by Dr. Xuejun Sun from Cross Cancer Institution) was first excited by the red beam (633 nm) and its emission above 650 nm wavelength was detected by the red detector. Then the same sample was excited by the green beam (488 nm) and detected by the same red detector again. As shown in Figure 11, both fitting curves of autocorrelation functions reveal similar amplitude ($G(0)$) and diffusion time (τ_D), which indicated that two lasers illuminate almost the same region. Since 488 nm is on the edge of the excitation spectral profile of Cy5, the emission light of Cy5 excited by 488 nm has low intensity and hence low signal to noise ratio. Therefore, the autocorrelation function of Cy5 excited by 488 nm is very noisy.

Calibration Measurement Two. To ensure that red and green detection volumes were well overlapped, Rhodamine 6G was excited at 488 nm and its emission from 505 to 550 nm was recorded by the green detector and that above 650 nm was detected by the red detector. Rhodamine 6G has a very broad emission spectrum ranging from 500 to 700 nm. Therefore, the concentration of Rhodamine 6G, together with the amplitude of the correlation function, measured by both detection wavelength should be the same. Figure 12 shows the autocorrelation curves and the cross correlation curves of Rhodamine 6G, as well as their fitting curves. In Table 6, the amplitudes of two autocorrelation functions and the cross correlation function are summarized, together with the observed number of the fluorescence species within each confocal volume and the diffusion time of Rhodamine 6G measured by fluorescence autocorrelation spectroscopy and

fluorescence cross-correlation spectroscopy (FCCS). In summary, the calibration measurements show an overlap of the two detection volume with the chosen objective with slightly different amplitudes ($G(0)$). There are two phenomena contributing to their difference. First, Rhodamine 6G has different photon efficiencies between 505 ~ 550 nm and 650 nm ~700 nm. Therefore the count rate of the green detector is much stronger than that of the red detector. This causes the slight differences in the amplitudes of the correlation function and their fitting curves. Second, the detection volume of the red laser beam is theoretically larger than that of green laser beam. Since the equatorial radius (w_{xy}) of the confocal volume is theoretically proportional to the wavelength of the laser beam, the red confocal volume is supposed to be larger than the green confocal volume. Therefore, it is reasonable that the observed numbers of the fluorescent species with the red confocal volume is larger than that from the green confocal volume, which agrees with my experimental data as shown in Table 6. Moreover, the cross confocal volume is not exactly the same as the red and the green confocal volume based on Equation (18).

Table 6: $G(0)$, N and τ_D of Rhodamine 6G measured by FCCS.

Channel	Count rate (kHz)	$G(0) \pm$ standard error	$N \pm$ standard error	$\tau_D \pm$ standard error (μs)
Red	6.828	0.0208 ± 0.0006	48 ± 1	$34.8 \pm 3e-6$
Green	61.781	0.02647 ± 0.00006	37.8 ± 0.1	$42.3 \pm 4e-7$
Cross		0.0187 ± 0.0002	53.5 ± 0.6	$46.6 \pm 2e-6$

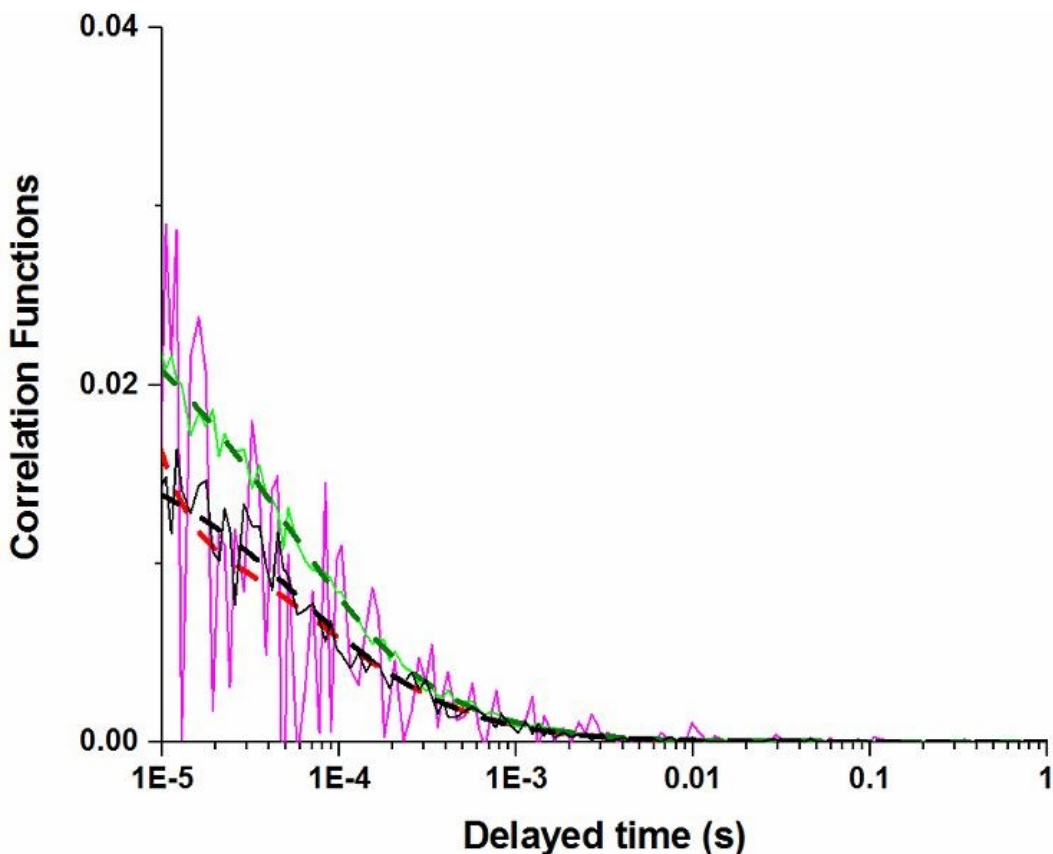


Figure 12: Autocorrelation functions and cross-correlation function of Rhodamine 6G. Red line is the fitting curve of data obtained by the red detector, Green line is from the green detector, Black line is data calculated based on the cross correlation function.

Calibration Measurement Three. To select the proper laser power, the total fluorescence count rates of Alexa Fluor[®] 488 C5-maleimide at different concentrations are plotted as a function of laser power in Figure 13. 0.1% ~ 3% of 25 mW Argon laser was used to excite the sample. The Alexa Fluor[®] 488 C5-maleimide concentration was determined using an Agilent Cary 60 UV/Vis spectrophotometer at $\lambda = 493 \text{ nm}$ with molar absorptivity = $7.0000 \times 10^4 \text{ cm}^{-1}\text{M}^{-1}$. As shown in Figure 13, the black line is for 1.312 nM of the dye, the red is for 656 nM, the green is for 328 nM, and the purple and the blue are 64 nM and 82 nM, respectively. A linear function ($y = ax + b$) was used to fit

the measured spot, and only the lower concentration samples (lower than 328 nM) showed linear fittings between the total count rate and the laser power. Moreover, when laser power was larger than 1%, the higher concentration samples were saturated and their count rates were lower than what was expected. Therefore, 1% of 25 mW Argon laser was chosen for the following experiments as the green laser beam to excite the sample at 488 nm. To ensure the brightness of red laser beam was close to that of the green, 5% of the 5 mW Helium-Neon laser was used as the red laser beam to excite sample at 633 nm.

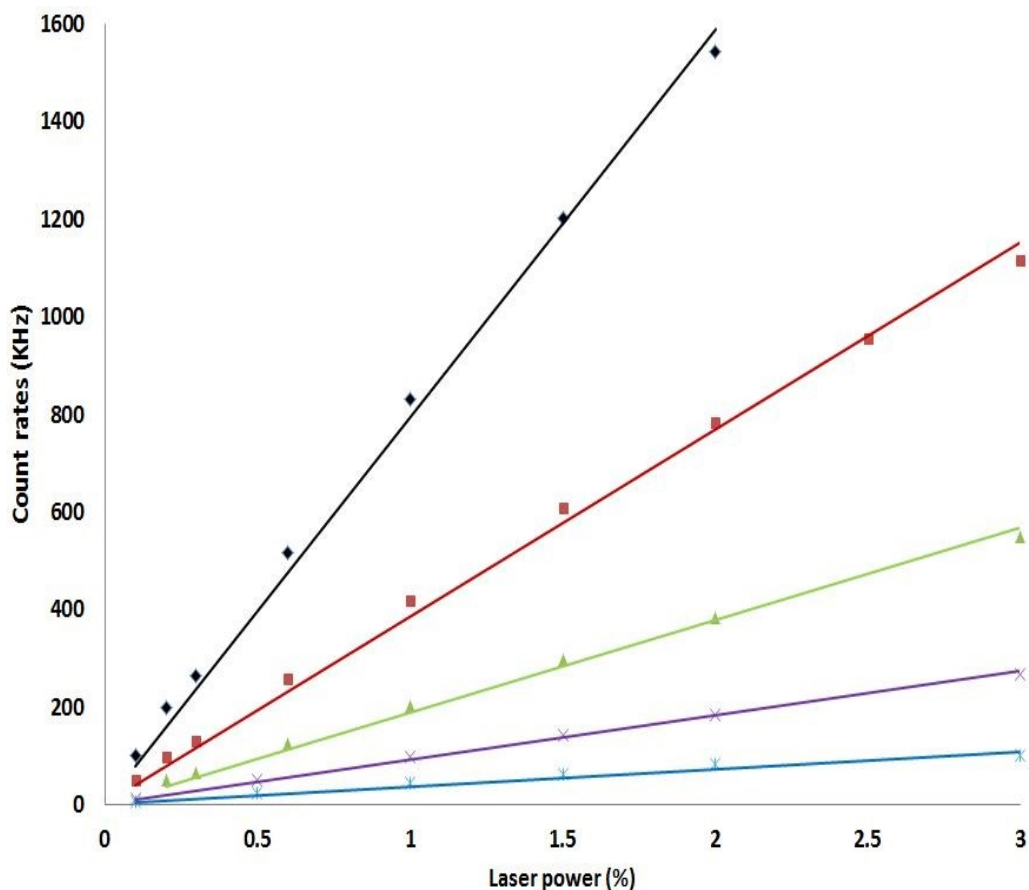


Figure 13: Count rate is a function of laser powers at different concentrations of Alexa Fluor® 488 C5-maleimide. Black is at 1312 nM, Red is at 656 nM, Green is at 328 nM, Purple is at 164 nM and Blue is at 82 nM.

Calibration Measurement Four. Oregon Green[®] 488 maleimide and Cy5 Tetrazine were chosen as the paired dye system in my FCCS experiments. To show that the cross talk of Oregon Green[®] 488 maleimide to the red channel is negligible, E_{GGG} , E_{RRR} , E_{RGG} , and E_{RRG} of one FCCS experiment were summarized in Table 7. E_{GGG} refers to the green channel count rate of Oregon Green[®] 488 maleimide excited by green laser, E_{RRR} refers to the red channel count rate of Cy5 Tetrazine excited by red laser, E_{RGG} refers to the red channel count rate of Oregon Green[®] 488 maleimide excited by green laser and E_{RRG} refers to the red channel count rate of Cy5 Tetrazine excited by green laser. By doing simple calculations, I got the following fractions: $\frac{E_{GGG}}{E_{RRR}} = 0.7$, $\frac{E_{GGG}}{E_{RGG}} = 18.5$, $\frac{E_{RRR}}{E_{RRG}} = 41.6$ and $\frac{E_{RGG}+E_{RRG}+E_{RRR}}{E_{RGG}} = 28.2$, which fulfilled the requirements (refer to Page 51) to ensure that the cross talk of Oregon Green[®] 488 maleimide to the red channel is negligible. This indicates that Cy5 Tetrazine was the only species detected by the red channel.

Table 7: Count Rates of Oregon Green[®] 488 maleimide and Cy5 Tetrazine in FCCS.

	E_{GGG}	E_{RRR}	E_{RGG}	E_{RRG}
Count Rate (KHz)	4.35	6.25	0.235	0.150

Calibration Measurement Five. The diffusion times (τ_D) of Oregon Green[®] 488 maleimide and Cy5 Tetrazine were measured by FCS as shown in Tables 8 and 9. In Table 8, three different concentrations of Oregon Green 488 Maleimide samples dissolved in 10 mM PBS at $pH = 7.40$ were measured at $T =$

298.15 K. Each row of the results including count rate, $G(0)$, N and τ_D obtained from 30 repeat measurements of the same Oregon Green 488 Maleimide sample. The resulting autocorrelation curves were fitted using the single component autocorrelation function, Equation (6) using Igor software. Some suggested fitting parameters were used, such as fit range started at 1 μs and $\frac{w_z}{w_{xy}}$ was equal to 10. The average diffusion time (τ_D) of Oregon Green[®] 488 maleimide in PBS at 298.15 K was determined to be $45.6 \pm 0.2 \mu\text{s}$.

Table 8: Fitting results of Oregon Green 488 maleimide in PBS at pH=7.40 in FCS.

Concentration of Oregon Green 488 Maleimide (nM)	Count rate (kHz)	$G(0)$ \pm standard error	N \pm standard error	τ_D \pm standard error (μs)
-	335	0.0070 ± 0.0002	146 ± 4	52.0 ± 0.1
-	83	0.0320 ± 0.0002	31.3 ± 0.2	40.1 ± 0.1
-	5	0.725 ± 0.005	1.38 ± 0.01	44.9 ± 0.1
Average \pm Standard Error				45.7 ± 0.2

Table 9 summarizes the fitting parameters of two Cy5 tetrazine samples dissolved in 10% of ethanol (by weight) at 298.15 K. Each row of the result including count rate, $G(0)$, N and τ_D obtained from 9 repeat measurements of the same sample. The resulting autocorrelation curves were fitted using the single component autocorrelation function in the defaulted Carl Zeiss software. The fit range started at 1 μs , free triplet state fraction was from 0% to 30%, free triplet time was from 1 μs to 10 μs and $\frac{w_z}{w_{xy}}$ was equal to 10. The average diffusion time (τ_D) of Cy5 tetrazine in 10% of ethanol (by weight) at 298.15 K was determined to be $107 \pm 1 \mu\text{s}$.

Table 9: Fitting results of Cy5 tetrazine in 10% of Ethanol using FCS.

Concentration of Cy5 tetrazine (nM)	Count rate (kHz)	G(0) \pm standard error	N \pm standard error	τ_D \pm standard error (μ s)
-	42.341	0.315 \pm 0.001	3.17 \pm 0.01	106 \pm 1
-	50.555	0.3250 \pm 0.0002	3.077 \pm 0.002	108.7 \pm 0.2
Average \pm Standard Error				107 \pm 1

Calibration Measurement Six – the green confocal volume. Alexa Fluor[®] 488 C5-maleimide was used to estimate the confocal volume of the green laser beam. 5.4 μ M Alexa Fluor[®] 488 C5-maleimide was dissolved with the 10 mM PBS at pH 7.4. The dye concentration was determined using an Agilent Cary 60 UV/Vis spectrophotometer at $\lambda = 493$ nm with absorption = 0.38 and molar absorptivity = 7.0000×10^4 $cm^{-1}M^{-1}$. Then, 5.4 μ M of Alexa Fluor[®] 488 C5-maleimide solution was diluted 10 times to 0.54 μ M, which is the first FCS sample. Next, two-fold serial dilutions were conducted to obtain 0.27 μ M, 0.13 μ M ... and 1.05 nM dye solutions. In Table 10, ten Alexa Fluor[®] 488 C5-maleimide solutions with different concentrations were measured using Laser-scanning microscope LSM 510/ConfoCor 2. Each row of the result including count rate, G(0), N and τ_D were obtained from 12 repeat measurements of the same sample. The resulting autocorrelation curves were fitted using the single component autocorrelation function in the defaulted Carl Zeiss software. The fit range started at 1 μ s, free triplet state fraction was from 0% to 30%, free triplet time was from 1 μ s to 10 μ s and $\frac{w_z}{w_{xy}}$ was equal to 10.

Table 10: Fitting results of Alexa Fluor® 488 C5-maleimide at different concentrations in PBS at pH=7.40 at 298.15 K in FCS.

Sample #	Concentration of Alexa Fluor® 488 (nM)	Count rate (kHz)	G(0) ± standard error	N ± standard error	τ_D ± standard error (μ s)
1	540	274	0.0040±0.0002	260±10	41±4
2	270	136	0.0080±0.0003	124±5	40±4
3	135	66	0.0170±0.0006	60±2	43±4
4	67.5	32	0.0390±0.0008	25±1	35±4
5	33.8	16	0.076±0.003	13.1±1	38±4
6	16.9	8	0.171±0.006	5.9±0.2	33±4
7	8.44	4	0.33±0.01	3.0±0.1	36±3
8	4.22	2	0.51±0.03	2.0±0.1	47±4
9	2.11	1.1	1.0±0.1	1.0±0.1	40±10
10	1.05	0.6	1.56±0.03	0.61±0.01	39±1
Average ± standard error					40 ±10

The estimated confocal volume of the green laser beam was obtained from the plot of N is a function of the concentration of Alexa Fluor® 488 C5-maleimide as shown in Figure 14, since $\frac{N}{c}$ is equal to the slope of the plot. The calculation of the green confocal volume using the slope is shown in Equation (32).

$$V_{eff} = \frac{N}{N_{Ac}} = \frac{(5.4 \pm 0.1) \times 10^8}{6.022 \times 10^{23}} = (8.9 \pm 0.2) \times 10^{-16} L = (0.89 \pm 0.02) fL \quad (32)$$

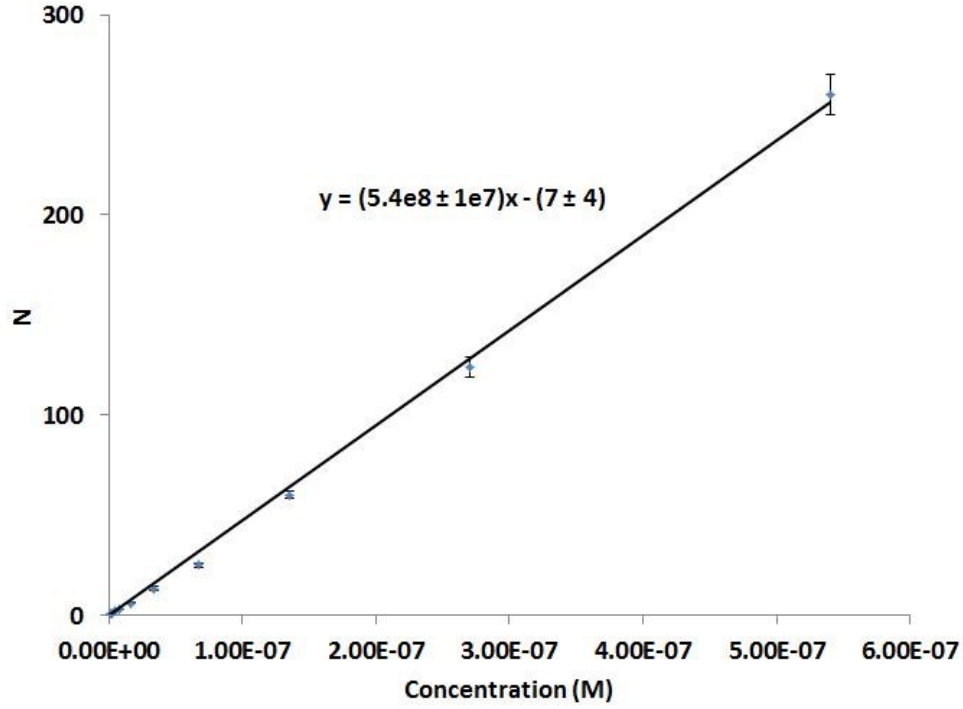


Figure 14: Observed number of fluorescent particles in a confocal volume, N , as a function of the concentrations of Alexa Fluor 488.

The value of the estimated green confocal volume fulfilled the requirement that confocal volume is small enough ($\sim 1 fL$) for observing obvious fluorescence fluctuations during the experiment. Moreover, this value agreed well with the green confocal volume calculated from the measured diffusion time (τ_D) of Alexa Fluor[®] 488 C5-maleimide with its known diffusion coefficient (D) as shown in Equations (33) ~ (35). According to Schwille¹¹⁸, the diffusion coefficient of Alexa Fluor[®] 488 is $435 \mu m^2 s^{-1}$ in water and $430 \mu m^2 s^{-1}$ in 10 mM PBS at 298.15 K.

$$w_{xy_Green} = \sqrt{430 \mu m^2 s^{-1} \times 4 \times (40 \pm 10) \mu s} = (260 \pm 70) nm \quad (33)$$

$$w_{z_Green} = w_{xy} \times 10 = (2600 \pm 700) nm \quad (34)$$

$$V_{eff_Green} = \pi^2 \times (260 \pm 70 \text{ nm})^2 \times (2600 \pm 700 \text{ nm}) = (1.0 \pm 0.4) fL \quad (35)$$

As above, the calculation of the equatorial radius (w_{xy}) of green confocal volume and the confocal volume using the measured diffusion time (τ_D) of Oregon Green 488-maleimide is shown in Equations (36)-(38).

$$w_{xy_Green} = \sqrt{409 \mu m^2 s^{-1} \times 4 \times (45.6 \pm 0.2) \mu s} = (273 \pm 1) nm \quad (36)$$

$$w_{z_Green} = w_{xy} \times 10 = (2730 \pm 10) nm \quad (37)$$

$$V_{eff_Green} = \pi^2 \times (273 \pm 1 \text{ nm})^2 \times (2730 \pm 10 \text{ nm}) = (1.135 \pm 0.009) fL \quad (38)$$

To determine whether the above three values are statistically the same, t-test was applied as shown in Equations (39) and (40).

$$t_{calc} = \frac{|\bar{x}_1 - \bar{x}_2|}{S_{pooled}} \sqrt{\frac{n_1 n_2}{n_1 + n_2}} \quad (39)$$

$$S_{pooled} = \sqrt{\frac{S_1^2(n_1 - 1) + S_2^2(n_2 - 1)}{n_1 + n_2 - 2}} \quad (40)$$

where \bar{x}_1 and \bar{x}_2 are the two means of interest, and n_1 and n_2 corresponds to the number of experiments to obtain \bar{x}_1 and \bar{x}_2 , respectively. S_1 and S_2 are the corresponding standard deviations.

Table 11 summarized the values of S_{pooled} , t_{calc} , degrees of freedom (df) and t_{table} for comparing the values from Equations (32), (35) and (38) by using t-tests. To sum up, the confocal volume calculated based on the measured diffusion time (τ_D) of Alexa Fluor[®] 488 C5-maleimide and those from the plot of N as a

function of the concentrations of Alexa Fluor[®] 488 C5-maleimide are statistically the same within the 95% confidence level, since t_{calc} , which is 0.26, is smaller than t_{table} , which is 2.101. However, the confocal volume calculated based on the measured diffusion time (τ_D) of Oregon Green 488 maleimide and those from the plot of N as a function of the concentrations of Alexa Fluor[®] 488 C5-maleimide are statistically different within the 95% confidence level. This may be due to the errors created from conversion of diffusion coefficient (D) of the dye in water to 10 mM PBS. In the further research, (273 ± 1) nm will be used as the equatorial radius (w_{xy}) of the green confocal volume and $(1.135 \pm 0.009) fL$ will be used as the green confocal volume.

Table 11: t-Tests for comparing two independent values.

	S_{pooled}	t_{calc}	df	t_{table}
0.89 ± 0.02 vs. 1.0 ± 0.4	0.9	0.26	18	2.101
1.0 ± 0.4 vs. 1.135 ± 0.009	1	0.15	11	2.201
1.135 ± 0.009 vs. 0.89 ± 0.02	0.06	5.4	11	2.201

Calibration Measurement Six – the red confocal volume. Cy5 tetrazine was used to estimate the confocal volume of the red laser beam by using its measured diffusion time ($\tau_D = 107 \pm 1$) in 10% ethanol (by weight), together with the corresponding diffusion coefficient (D). Since the diffusion coefficient of Cy5 in

10% ethanol could not be found in references, it was calculated from the diffusion coefficient of Cy5 in water at 298.15 K using the Stokes-Einstein equation, Equation (11), with the assumption that hydrodynamic radius of Cy5 was constant in both water and 10% ethanol at 298.15 K. In addition, the viscosity of 10% of ethanol at 298.15 K was required. It was obtained by fitting the known viscosity 10% of ethanol at other different temperatures with a double exponential function.

Table 12: Viscosity of 10% ethanol (by weight) at different temperatures.¹¹⁹

Temp. (K)	273.15	283.15	293.15	303.15	313.15	323.15	333.15	343.15	353.15
Viscosity (mPa·s)	3.311	2.179	1.538	1.16	0.907	0.734	0.609	0.514	0.43

Table 12 shows the viscosity of 10% ethanol (by weight) under different temperatures¹¹⁹, which unfortunately does not include the viscosity at 298.15 K. Hence, a double exponential function with offsets, Equation (41), was used to fit these data to obtain the viscosity at 298.15 K.

$$y = y_0 + A_1 e^{\left(\frac{x_0 - x}{\tau_1}\right)} + A_2 e^{\left(\frac{x_0 - x}{\tau_2}\right)} \quad (41)$$

In Figure 15, the red dashed line is based on the referenced data and the blue line is the fitting curve. The two double exponential function with $y_0 = 0.12 \pm 0.09$, $A_1 = 1.5 \pm 0.3$, $\tau_1 = 13 \pm 1$, $A_2 = 1.7 \pm 0.2$, and $\tau_2 = 50 \pm 10$ fitted quite well with the reference data. Therefore, from the fitting curve, the viscosity of 10% ethanol (by weight) at 298.15 K was determined to be 1.340 mPa·s.

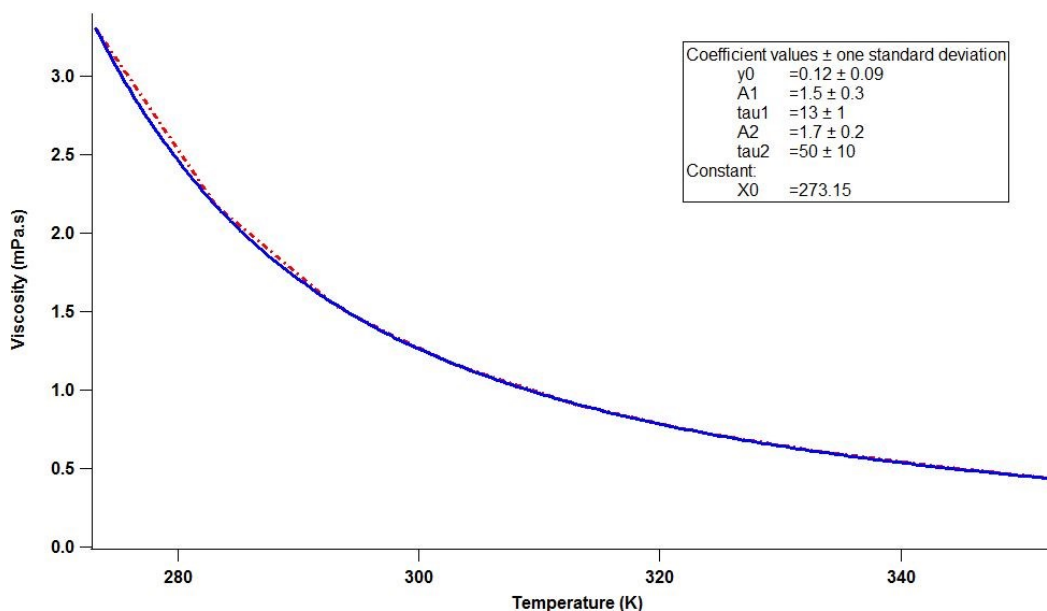


Figure 15: Viscosity of 10% ethanol as a function of temperature.

Table 13: Viscosity of water, 10 mM PBS and 10% Ethanol at 298.15 K.

	Water	10 mM PBS	10% of Ethanol
Viscosity at 298.15K (mPa·s)	0.890*	0.900**	1.340***

*from reference.¹²⁰

**from reference.¹²¹

***from the above fitting by using Equation (30).

Table 13 summarizes the viscosity of water, 10 mM PBS and 10% of ethanol (by weight) at 298.15 K. These data allowed me to calculate the diffusion coefficients of the dyes of interest in 10 mM PBS or in 10% of ethanol at 298.15 K.

The calculated diffusion coefficients under specific conditions are summarized in Table 14. As we can see, the diffusion time of Cy5 tetrazine in 10 mM PBS at 298.15 K was expected to be $72 \pm 0.7 \mu\text{s}$ and the corresponding diffusion coefficient was expected to be $356 \mu\text{m}^2\text{s}^{-1}$. Equations (42)-(44) show the calculation of the red confocal volume. In my further research, $(320 \pm 3) \text{ nm}$ will

be used as the equatorial radius (w_{xy}) of red confocal volume and $(1.82 \pm 0.03) fL$ will be used as the red confocal volume.

$$w_{xy_Red} = \sqrt{356 \mu\text{m}^2\text{s}^{-1} \times 4 \times (72 \pm 0.7) \mu\text{s}} = (320 \pm 3) \text{nm} \quad (42)$$

$$w_{z_Red} = w_{xy} \times 10 = (3200 \pm 30) \text{nm} \quad (43)$$

$$V_{eff_Red} = \pi^{\frac{3}{2}} \times (320 \pm 3 \text{ nm})^2 \times (3200 \pm 30 \text{ nm}) = (1.82 \pm 0.03) fL \quad (44)$$

Table 14: Calculated diffusion coefficients (D) and diffusion times (τ_D) of different dyes in water, 10 mM PBS and 10% Ethanol at 298.15 K

Dyes	Referenced D in water ($\mu\text{m}^2\text{s}^{-1}$)	Calculated D in PBS ($\mu\text{m}^2\text{s}^{-1}$)	Calculated D in 10% Ethanol ($\mu\text{m}^2\text{s}^{-1}$)	τ_D in PBS (μs)	τ_D in Ethanol (μs)
Alexa Fluor [®] 488 maleimide	435*	430	-	40 ± 10 ***	-
Oregon Green [®] 488 maleimide	414**	409	-	45.6 ± 0.2 ***	-
Cy5 Tetrazine	360**	356	239	72 ± 0.7 ****	107 ± 1 ***

*from reference.¹¹⁸

**from reference.¹²²

***from my FCS experiments.

****calculated based on Equation (10).

Calibration Measurement Six – the cross confocal volume. The estimated cross confocal volume in the future research will be $(1.49 \pm 0.01) fL$ as shown in Equation (45).

$$V_{eff_Cross} = \left(\frac{\pi}{2}\right)^{\frac{3}{2}} [(273 \pm 1 \text{ nm})^2 + (320 \pm 3 \text{ nm})^2][(2730 \pm 10 \text{ nm})^2 + (3200 \pm 30 \text{ nm})^2]^{\frac{1}{2}} = (1.49 \pm 0.01) fL \quad (45)$$

3.5.2 Hydrodynamic diameters of α -synucleins by FCS

Sample preparations and method. Samples used in this section are monomeric α -synucleins and the engineered dimers, tetramers and octamers with C-terminal Cysteine labelled with Oregon Green 488 maleimide or Cy5-tetrazine based on the sulfhydryl maleimide Reaction Two or Trans-cyclooctenes (TCO) Tetrazine Reaction. Each sample was measured at the nanomolar concentration and has more than 50 times of repeat measurements. Each resulting autocorrelation curve was fitted by the two component autocorrelation function in the defaulted Carl Zeiss software with suggested fitting parameters. The diffusion time of Oregon Green 488 maleimide was 45.6 μ s, the diffusion time of Cy5 tetrazine was 72 μ s, the fit range started at 1 μ s, free triplet state fraction was from 0% to 30%, free triplet time was from 1 μ s to 10 μ s and $\frac{w_z}{w_{xy}}$ was equal to 10. All diffusion coefficients were calculated using Equation (10) with $w_{xy_green} = 273$ nm and $w_{xy_red} = 320$ nm, respectively. All hydrodynamic diameters were calculated using Equation (11) with T = 298.15 K and viscosity of 10 mM of PBS = 0.00090 Pa·s.

3.5.3 Aggregation tests by FCS

Sample preparations and method. In this section, only monomeric α -synucleins, the engineered tetramers and Alexa Flour 488 C5 maleimide were ready for the experiments. Therefore, both proteins were labelled with Alexa Flour 488 C5 maleimide by using the corresponding labelling protocol.

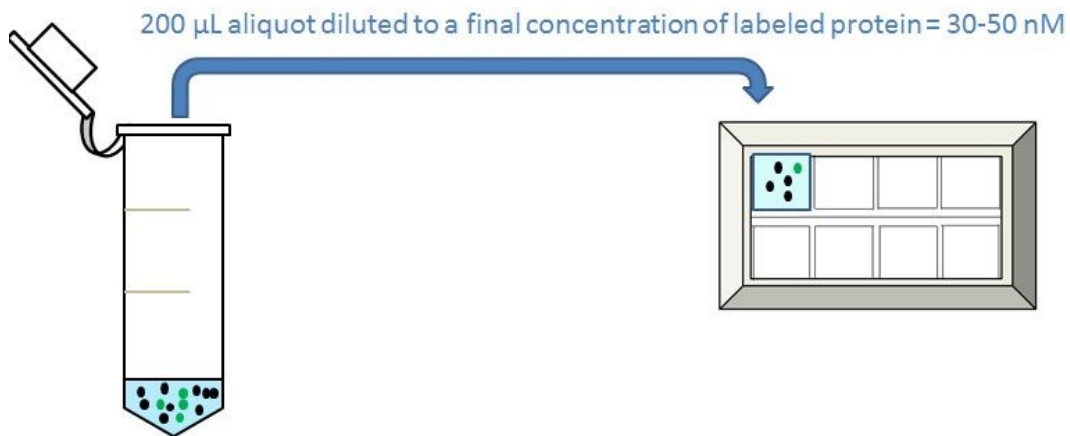


Figure 16: Scheme of the aggregation tests by using FCS.

In Figure 16, the labelled α -synuclein of one kind was mixed with unlabelled α -synuclein as the initial samples used in the experiment. Next, the mixture was incubated at 310.15 K with continuous shaking at 250 rpm. 200 μ L aliquot were taken out from the mixture at specific incubation time as indicated below, starting from $t = 0$ hour. Aliquots were rapidly diluted 1~2 folds, so that the final labelled protein concentration was 30~50 nM. Then, each diluted sample of Figure 32 had 12 repeated measurements and each sample of Figure 33 had more than 70 repeated measurements at 298.15 K using the laser-scanning microscope LSM 510/ConfoCor 2. The resulting autocorrelation curves were fitted using the two-component autocorrelation function in the defaulted Carl Zeiss software with suggested fitting parameters including: diffusion time of Alexa Fluor 488 C5 maleimide as 40 μ s, the fit range started at 1 μ s, free triplet state fraction was from 0% to 30%, free triplet time was from 1 μ s to 10 μ s; and $\frac{w_z}{w_{xy}}$ was equal to 10.

3.5.4 Aggregation tests by dual-color FCCS.

Sample preparations. Large amounts of the monomeric or the engineered dimeric, tetrameric and octameric α -synucleins were labelled with Oregon Green 488-maleimide and Cy5 tetrazine, respectively. Each of my labelled α -synuclein samples has the same monomer concentration (7.75 mg/mL) at the initial incubation time. For example, 536 μ M of labelled monomeric α -synucleins and 67 μ M of labelled octameric α -synucleins were considered as having the same monomer concentration.

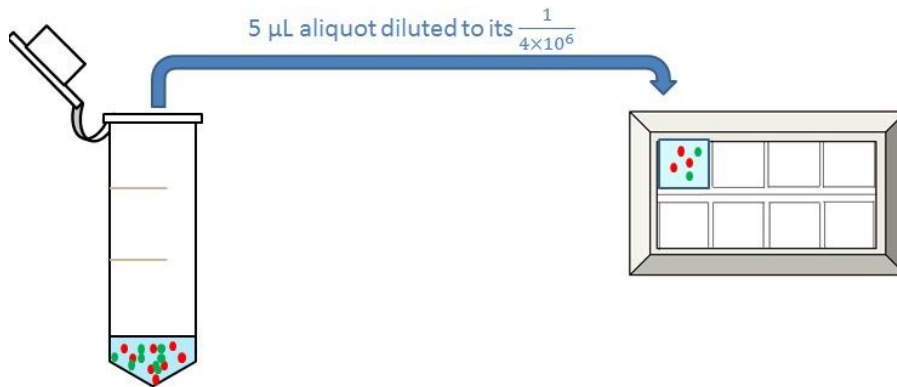


Figure 17: Scheme of the aggregation tests using dual-color FCCS.

In Figure 17, 125 μ L of one kind of α -synuclein labelled with Cy5 tetrazine (the red species) were mixed with 125 μ L of another kind of α -synuclein labelled with Oregon Green 488 maleimide (the green species) as initial samples used in FCCS. Next, the mixture was incubated at 310.15 K with continuous shaking at 250 rpm to initiate the aggregation process. 5 μ L aliquots were taken out from the mixture every one hour, starting at $t = 0$ hour, and were rapidly diluted with 10 mM PBS at $\text{pH} = 7.4$ by a factor of 2.5×10^{-5} to a final concentration of ~ 134 pM. The diluted sample was immediately measured by FCCS at 298.15 K using the laser-

scanning microscope LSM 510/ConfoCor 2 for 50 repeat measurements. The resulting cross-correlation curve was fitted by the single component correlation function and the two autocorrelation curves were fitted by the two component autocorrelation function in the defaulted Carl Zeiss software with suggested fitting parameters including diffusion time of Oregon Green 488 maleimide of 45.6 μs and diffusion time of Cy5 tetrazine of 72 μs . The fit range, free triplet state fraction, free triplet time and $\frac{w_z}{w_{xy}}$ were set the same as those of the calibration experiments.

Table 15: Codes and repeated times of all dual-color FCCS experiments.

	Snca1_Cys_OR M488 (536 μM)	Snca2_Cys_OR M488 (268 μM)	Snca4_Cys_OR M488 (134 μM)	Snca8_Cys_OR M488 (67 μM)
Snca1_Cys_ TMP_Cy5 (536 μM)	FCCS 11 (Repeat 4 times)	FCCS 12 (Repeat 3 times)	FCCS 14 (Repeat 3 times)	FCCS 18 (Repeat 4 times)
Snca2_Cys_ TMP_Cy5 (268 μM)	FCCS 21 (Repeat 2 times)	FCCS 22 (Repeat 2 times)	-	-
Snca4_Cys_ TMP_Cy5 (134 μM)	FCCS 41 (Repeat 4 times)	-	FCCS 44 (Repeat 4 times)	-
Snca8_Cys_ TMP_Cy5 (67 μM)	FCCS 81 (Repeat 4 times)	-	-	FCCS 88 (Repeat 2 times)

Table 15 summarizes the codes of each FCCS experiment and the number of repeat measurements. In this table, Snca1_ORM488 and Snca1_Cy5 were the abbreviations for monomeric α -synucleins labelled with Oregon Green 488-maleimide and Cy5 tetrazine, respectively. Similar abbreviations were also used for the rest of the labelled proteins. Each FCCS experiment shown below has a

name in the format of “FCCS xx”, the first digits of which indicates the type of α -synuclein labelled with Cy5 tetrazine. For example, the FCCS experiment was called “FCCS 41”, when tetrameric α -synuclein with Cy5 tetrazine and monomeric α -synucleins with Oregon Green 488-maleimide were the initial red and green species.

Finally, in order to understand whether continuous shaking could affect the aggregation process, 125 μ L of octameric α -synuclein (67 μ M) labelled with Cy5 tetrazine were mixed with 125 μ L of octameric α -synuclein (67 μ M) labelled with Oregon Green 488 maleimide (the green species), and then it was incubated of 310.15 K without shaking as a control group. Each controlled experiment of the same sample was measured for 50 times and each control group with newly made sample was repeated one more time.

Data analysis. Equations (46) and (47) were obtained after rearrange of Equation (17).

$$\frac{N_{rg}}{N_r} = \frac{G_{rg}(0)}{G_g(0)} \quad (46)$$

$$\frac{N_{rg}}{N_g} = \frac{G_{rg}(0)}{G_r(0)} \quad (47)$$

where N_{rg} is the absolute number of fluorescent aggregates observed within the cross confocal volume, N_r is the absolute number of red fluorescent species observed within the red confocal volume and N_g is the absolute number of green fluorescent species observed within the green confocal volume. The physical

meaning of $\frac{N_{rg}}{N_r}$ refers as the fraction of red fluorescent species which were used to form conjugates. It is advantageous to present FCCS data in the format $\frac{N_{rg}}{N_r}$ instead of using the absolute number. Dilution of a very small amount of aliquot (5 μ L) caused large errors between the absolute numbers of fluorescent species observed under confocal volume (N) at different incubation times for each FCCS experiment. Presenting FCCS data as $\frac{N_{rg}}{N_r}$ or $\frac{N_{rg}}{N_g}$ solves the problem. Considering the slight difference between the red, green and cross confocal volumes, $\langle n_r \rangle$, $\langle n_g \rangle$ and $\langle n_{rg} \rangle$ were used to correct for the different confocal volume as shown in Equations (48) and (49).

$$\frac{\langle n_{rg} \rangle}{\langle n_r \rangle} = \frac{G_{rg}(0)}{G_g(0)} \times \frac{V_{eff_Red}}{V_{eff_Cross}} = \frac{G_{rg}(0)}{G_g(0)} \times \frac{1.82}{1.49} \times 100\% \quad (48)$$

$$\frac{\langle n_{rg} \rangle}{\langle n_g \rangle} = \frac{G_{rg}(0)}{G_r(0)} \times \frac{V_{eff_Green}}{V_{eff_Cross}} = \frac{G_{rg}(0)}{G_r(0)} \times \frac{1.135}{1.49} \times 100\% \quad (49)$$

The final FCCS aggregation data was represented as a plot of $\frac{\langle n_{rg} \rangle}{\langle n_r \rangle}$ or $\frac{\langle n_{rg} \rangle}{\langle n_g \rangle}$ as a function of the incubation time. Then an exponential growth function, Equation (50), was used to fit the plot.

$$y = y_0 + A \times (1 - e^{(-x \cdot k)}) \quad (50)$$

From the fitting curves, two important values were obtained: (i) the amplitude of the fitting curve, A , which gives the difference between the start-point and endpoint of each aggregation test; and (ii) the parameter, k , which is the

reciprocal of the growth time. The growth time is defined as the time to reach $\frac{1}{e}$ of the final value.

Chapter 4: Results and Discussions

The objective of this research is to establish a generic approach to study the aggregation between engineered α -synuclein oligomers and monomers using dual-color FCCS. To do this, several experiments are conducted. These experiments include: (i) properly labelling of the protein of interest; (ii) efficiently purifying the labelled protein; (iii) ensuring the quantum yields of fluorescent dyes keep constant once they are mixed with or bind to the protein of interest; (iv) measuring the initial hydrodynamic size of the protein of interest before aggregation by DLS; (v) validating the initial hydrodynamic size of the protein by FCS; and (vi) monitoring the aggregation process between the engineer α -synuclein oligomers and monomer by both FCS and dual-color FCCS. All experimental results are summarized in this Chapter.

4.1 Purification and labelling efficiency

4.1.1 Distinguishing non-specific binding from covalent labelling

Results. To ensure that unconjugated dye and protein were baseline-separated, each FPLC purification experiment was conducted with three control samples: (i) the dye; (ii) the α -synuclein before labelling; and (iii) the mixture of unlabelled α -synuclein and the dye.

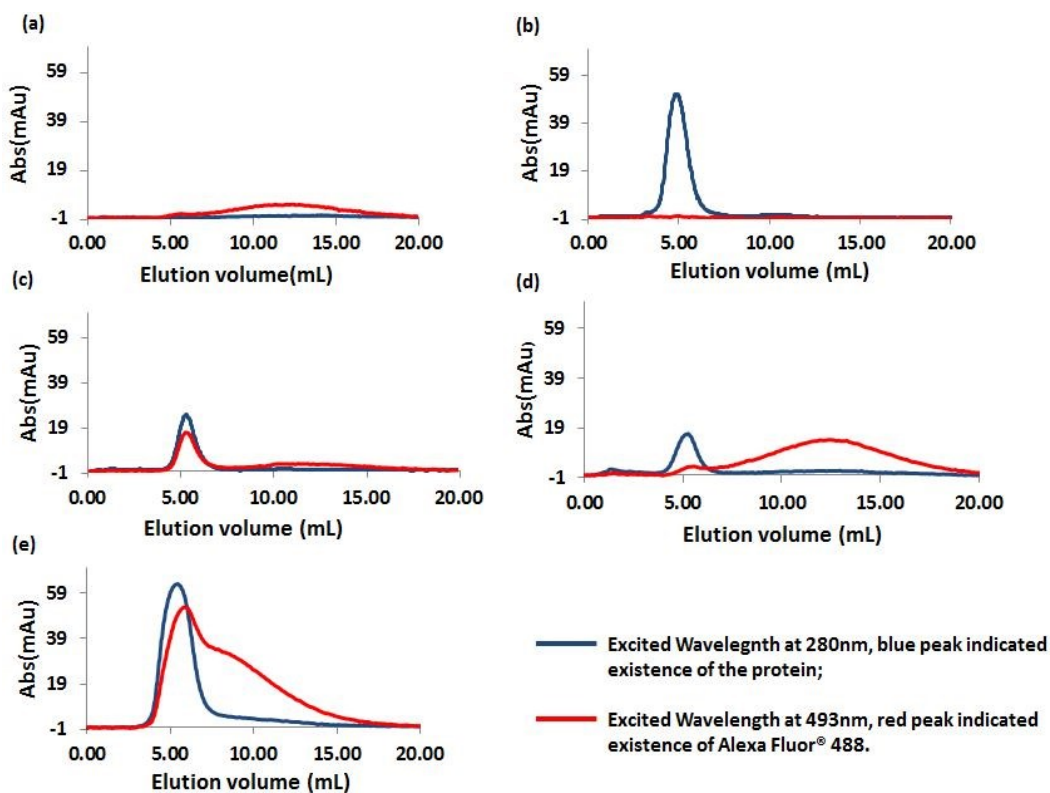


Figure 18: Comparison of FPLC elution profiles for Alexa Fluor® 488 C5-Maleimide and Snca1. (a) Alexa Fluor® 488 at pH 7.40, (b) Snca1 at pH 7.40, (c) Non-reacted the dye and Snca 1 at pH 7.40, (d) Non-reacted dye and Snca 1 at pH 4.68 and (e) Snca1_alex Fluor® 488 C5-Maleimide .

Figure 18 summarizes the FPLC elution profiles of samples containing Alexa Fluor® 488 C5 Maleimide and/or monomeric α -synuclein (Snca1). In Figure 18 (a), 3 μ M of Alexa Fluor® 488 C5 Maleimide at pH 7.40, 1 mL, was loaded into the desalting column, and eluted within 5 to 20 mL as shown by a broad peak. In Figure 18 (b), 0.4 mg/mL of Snca1 at pH 7.40, 1 mL, was loaded into the desalting column. Snca1 always eluted earlier than the dye (from 3 to 7 mL), because the protein has a larger hydrodynamic size so that it will not diffuse inside of the pores of stacking particles. In Figure 18 (c), 1 mL of a mixture of 0.4 mg/mL of Snca1 (168 μ M) and 3 μ M of Alexa Fluor® 488 C5 Maleimide at pH 7.40 without initiating the labelling reaction was loaded into the desalting column.

Both the dye and the protein eluted out at the same time, as indicated by the overlap of peaks measured at 493 and 280 nm. This figure demonstrated that Alexa Fluor 488 non-specifically bind to Snca1 at pH 7.40. Figure 18 (d) used the exact same samples as that of Figure 18 (c), except that elution buffer was controlled at lower pH (pH = 4.68). The protein and the dye were able to be separated and the protein eluted earlier than the dye. In Figure 18 (e), the loaded sample was 1 mL of monomeric α -synuclein (2.7 mg/mL) labelled with Alexa Fluor[®] 488 C5-Maleimide following the sulfhydryl maleimide labelling Method One. The dye and the protein eluted at the same time. To sum up, Alexa Fluor[®] 488 C5 Maleimide was not a suitable dye for labelling α -synuclein, because it bound non-specifically to the protein at pH = 7.40 (Figure 18 (c)) and could not be baseline-separated from the protein using the desalting column.

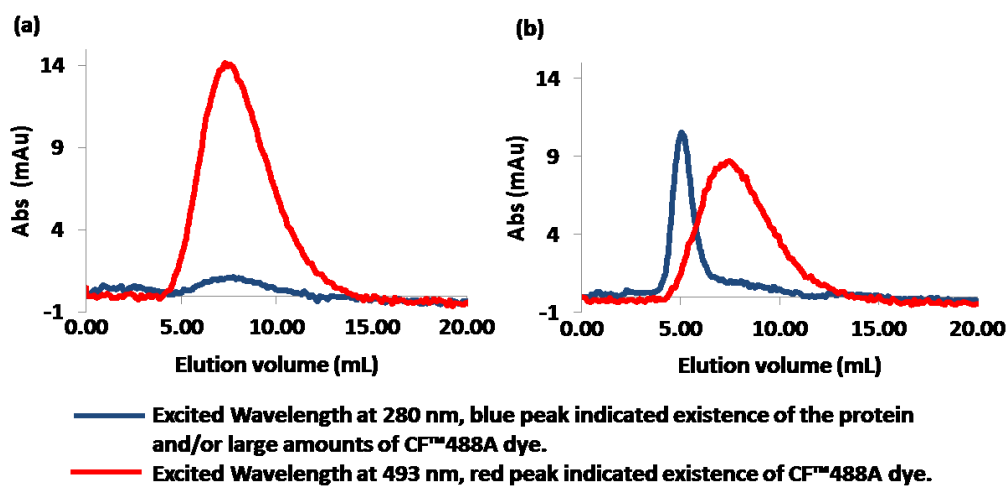


Figure 19: Comparison of FPLC elution profiles for CF[™] 488A Dye and α -synuclein. (a) CF[™] 488A Dye, and (b) Snca1 mixed with CF[™] 488A Dye without labelling reaction.

Figure 19 summarizes the FPLC elution profiles of samples containing CF[™] 488A Dye and/or monomeric α -synuclein (Snca 1). In Figure 19 (a), 5 μ M of

CFTM 488A Dye at pH 7.40, 1 mL, was loaded to the desalting column. CFTM 488A Dye eluted out at 4 mL ~ 15 mL with both absorbance at 280 nm and 493 nm. In Figure 19 (b), 1 mL of the mixture of 0.3 mg/mL of monomeric α -synuclein (126 μ M) and 3 μ M of CFTM 488A Dye at pH 7.40 without labelling reaction were loaded, the protein and the dye could not be completely separated using the desalting column.

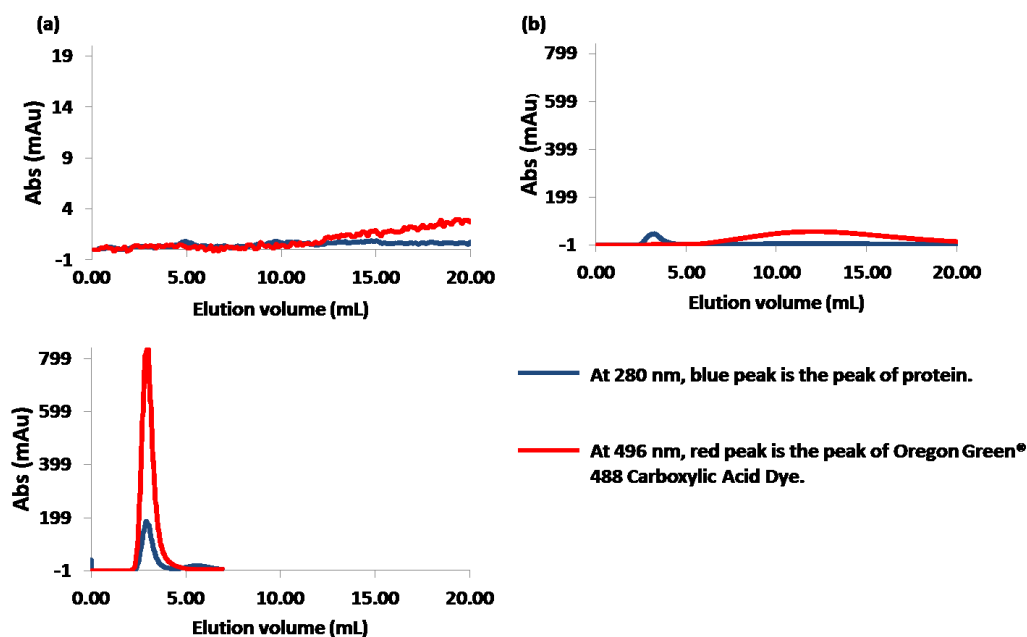


Figure 20: Comparison of FPLC elution profiles for Oregon Green® 488 Carboxylic Acid Succinimidyl Ester, 6-isomer dye and α -synuclein. (a) Oregon Green® 488 Carboxylic Acid Dye, (b) The mixture of Snca8 and the dye, and (c) Snca8_ ORNH488.

Figure 20 shows the FPLC elution profiles of samples containing Oregon Green® 488 Carboxylic Acid Succinimidyl Ester, 6-isomer dye and/or octameric α -synuclein (Snca8). In Figure 20 (a), 0.5 μ M of Oregon Green® 488 Carboxylic Acid dye at pH 7.40, 1 mL, was loaded onto the desalting column. It started eluting out at 12 mL, which demonstrated a possibility of being entirely separated

from α -synuclein, since α -synuclein eluted at 3 ~ 4 mL . In Figure 20 (b), 1 mL of the mixture of 1.5 mg/mL of Snca8 and 66 μ M of Oregon Green[®] 488 Carboxylic Acid dye at pH 7.40 without labelling reaction were loaded. The protein and the dye were baseline-separated as expected. In Figure 20 (c), 1.5 mg/mL of Snca8 labelled with Oregon Green[®] 488 Carboxylic Acid Dye (Snca8_ORNH488) at pH 7.40 following the Succinimidyl Ester Amine labelling method, 1 mL, was loaded. Its elution volume at 3 ~ 4 mL contained the purified Snca8_Oregon 488 conjugates. To conclude, Oregon Green[®] 488 was an appropriate dye for labelling α -synuclein.

Considering the specific needs of the following FCS experiments, it is the best that each protein is labelled with a single dye. Oregon Green[®] 488 Maleimide was eventually chosen as the best dye for labelling α -synuclein. However, FPLC was not the best purification method in my research, since it is limited to low concentration and low volume of dye.

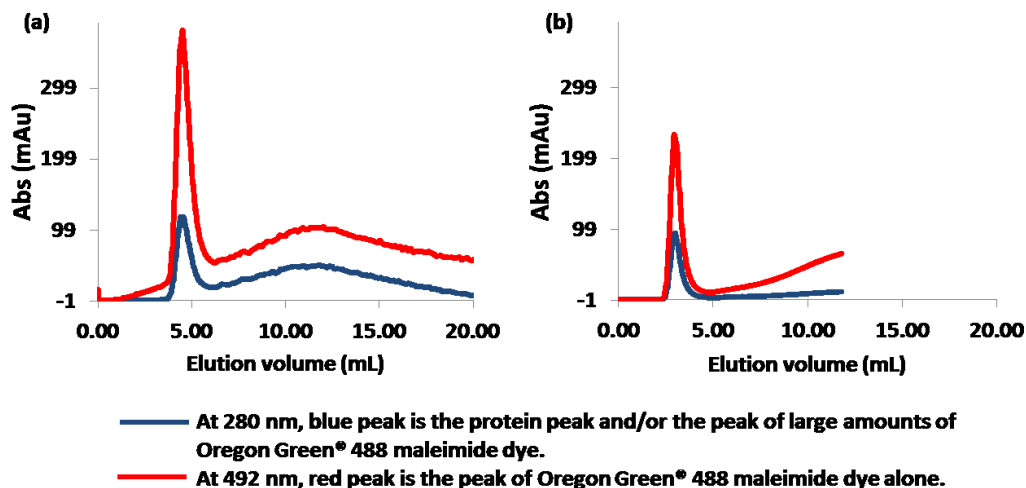


Figure 21: Comparison of FPLC elution profiles for Oregon Green® 488 Maleimide and α -synuclein. (a) Snca4_ORM488 using sulfhydryl maleimide labelling Method One. (b) Snca4_ORM488 using sulfhydryl maleimide labelling Method Two.

Figure 21 demonstrates two FPLC elution profiles of tetrameric α -synuclein labelled with Oregon Green® 488 Maleimide (Snca4_ORM488). In Figure 21 (a), 1 mL of 2 mg/mL Snca4 labelled with Oregon Green® 488 Maleimide Dye at pH 7.40 followed by the sulfhydryl maleimide labelling Method One. Unfortunately, the labelled protein and the free dye could not be completely separated, since peak of the protein and dye slightly overlapped which is due to the large amounts of dye. In Figure 21 (b), the same amounts of protein were labelled with Oregon Green® 488 Maleimide Dye at pH 7.40 followed by the sulfhydryl maleimide labelling Method Two, the labelled protein and the free dye could be completely separated, because less dyes were used for labelling.

Discussion. The results reported above confirm that Alexa Fluor® 488 C5 Maleimide and CFTM 488A Dye bind non-specifically with α -synuclein at pH 7.40 and these cannot be separated from the protein using the desalting column. The

non-specific binding between the dye and α -synuclein is probably due to electrostatic interactions between the charged dyes and the charged α -synuclein. This hypothesis is supported by the result that Alexa Fluor® 488 C5 Maleimide and α -synuclein can be largely separated at low pH, when the charge distributions of α -synuclein are completely changed (anionic Alexa Fluor 488 appears fully ionized within pH 3~10).¹²³ Therefore, Oregon Green® 488 Maleimide, as an uncharged dye, is the best dye for labelling α -synuclein.

The above results also show that FPLC is not the best protein purification method for this protein system. It is able to measure absorbance of each small eluted fraction volume automatically, but it is limited in purifying small quantities of labelled α -synuclein at each sample run. Because higher concentrations of fluorescent dye are required for labelling large quantities of α -synuclein for the future aggregation tests, other purification methods were explored.

4.1.2 High labelling efficiency demonstrated by centrifugal purification

Selected experimental results. Based on the FPLC results, Alexa Fluor® 488 were bound non-specifically with α -synuclein under “physiological” conditions (10 mM PBS at pH = 7.4). Therefore, only Oregon Green 488 maleimide and Cy5 tetrazine were used to label the engineered α -synuclein monomer and oligomers in this section and these labelled proteins were used in subsequent aggregation tests. Some selected results presented below demonstrate how well both dyes conjugated with the protein and that excess dyes could be effectively removed.

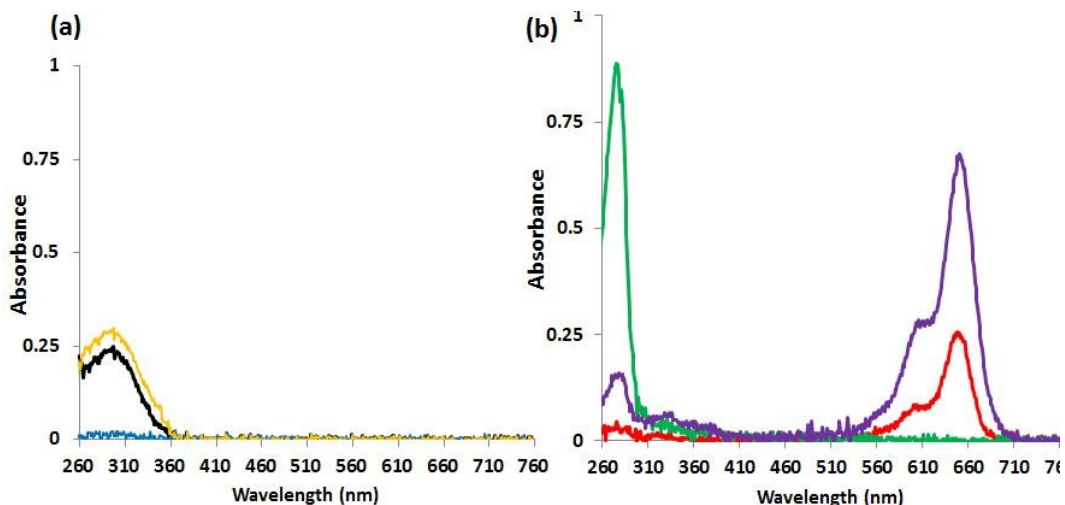


Figure 22: (a) Spectra of TCO-PEG3-Maleimides (TPM) (yellow), the first filtrate volume (black) and the second filtrate volume (blue) from centrifugation of the Snca4 labelled with large amounts of TPM. (b) Spectra of Snca4_TPM (green), spectra of Cy5 tetrazine (red) and spectra of Snca4_TPM_Cy5 (purple).

Figure 22 (a) and (b) display results of coupling the tetrameric α -synuclein (Snca4) and TCO-PEG3-Maleimides (TPM) and then Cy5 tetrazine. As mentioned above, the sulfhydryl-maleimide reaction required a 5-30 fold molar excess of the maleimide reagents for each mole of protein to ensure high labelling efficiency. Therefore, it is very important to remove the excess TPM before Cy5 tetrazine was added to the protein. Figure 22 (a) shows the absorbance spectra of 120 μ M of TPM solution (yellow line), the first filtrate volume (black line) and the second filtrate volume (blue line) of the Snca4 labelled with 10 moles excess of TPM. Comparison between the first and second filtrate volume absorbance spectra revealed that excess TPM was completely removed from the protein solution by two centrifugations with a 10 K Amicon[®] Ultra-15 Centrifugal Filter. The purified Snca4_TPM spectrum is shown in Figure 22 (b) in green. Then, the purified Snca4_TPM was conjugated with the same moles of Cy5-tetrazine and

then purified using another 10 K Amicon[®] Ultra-15 Centrifugal Filter. A 5 μ L aliquot of the final purified Snca4_TPM_Cy5 tetrazine was diluted 5 times. Its absorbance spectrum is shown in Figure 22 (b) in purple. Compared with the spectrum of Cy5 tetrazine solution, the purple spectrum shows successful labelling between Snca4_TPM and Cy5 tetrazine. The labelling efficiency is calculated by Equation (28).^{113,114}

$$\frac{\text{Concentration of dye}}{\text{Concentration of protein}} = \frac{\frac{A(650 \text{ nm})}{\epsilon(\text{Cy5 tetrazine})}}{\frac{[A(280 \text{ nm}) - A(650 \text{ nm}) \times CF]}{\epsilon(\text{Protein})}}$$

$$= \frac{0.66 / (2.50000 \times 10^5 \text{ M}^{-1} \text{ cm}^{-1})}{(0.15 - 0.66 \times 0.08) / (23840 \text{ M}^{-1} \text{ cm}^{-1})} = 0.65 \quad (28)$$

where CF is the correction factor, which is equal to $\frac{A(650 \text{ nm})}{A(280 \text{ nm})}$ for a sample only contained Cy5 tetrazine. Its value is 0.08.¹¹³ Knowing that the volume of tetrameric α -synuclein solution before adding Cy5 was the same as the volume of the final purified sample, the green and the purple spectra yield the retentate recovery of the centrifugal filter as calculated by Equation (29).

$$\text{Retentate recovery} = \frac{A(280) \text{ of labeled protein} \times \text{dilution factor}}{A(280) \text{ of protein before adding dye}}$$

$$= \frac{0.15 \times 5}{0.80} \times 100\% = 97\% \quad (29)$$

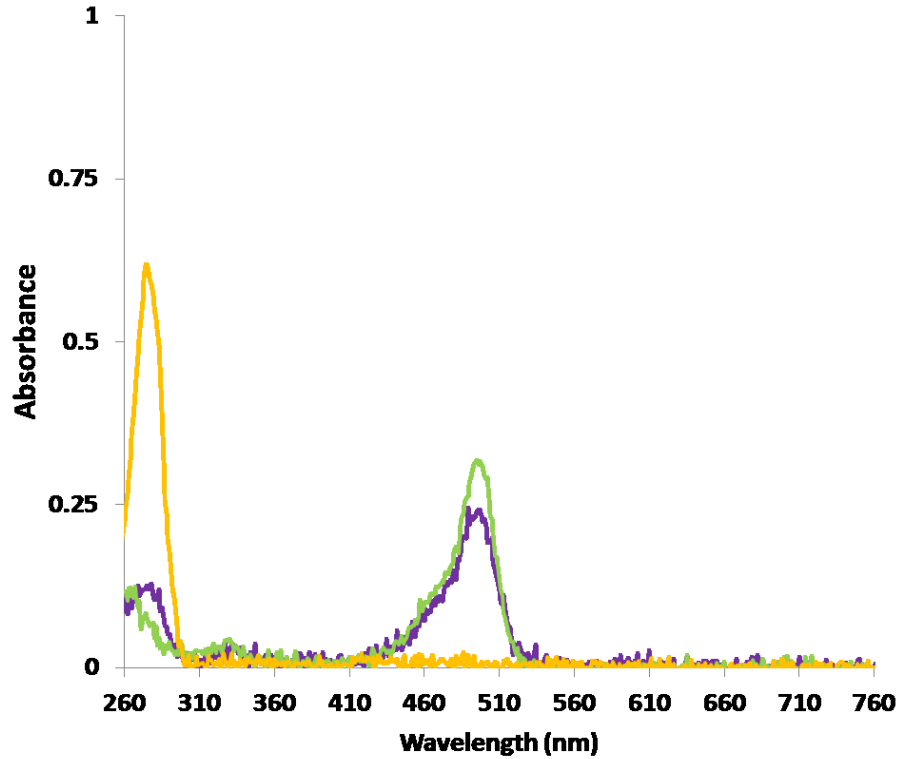


Figure 23: Spectra of Oregon Green 488 maleimide (green), Snca4 before labelling (yellow) and 5 μL of Snca4 ORM488 diluted by 20 times (purple).

Figure 23 demonstrates a removal of excess Oregon Green 488 maleimide from tetrameric α -synuclein (Snca 4) solution by centrifugation. The figure shows the spectra of samples that contained only Oregon Green 488 maleimide (green line), only Snca 4 (yellow line) and of a 5 μL Snca 4 ORM488 aliquot diluted by 20 times (purple line). Comparing the green and the purple spectra at 493 nm and 280 nm, a successful conjugation between tetrameric α -synuclein and Oregon Green 488 maleimide is demonstrated. Its labelling efficiency is calculated by Equation (30).

$$\frac{\text{Concentration of dye}}{\text{Concentration of protein}} = \frac{\frac{A(492 \text{ nm})}{\epsilon(\text{Oregon 488})}}{\frac{[A(280 \text{ nm}) - A(492 \text{ nm}) \times CF]}{\epsilon(\text{Protein})}}$$

$$= \frac{0.23 / (8.7000 \times 10^4 \text{ M}^{-1} \text{ cm}^{-1})}{(0.10 - 0.23 \times 0.12) / (23840 \text{ M}^{-1} \text{ cm}^{-1})} = \mathbf{0.97} \quad (30)$$

Discussion. To sum up, the Amicon[®] Ultra Centrifugal Filters with centrifugation is a faster and cleaner method to remove excess dyes and TPM from the α -synuclein solution, especially when large quantities of protein are labelled. It also shows a very high protein recovery after purification. More importantly, in combination with an Agilent Cary 60 UV/Vis spectrophotometer, only very small aliquots (5 ~ 100 μ L) of final samples are needed to obtain protein concentration and labelling efficiency.

4.1.3 HPLC-MS confirms covalent labelling at high efficiency

Experimental data. Figure 24 is a MS spectrum consisted of both labelled and unlabelled monomeric α -synuclein. The multiple small peaks of one large peak indicate differing numbers of methionine of the protein that were oxidized during the electrospray ionization. Therefore, there always was a mass difference around 16 Da between the nearby peaks arising from an addition of oxygen atom.

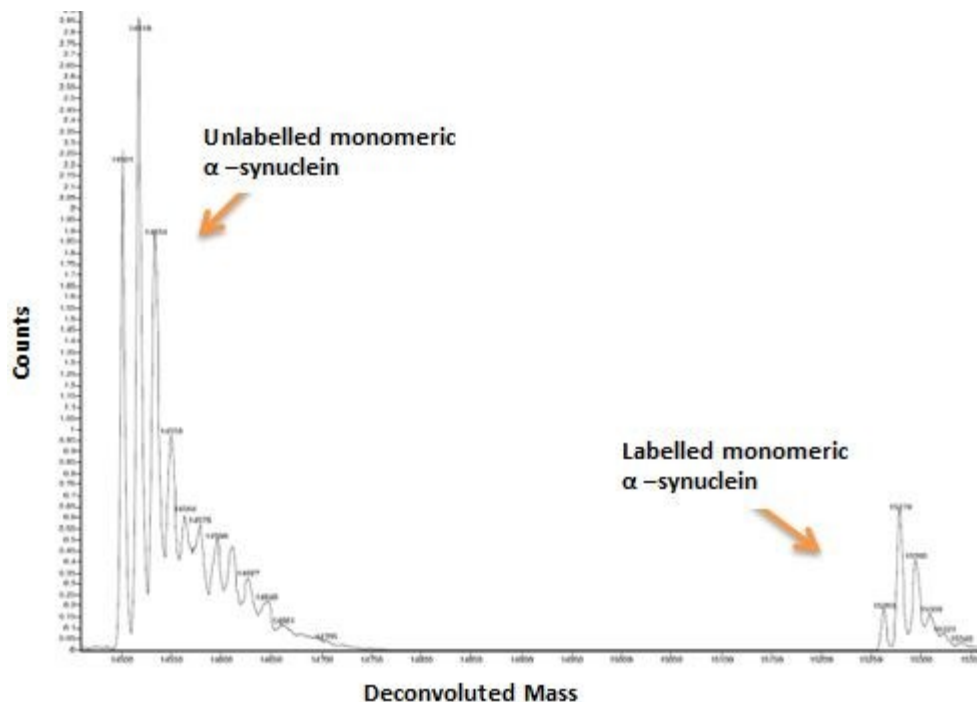


Figure 24: MS spectra for labelled and unlabelled monomeric α -synuclein.

The labelling efficiency was defined as the percentage of the labelled protein versus the total protein in concentration. Based on the counts in Figure 24, about 19% of proteins were labelled in the sample, which agreed well with the results obtained by the labelling efficiency calculation as shown in equation (31).

$$\frac{\text{Concentration of dye}}{\text{Concentration of protein}} = \frac{\frac{A(492 \text{ nm})}{\epsilon(\text{Alexa 488})}}{\frac{[A(280 \text{ nm}) - A(492 \text{ nm}) \times CF]}{\epsilon(\text{Protein})}}$$

$$= \frac{0.090 / (7.3000 \times 10^4 \text{ M}^{-1} \text{ cm}^{-1})}{(0.045 - 0.090 \times 0.11) / 5960 \text{ M}^{-1} \text{ cm}^{-1}} = \mathbf{0.21} \quad (31)$$

4.1.4 HPLC-MS confirms coupling of TPM with α -synuclein

Results. The MS spectra in Figures 25 and 26 confirm the coupling between TPM and α -synuclein monomer and dimer. In Table 16, the molecular masses of Sncax_Cys_TPM were 627 Da heavier than the corresponding mass of the protein

in Table 3. This difference was due to the mass of one cysteine and TPM. To sum up, the MS experimental data match well with the expected data. This shows that the labelling protocol of the sulfhydryl maleimide reaction functioned well.

Table 16: Expected mass and experimental result of Sncax_Cys_TPM.

		Snca1_Cys TPM	Snca2_Cys TPM	Snca4_Cys TPM	Snca8_Cy s TPM
Expected Mass (Da)		15087	29730	59017	117590
MS Mass (Da) with different numbers of oxidized methionines	0	15088	29731	59018	-
	1	15105	29746	-	-
	2	15120	29762	-	-
	3	15137	29778	-	-
	4	15152	29795	59073	-
	5		29812	-	-
	6		29825	-	-
	7		29846	-	-
	8		29859	-	-

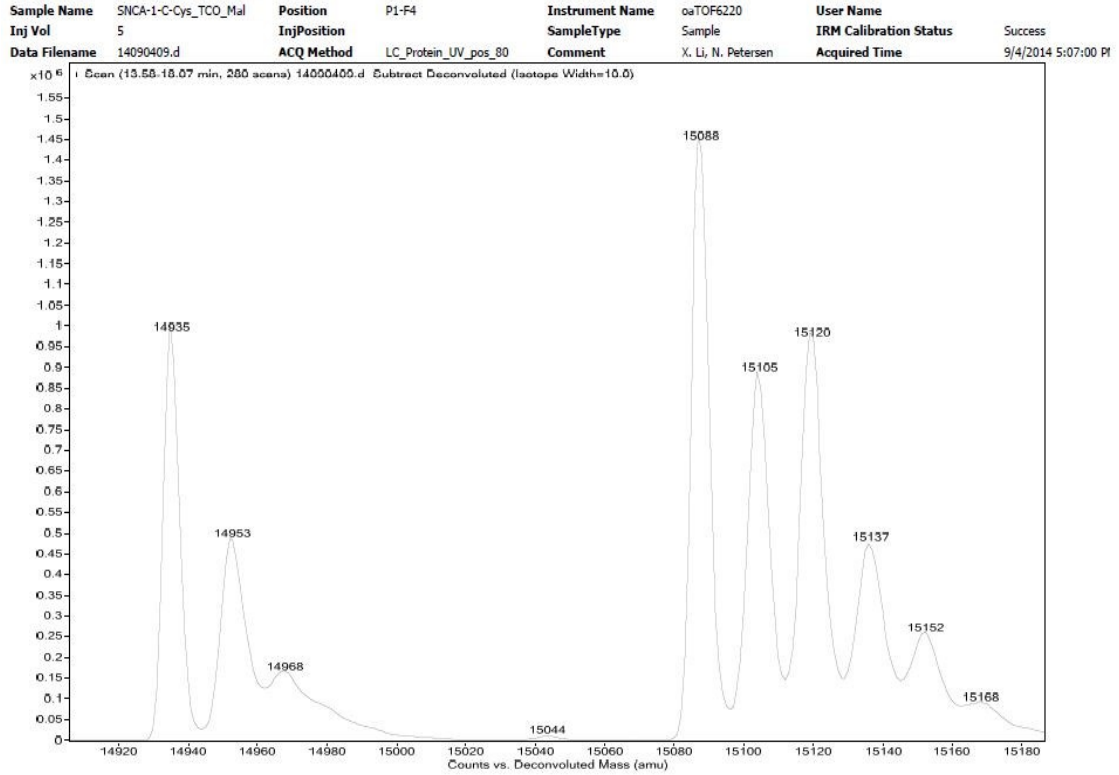


Figure 25: MS spectrum for Sncal_Cys_TPM.

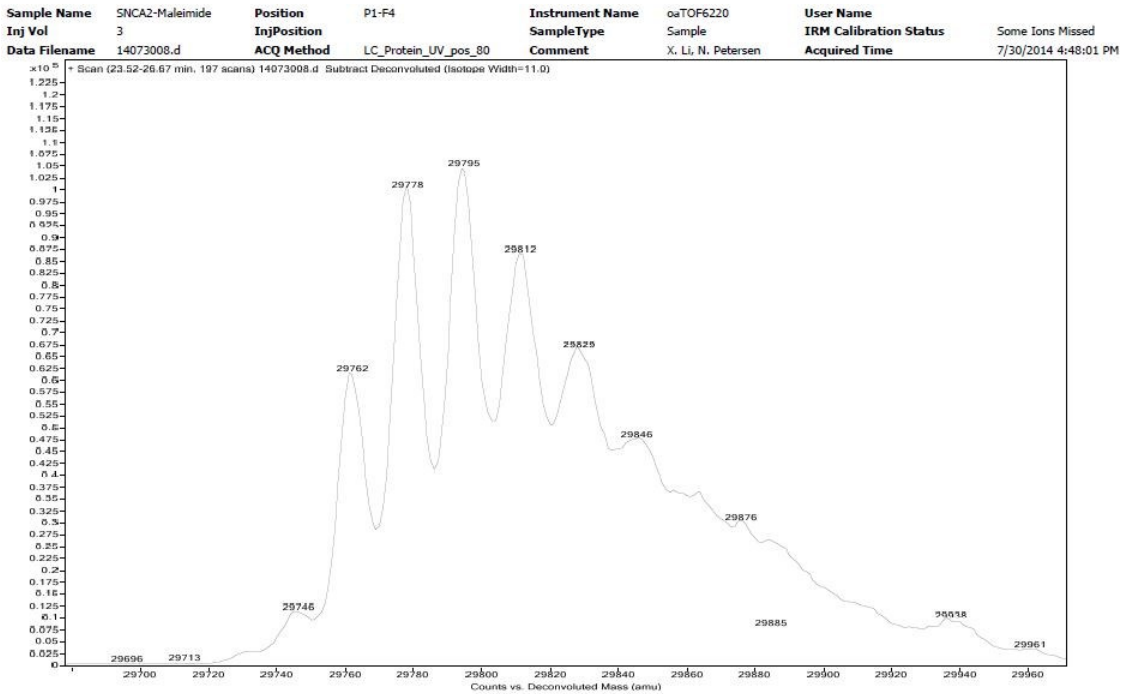


Figure 26: MS spectrum for Sncal2_Cys_TPM.

4.2 Quantum yield of Oregon green 488 is affected by conjugation to α -synucleins

Results. Figures 27 and 28 show examples of the emission spectra of samples consisted of either Cy5 tetrazine or Oregon Green 488 maleimide. The blue line is the emission spectrum of pure Cy5 tetrazine solution with its absorbance equal to 0.023 and the red line is for a mixture of monomeric α -synuclein and Cy5 tetrazine (Abs = 0.029) without conjugation.

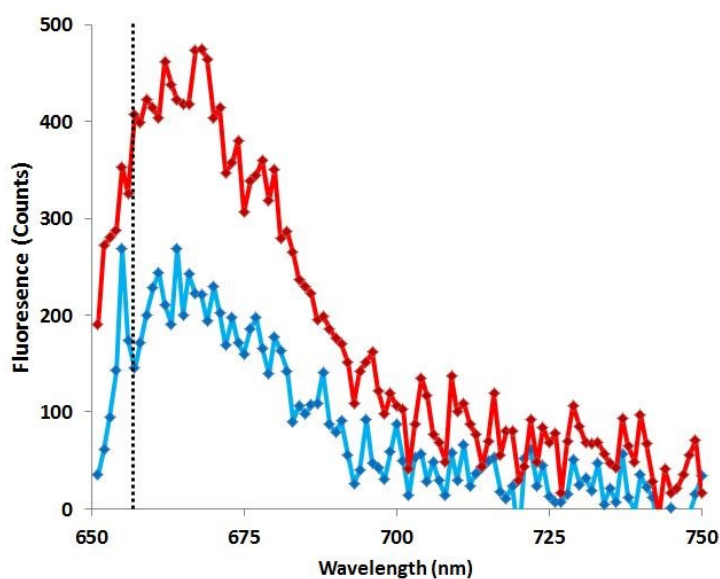


Figure 27: Fluorescence as a function of emission wavelengths for Cy5 tetrazine (Blue) and the mixture of Sncal_Cys and Cy5 tetrazine (Red). Dashed line indicated the starting point (656 nm) of all integrated emission.

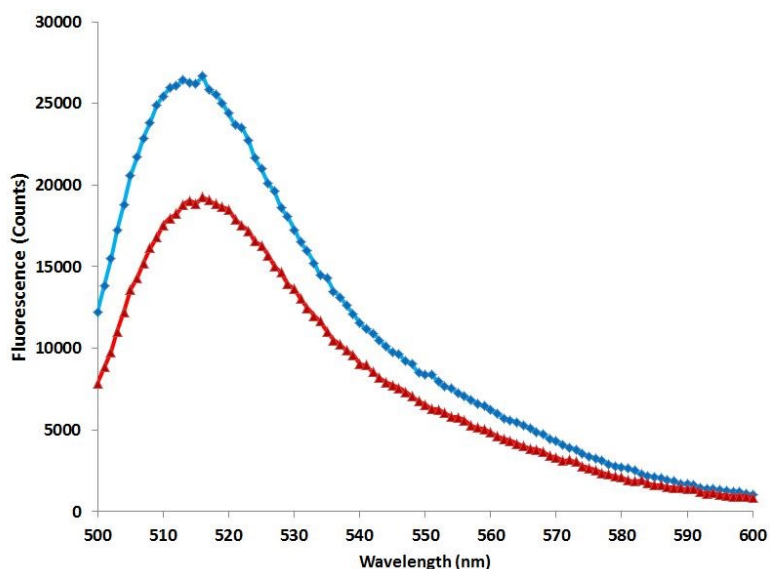


Figure 28: Fluorescence as a function of emission wavelength for Oregon Green 488 maleimide (Blue) and the mixture of Snca1_Cys and the dye (Red).

Table 17: Summary of relative quantum yields for Cy5 tetrazine alone, in mixture with proteins and conjugated to proteins.

	\langle Integrated Emission \rangle (656 – 750 nm)	\langle Absorption \rangle (650 nm)	“Absolute” quantum yield	Relative quantum yield
Cy5	$(8.7 \pm 0.4) \times 10^3$	0.0226 ± 0.0008	$(3.8 \pm 0.2) \times 10^5$	1.0
Snca1 and Cy5 (no conjugation)	$(1.4 \pm 0.2) \times 10^4$	0.0293 ± 0.0004	$(4.9 \pm 0.5) \times 10^5$	1.3 ± 0.1
Snca2 and Cy5 (no conjugation)	$(1.12 \pm 0.06) \times 10^4$	0.0308 ± 0.0006	$(3.6 \pm 0.2) \times 10^5$	0.95 ± 0.08
Snca4 and Cy5 (no conjugation)	$(1.15 \pm 0.02) \times 10^4$	0.026 ± 0.002	$(4.4 \pm 0.4) \times 10^5$	1.2 ± 0.1
Snca8 and Cy5 (no conjugation)	$(1.01 \pm 0.06) \times 10^4$	0.027 ± 0.001	$(3.7 \pm 0.3) \times 10^5$	1.0 ± 0.1
Snca1_Cy5	$(1.4 \pm 0.1) \times 10^4$	0.033	$(4.2 \pm 0.3) \times 10^5$	1.11 ± 0.09

Snca2_Cy5	$(1.1 \pm 0.1) \times 10^4$	0.026	$(4.2 \pm 0.4) \times 10^5$	1.1 ± 0.1
Snca4_Cy5	$(1.1 \pm 0.1) \times 10^4$	0.043	$(2.6 \pm 0.2) \times 10^5$	0.68 ± 0.09
Snca8_Cy5	$(1.098 \pm 0.001) \times 10^4$	0.029	$(3.795 \pm 0.004) \times 10^5$	1.00 ± 0.05

Tables 17 and 18 summarizes all experimental data including the average of the integrated emission, the average of sample absorption of sample, the “absolute” quantum yield, the relative quantum yield of the samples and the standard of the mean. The “absolute” quantum yield of fluorescence is defined as the ratio between the average integrated emission and the average absorption of three repeat measurements. The “absolute” quantum yield of fluorescence is calculated without full calibration of the instrument detection efficiency.

Table 18: Summary of relative quantum yields for Oregon Green 488 C5 maleimide alone, in mixture with proteins and conjugated to proteins.

	⟨Integrated Emission⟩ (500 – 600 nm)	⟨Absorption⟩ (492 nm)	“Absolute” quantum yield	Relative quantum yield
ORM488	$(1.13 \pm 0.03) \times 10^6$	0.0332 ± 0.0008	$(3.4 \pm 0.1) \times 10^7$	1.0
Snca1 and 488 (no conjugation)	$(7.9 \pm 0.3) \times 10^5$	0.029 ± 0.001	$(2.7 \pm 0.1) \times 10^7$	0.79 ± 0.05
Snca2 and 488 (no conjugation)	$(9.4 \pm 0.5) \times 10^5$	0.030 ± 0.001	$(3.1 \pm 0.2) \times 10^7$	0.91 ± 0.07
Snca4 and 488 (no conjugation)	$(9.6 \pm 0.2) \times 10^5$	0.0314 ± 0.0008	$(3.1 \pm 0.1) \times 10^7$	0.91 ± 0.04
Snca8 and 488 (no conjugation)	$(9.7 \pm 0.5) \times 10^5$	0.0298 ± 0.0005	$(3.3 \pm 0.2) \times 10^7$	0.97 ± 0.07

Snca1_488	$(5.9 \pm 0.6) \times 10^5$	0.0293	$(2.0 \pm 0.2) \times 10^7$	0.6 ± 0.1
Snca2_488	$(1.0760 \pm 0.0005) \times 10^6$	0.0335	$(3.207 \pm 0.002) \times 10^7$	0.94 ± 0.03
Snca4_488	$(9.89 \pm 0.07) \times 10^5$	0.0453	$(2.18 \pm 0.01) \times 10^7$	0.64 ± 0.03
Snca8_488	$(7.48 \pm 0.02) \times 10^5$	0.0381	$(1.964 \pm 0.004) \times 10^7$	0.58 ± 0.03

Setting the quantum yield of the dye equal to 1, the relative quantum yield of the mixtures and labelled protein are presented as the ratio of the “Absolute” quantum yield of the dye and those of the labelled protein. “Snca1 and Cy5 (no conjugation)” refers to a mixture of monomeric α -synuclein and Cy5 tetrazine without conjugation. “Snca1 and Cy5 (no conjugation)” is a control group to check whether the quantum yield of dye changes or not in the presence of α -synuclein. While “Snca1_Cy5” means a purified sample of monomeric α -synuclein labelled with Cy5 tetrazine. The same rule was applied to the names of the rest of samples. To sum up, neither the presence of α -synucleins nor the conjugation with α -synucleins affected the quantum yield of the Cy5 tetrazine (less than 10% changes). However, the quantum yield of the Oregon Green 488 maleimide was decreased a little when it was conjugated with the protein. This result was helpful for the further studies about the aggregation of α -synucleins using fluorescence correlation spectroscopy.

4.3 Determination of hydrodynamic size of labelled α -synucleins

4.3.1 Hydrodynamic diameters of α -synucleins by DLS

Data analysis. The DLS measurement results are presented in several ways, and data analyses are required to select the most adequate to describe the size

distribution of each measurement. The most common way to describe DLS data is the intensity particle size distribution, which is directly generated by the Malvern Software based on Equations (1), (2) and (11). If there is more than one particle size being detected in the sample, the weighted average of two intensity values is called the Z-average size. However, these two ways of data presentations are only accurate for measuring solutions consisting of a single particle size. The reason is that the Rayleigh scattering intensity of a particle is proportional to the 6th power of its hydrodynamic radius.⁹⁸ Therefore, existence of any large sized impurity, such as small amounts of dusts or protein aggregates, will greatly influence the intensity particle size distribution and the Z-average size.

Although my DLS samples were carefully filtered before measurements, ~ 0.2% of molecules were detected as large aggregates, which turn out to greatly amplify the value of the intensity particle size distribution and Z-average size. In this case, the volume-weighted particle size distribution is a more appropriate value to report.

Experimental results. The intensity hydrodynamic diameter distributions of monomeric, dimeric, tetrameric and octameric α -synuclein labelled with TPM are presented in Figure 29, to show that the existence of a small amount of aggregates can affect the intensity particle size distributions greatly.

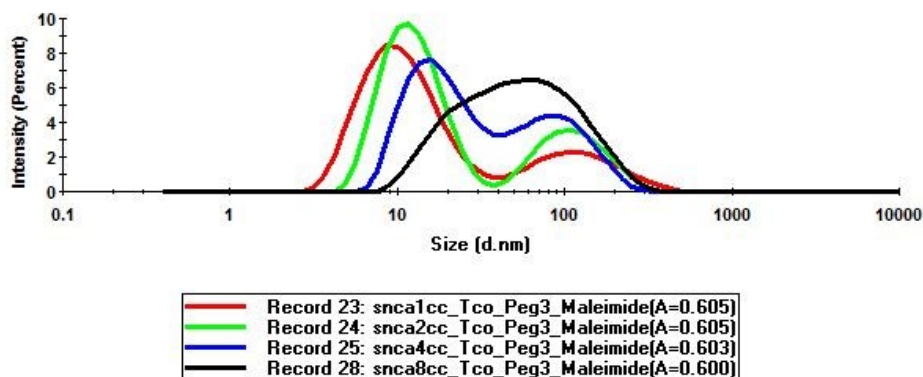


Figure 29: Intensity particle size distributions of Snca1, 2, 4 and 8_Cys_TCM.

Figure 30 summarizes the weighted-volume hydrodynamic diameter distributions for 1.4 mg/mL of monomeric, dimeric, tetrameric and octameric α -synuclein labelled with TPM in 10 mM of PBS at pH 7.4.

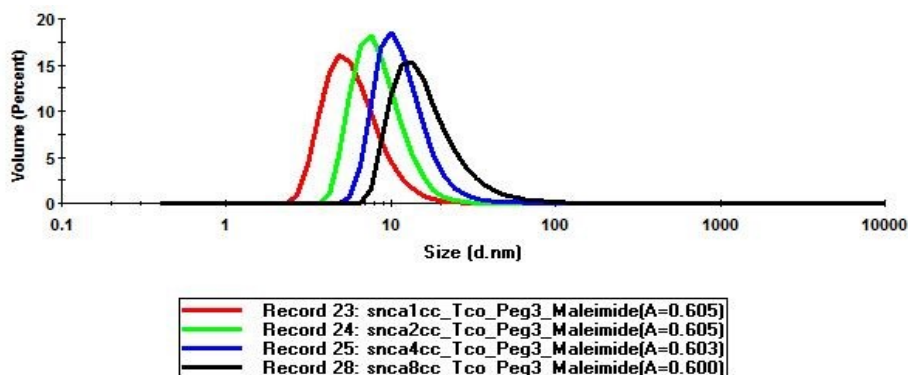


Figure 30: Weighted-volume particle size distributions of Snca1, 2, 4 and 8_Cys_TPM.

The correlograms and their fitting data of monomeric, dimeric, tetrameric and octameric α -synuclein labelled with TPM are presented in Figure 31. As shown in the figure, Snca1_TPM is the smallest and fastest diffusing protein; its measured correlation curve has decayed to the half of its amplitude within the shortest time.

Snca8_TPM requires the longest time for a half loss of correlation, and correlation curves of dimeric and tetrameric α -synuclein are in between.

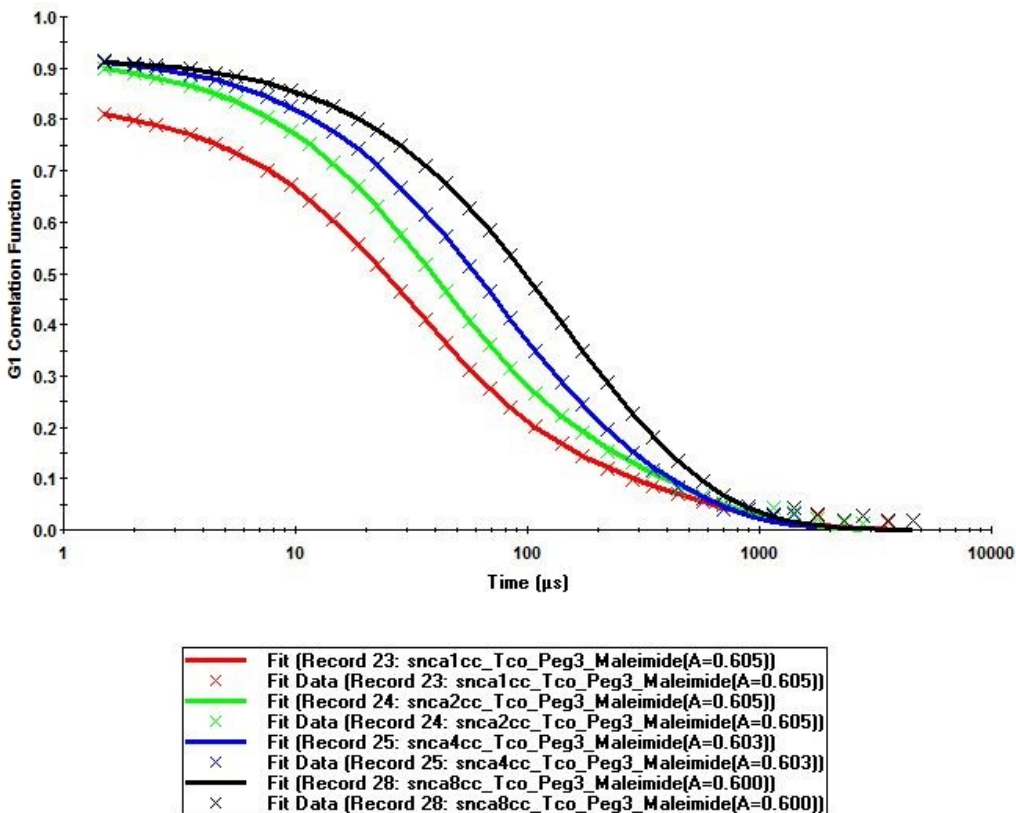


Figure 31: Fitted correlograms of Snca1, 2, 4, and 8_Cys_TPM.

Table 19: Weighted-volume particle size distributions for α -synucleins.

Sample Names	Hydrodynamic Diameter \pm Standard Error (nm)	% Volume of the major peak
Snca1_TPM	6.2 ± 0.9	100.0
Snca2_TPM	8.7 ± 0.8	99.9
Snca4_TPM	12 ± 2	100.0
Snca8_TPM	18 ± 3	100.0

Table 19 summarizes the diameters (in nanometers) and their standard error of the mean based on the weighted volume, together with the volume percentage of the

major component in each sample. According to the technical notes of Malvern Company, the resolution of a DLS measurement is not high; approximately three times difference in size can eventually be practically baseline-separated. Therefore, DLS measurements are not the most accurate method to determine the hydrodynamic sizes of α -synucleins.

4.3.2 Hydrodynamic diameters of α -synucleins by FCS

Results. Monomeric, dimeric, tetrameric and octameric α -synucleins were labelled with Oregon Green 488 Maleimide and Cy5 tetrazine in 10 mM PBS at pH = 7.4, respectively. Then those samples were measured using FCS to determine their hydrodynamic sizes for comparison with those from DLS.

Table 20: Fitting results of labelled Snca1, 2, 4 and 8 in PBS at pH = 7.40 and comparison of the hydrodynamic diameters obtained from FCS and DLS.

	Repeat #	τ_D \pm standard error (μ s)	D \pm standard error (μ m ² s ⁻¹)	Hydrodynamic Diameter (nm)	
				FCS Data	DLS Data
Snca1_ORM488	50	240 \pm 4	79 \pm 1	6.3 \pm 0.1	6.2 \pm 0.9
Snca1-TPM_Cy5	95	357 \pm 7	75 \pm 2	6.8 \pm 0.1	
Snca2_ORM488	100	306 \pm 4	61.9 \pm 0.7	8.0 \pm 0.1	8.7 \pm 0.8
Snca2-TPM_Cy5	50	470 \pm 20	58 \pm 2	8.8 \pm 0.3	
Snca4_ORM488	58	500 \pm 10	38.5 \pm 0.9	13.1 \pm 0.3	12 \pm 2
Snca4-TPM_Cy5	100	670 \pm 10	38.6 \pm 0.9	13.2 \pm 0.3	
Snca8_ORM488	93	690 \pm 20	28.4 \pm 0.6	17.9 \pm 0.4	18 \pm 3
Snca8-TPM_Cy5	100	970 \pm 30	28.4 \pm 0.8	18.4 \pm 0.6	

Table 20 summarizes the hydrodynamic diameters of monomeric, dimeric, tetrameric and octameric α -synucleins in 10 mM PBS at pH = 7.40 based on their

measured diffusion times using FCS. All diffusion times shown in the table were the average of more than 50 repeat measurements of the same sample. The resulting autocorrelation curves were fitted by the two component autocorrelation function in the defaulted Carl Zeiss software with suggested fitting parameters: diffusion time of Oregon Green 488 maleimide was 45.6 μs ; diffusion time of Cy5 tetrazine was 72 μs ; the fit range started at 1 μs ; free triplet state fraction was from 0% to 30%; free triplet time was from 1 μs to 10 μs ; and $\frac{w_z}{w_{xy}}$ was equal to 10. All diffusion coefficients were calculated using Equation (10) with $w_{xy_green} = 273$ nm and $w_{xy_red} = 320$ nm, respectively. All hydrodynamic diameters were calculated using Equation (11) with $T = 298.15$ K and viscosity of 10 mM of PBS = 0.00090 Pa·s. To sum up, the hydrodynamic diameters of α -synuclein monomer and oligomers labelled with Oregon Green 488 Maleimide or Cy5 tetrazine obtained from FCS agreed well with those measured by DLS. DLS measurements were conducted using ~ 1 mM of protein sample, while ~ 10 nM of protein sample were used in FCS measurements. This result also suggests that the hydrodynamic radius of α -synuclein may be independent of the protein concentration, which is useful for future aggregation studies.

4.3.3 Hydrodynamic diameters of α -synucleins are independent of the protein concentration.

Results. Constant concentration of tetrameric α -synuclein labelled with Alexa Fluor[®] 488 C5-maleimide (snca4-488) solutions were mixed with different concentrations of unlabelled tetrameric α -synuclein (snca4) in 10 mM PBS at pH

= 7.4. Those samples were measured using FCS to find out whether the hydrodynamic size of α -synuclein changes with its concentration.

Table 21: Fitting results of labelled Snca4 with different concentration of unlabelled Snca4 in PBS at pH=7.40.

Concentration of snca4-488 (nM)	Concentration of unlabelled snca4 (nM)	Count rate (kHz)	G(0) \pm standard error	N \pm standard error	τ_D \pm standard error (μ s)
34	10898	18	0.099 \pm 0.002	10.1 \pm 0.2	478 \pm 8
34	5449	20	0.117 \pm 0.004	8.6 \pm 0.3	460 \pm 10
34	2724	21	0.100 \pm 0.002	10.0 \pm 0.2	450 \pm 10
34	1362	23	0.091 \pm 0.001	11.0 \pm 0.2	470 \pm 10
34	681	14	0.137 \pm 0.003	7.3 \pm 0.1	490 \pm 20
34	341	18	0.101 \pm 0.002	9.9 \pm 0.2	460 \pm 10
34	170	11	0.152 \pm 0.003	6.6 \pm 0.1	500 \pm 10
34	85	13	0.136 \pm 0.001	7.38 \pm 0.04	420 \pm 20
Average \pm Standard Error					460 \pm40

Table 21 demonstrates the experimental data of the former experiments. Each row of the result including count rate, G(0), N and τ_D were obtained from 12 repeat measurements of the same sample. The resulting autocorrelation curves were fitted by using the two component autocorrelation function in the defaulted Carl Zeiss software with suggested fitting parameters: range started at 1 μ s; free triplet state fraction was from 0% to 30%; free triplet time was from 1 μ s to 10 μ s; and $\frac{w_z}{w_{xy}}$ was equal to 10. As a result, the hydrodynamic sizes of tetrameric α -synuclein show a broad distribution. But there is no statistic difference between the diffusion times of Snca4-488 under different protein concentrations.

4.3.4 Overall Discussion

As mentioned in Section 1.2.2, empirical equations to predict the hydrodynamic radius of a protein based on its numbers of amino acid were established ($R_h =$

$4.75 \times N^{0.29} \text{Å}$ for native folded protein and $R_h = 2.21 \times N^{0.57} \text{Å}$ for unfolded protein, N is the number of amino acids in the protein of interest²¹. With the assumption that the hydrodynamic radius of a protein is half of its hydrodynamic diameter, the hydrodynamic diameters of α -synucleins under different folding conditions were calculated based on the empirical equations and are summarized in Table 22. Compared with my experimental data of DLS, and FCS, it is also shown that α -synuclein is intrinsically disordered protein with partial compactness under the “physiological” conditions (10 mM PBS and pH = 7.4), which is in good agreement with previous research.^{8,46,86} Moreover, α -synuclein is intrinsically disordered even when it binds to TPM or when it is labelled with the dye. This is supported by comparing my FCS and DLS data with the DLS data of unlabelled and non-mutated α -synuclein monomer, dimer, tetramer and octamer obtained by Marion Becker.¹²⁴

Table 22: Comparison of the estimated hydrodynamic diameters of Snca1, 2, 4, and 8 with DLS and FCS results.

Protein Name	N	Estimated D_h (nm)		Measured D_h (nm)		
		Natively folded	Completely unfolded	DLS (Sncax)	DLS (Sncax_Cys_TPM)	FCS (Sncax_Cys_TPM_Dyes)
Snca1	141	4.0	7.4	6.2±0.6	6.2±0.9	6.3±0.1
						6.8±0.1
Snca2	284	4.8	11.0	9.0±0.6	8.7±0.8	8.0±0.1
						8.8±0.3
Snca4	570	6	16.4	13.2±0.2	12±2	13.1±0.3
						13.2±0.3
Snca8	1142	7.4	24.4	18.9±0.5	18±3	17.9±0.4
						18.4±0.6

4.4 Aggregation of labelled α -synucleins

4.4.1 Aggregation tests by FCS

In the first aggregation experiment, a small amount of labelled α -synucleins and a large excess of unlabelled α -synucleins were incubated together, and the mixture was measured by FCS to determine whether the diffusion of the labelled protein would change if aggregation occurred. Figure 32 (a) displays the distributions of the measured diffusion time of a sample which contains $\sim 0.3 \mu\text{M}$ of labelled monomeric α -synuclein and $150 \mu\text{M}$ unlabelled monomer over 120 hours. There is no apparent change in the distribution of diffusion times after the sample was incubated at 310.15 K for 120 hours with continuous shaking at 250 rpm. Figure 32 (b) displays the distributions of the measured diffusion time of a sample which contained $\sim 0.03 \mu\text{M}$ of labelled tetrameric α -synuclein and $10 \mu\text{M}$ of unlabelled tetrameric protein at incubation times over 6 hours. No change in distribution is discovered, although there are a few outliers of very large diffusion times after 0.4 hours.

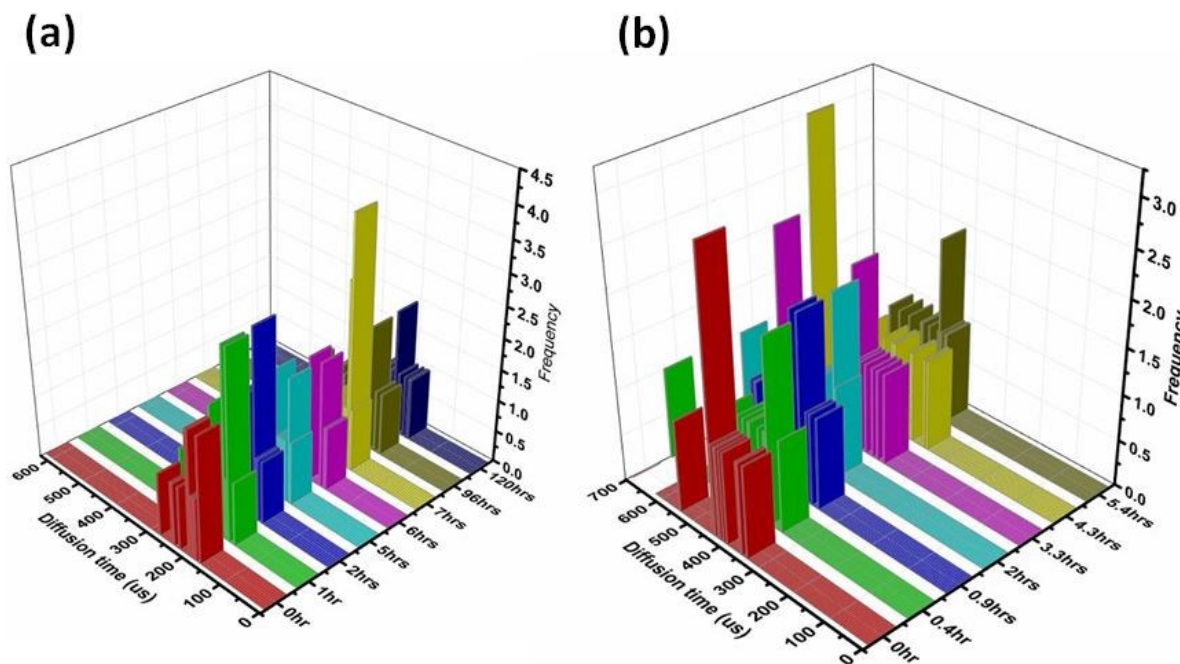


Figure 32: (a) Distribution of the diffusion time of Sncal_Cys_Dye with Sncal_Cys at different incubation times. (b) Distribution of the diffusion time of Sncal4_Cys_Dye with Sncal4_Cys at different incubation times.

Figure 32 shows the distributions of the measured diffusion time of a sample which contained the same concentrated labelled tetrameric α -synuclein ($\sim 0.03 \mu\text{M}$) and $150 \mu\text{M}$ unlabelled monomer at different incubation times. Again, the distribution of the diffusion time was not dramatically changed with the incubation time, but there were several measurements of fluorescent species with diffusion times around $1000 \mu\text{s}$ at $t = 11$ hours. Most interestingly, the average of the measured diffusion time of labelled tetramer at $t = 0$ in Figure 32 appeared larger than those in Figure 32 (b). Two possibilities to explain this difference: (i) the initial labelled tetramers in Figure 33 were originally more aggregated than those in Figure 32(b); or (ii) the presence of $150 \mu\text{M}$ of unlabelled monomer and $10 \mu\text{M}$ of unlabelled tetramer showed different effects on the diffusion of the

labelled tetramer, and large amounts of unlabelled monomers at high concentration were rapidly incorporated by the small amounts of labelled tetramer at $t = 0$. Considering the molecular weight (or the molecular hydrodynamic volume) of a molecule is proportional to the third power of its diffusion time (or its hydrodynamic radius), the measured diffusion time would not be the most suitable scale for the aggregation test.

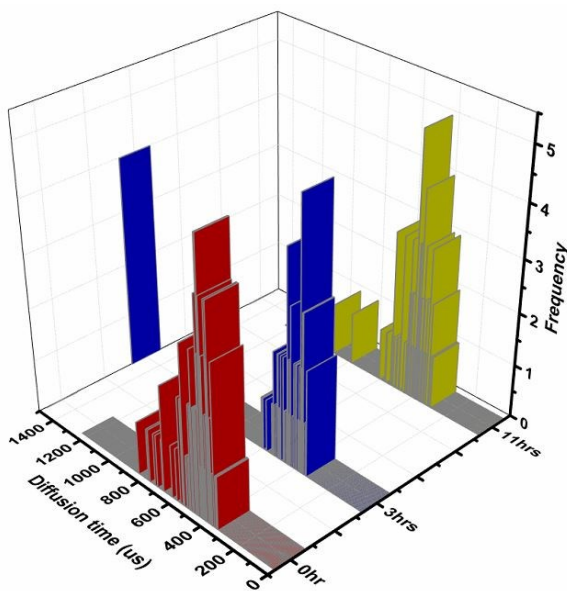


Figure 33: Distribution of the diffusion time of Sna4_Cys_Dye incubated with Sna1_Cys at different times.

4.4.2 Aggregation tests by dual-color FCCS.

Dual-color FCCS measurements are, in principle, more sensitive tests for co-aggregation of species that form oligomers, because only those species that contain both fluorophores are detected in the cross-correlation. In this section, whether two differently labelled α -synuclein proteins will rapidly form small aggregates by mixing equal molar amounts of red and green fluorescently labelled monomers, dimers, tetramers and octamers are explored. There are two specific

objectives with these experiments: (i) to find out whether each kind of α -synucleins (monomers and the engineered α -synuclein oligomers) can aggregate alone under “physiological” conditions (10 mM PBS at pH = 7.4) within short incubation time (~8 hrs). This part refers to “self-aggregation” in the subsequent discussion; and (ii) to understand whether α -synuclein monomers can be incorporated into aggregates of the engineered dimers, tetramers and octamers, which is the “cross-aggregation” tests in the subsequent discussion.

Figure 34 demonstrates the autocorrelation functions and cross-correlation function in a self-aggregation test. The sample for the test consists of 125 μ L of octameric α -synuclein (67 μ M) labelled with Cy5 tetrazine and 125 μ L of octameric α -synuclein (67 μ M) labelled with Oregon Green 488 Maleimide. Figure 34 (a) shows the correlation functions when two solutions mixed at $t = 0$ hour, and Figure 34 (b) shows that of $t = 6$ hours with continuous shaking at 250 rpm and 37°C. It is apparent that the cross correlation function in Figure 34 (b) have a higher $G(0)$ than that in Figure 34 (a). Moreover, and the cross correlation function in Figure 34 (b) had a larger diffusion time (τ_D) than those of autocorrelation functions of the same figure. All this evidence indicates that α -synucleins labelled with different dyes can form aggregates during the 6 hours incubation under the above conditions. α -Synuclein monomers, the engineered dimers and tetramers are also measured by dual-color FCCS. The important fitting values, such as $G(0)$ from autocorrelation functions and cross correlation functions, are used in the following data analysis.

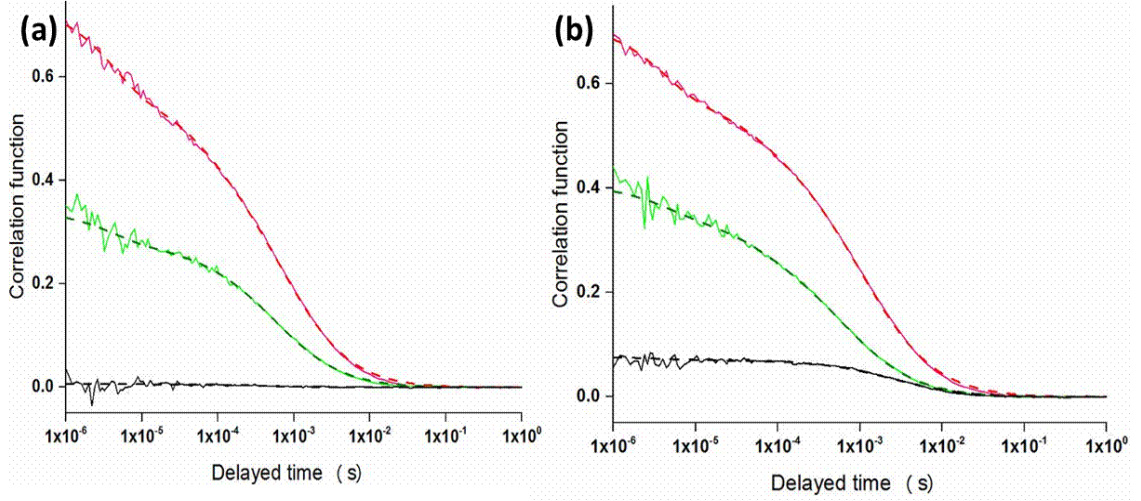


Figure 34: (a) Autocorrelation functions and cross-correlation function of a mixture of Snca8 ORM488 and Snca8 Cy5 at $t = 0$ hour. (b) Autocorrelation functions and cross-correlation function of a mixture of Snca8 ORM488 and Snca8 Cy5 at $t = 6$ hours. Red dashed line is the fitting curve of data obtained by the red detector, Green dashed line is from the green detector and Black dashed is data calculated based on the cross correlation.

Figure 34 (a) and (b) respectively display the $\frac{\langle n_{rg} \rangle}{\langle n_r \rangle}$ and $\frac{\langle n_{rg} \rangle}{\langle n_g \rangle}$ in percentage (calculated from $G(0)$, refers to 3.5.4) as functions of the incubation time for selected aggregation experiments of mixture of green and red dye labelled α -synuclein monomers (FCCS11 in red), dimers (FCCS22 in black), tetramers (FCCS44 in blue) and octamers (FCCS88 in purple). Then these experimental data are fitted to the exponential growth function, Equation (50). Two important fitting parameters are revealed: one is the amplitude of the fitting curve, A , which is the difference between the start-point and the endpoint of a growth curve; and the other is k , which is the reciprocal of the growth time. The growth time is defined as the time to reach $\frac{1}{e}$ of the final value.

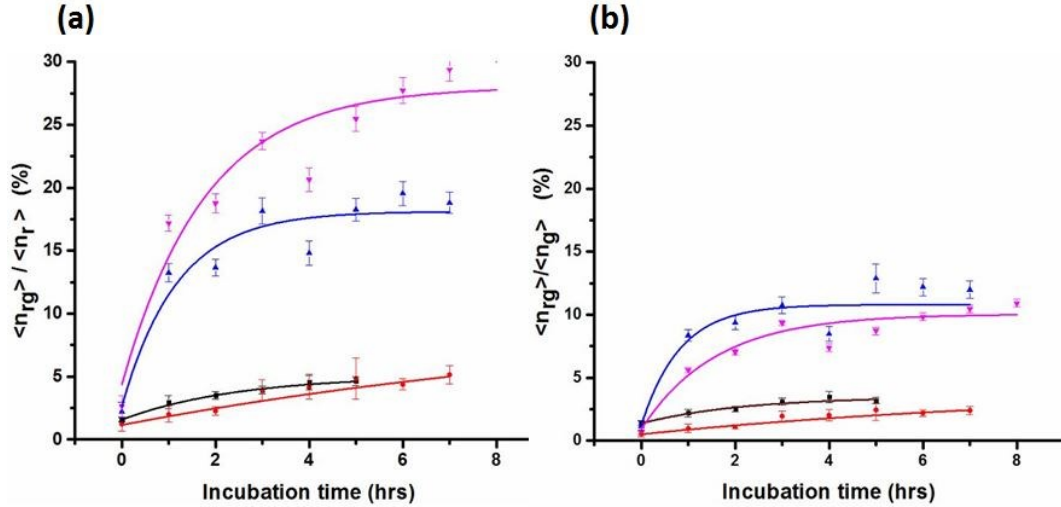


Figure 35: (a) $\frac{\langle n_{rg} \rangle}{\langle n_r \rangle}$ as a function of incubation time; (b) $\frac{\langle n_{rg} \rangle}{\langle n_g \rangle}$ as a function of incubation time for FCCS 11 (red), FCCS 22 (black), FCCS 44 (blue) and FCCS 88 (purple).

Self-aggregation: Analysis of the amplitude of fitting curves. It was evident from Figure 35 (a) that the extent and the rate of increase of the FCCS 88 fractions were the largest while those of the FCCS 11 were the smallest, and those of FCCS 22 and 44 were in between. Figure 35 (b) shows an overall similar trend, but with relatively smaller changes in these fractions. This indicates that more red dye labelled α -synuclein is incorporated into the aggregates than the green dye labelled α -synuclein. Moreover, it is interesting to point out that the extent and the rate of the FCCS 44 aggregation curve are larger than those of the FCCS 88 in Figure 35 (b).

Table 23 summarizes the amplitude (in %) with its standard error of the fitting curves of all FCCS self-aggregation experiments. Each test reveals the average amplitude of 50 repeated measurements of the same sample. Same test is repeated 3~4 times and newly prepared samples are used each time. Finally the average

amplitude of all tests of one kind of aggregation is summarized in the last column of Table 23. Since not all experimental data can be well fitted with the exponential growth function, the improper fitting measurement was labelled as “ \emptyset ” in the following tables. Moreover, some fitting gave a standard error which was even larger than the average value; these experimental data were also not considered into the average fitting values.

Table 23: Summary of fitting amplitude of FCCS self-aggregation tests.

	Amplitude of the fitting (%) \pm standard error					
	Codes	Test 1	Test 2	Test 3	Test 4	Average of Tests 1~4
$\frac{\langle n_{rg} \rangle}{\langle n_r \rangle}$	FCCS 11	3 \pm 3(\emptyset)	5.2 \pm 0.2	3 \pm 1	2 \pm 2	3\pm2
	FCCS 22	10 \pm 10(\emptyset)	8 \pm 6	-	-	8\pm6
	FCCS 44	\emptyset	15 \pm 2	11 \pm 3	13.6 \pm 0.6	13\pm4
	FCCS 88	24 \pm 3	21 \pm 3	-	-	23\pm4
$\frac{\langle n_{rg} \rangle}{\langle n_g \rangle}$	FCCS 11	2 \pm 2(\emptyset)	2.0 \pm 0.7	2.0 \pm 0.8	3.0 \pm 0.3	2\pm1
	FCCS 22	4 \pm 2	4 \pm 3	-	-	4\pm4
	FCCS 44	\emptyset	10 \pm 1	9 \pm 2	10.4 \pm 0.6	10\pm2
	FCCS 88	9 \pm 1	8 \pm 1	-	-	9\pm1

First of all, $\frac{\langle n_{rg} \rangle}{\langle n_r \rangle}$ always had a larger value than $\frac{\langle n_{rg} \rangle}{\langle n_g \rangle}$ of the corresponding aggregation test (such as $\frac{\langle n_{rg} \rangle}{\langle n_r \rangle} > \frac{\langle n_{rg} \rangle}{\langle n_g \rangle}$ in FCCS 88), which again indicated that Cy5 tetrazine labelled α -synuclein were more easily recruited in the aggregation than those of the Oregon Green 488 maleimide labeled α -synucleins. Second, as shown in Table 23, there were 23% of Cy5 labelled octameric α -synucleins and 9% of

Oregon 488 labelled octameric α -synucleins in the FCCS 88 experiments were used to form aggregates within 8 hours, while only 3% of red dye labelled monomer and 2% of green dye labelled monomeric α -synucleins aggregated under the same incubation condition (FCCS 11). The percentages of dimeric and tetrameric α -synuclein that used to form aggregates in the same experimental condition were lower than that of octamer and higher than those of monomer (FCCS 22 and FCCS 44). This result indicated that the engineered octameric α -synucleins aggregated the fastest while the monomers of α -synuclein were the slowest.

Cross-aggregation: Analysis of the amplitude of fitting curves. Figure 36 (a) ~ (d) display the $\frac{\langle n_{rg} \rangle}{\langle n_r \rangle}$ and $\frac{\langle n_{rg} \rangle}{\langle n_g \rangle}$ in percentage as functions of the incubation time for selected cross-aggregation experiments of FCCS 12, FCCS 21 (black), FCCS 14, FCCS 41 (blue) and FCCS 18, and FCCS 81 (purple). All cross-aggregation curves are also fitted with the exponential growth function, Equation (50), to obtain the parameters A and k . All fitting parameters are summarized in Tables 24 and 26. Table 24 includes the amplitude (in %) with its standard error of the fitting curves for all cross-aggregation experiments. Same as before, each test reveals the average amplitude of 50 repeated measurements of the same sample and same test is repeated for 3-4 times while newly prepared samples are used each time. Finally the average amplitude of all tests of one kind of aggregation is calculated in the last column of Table 24.

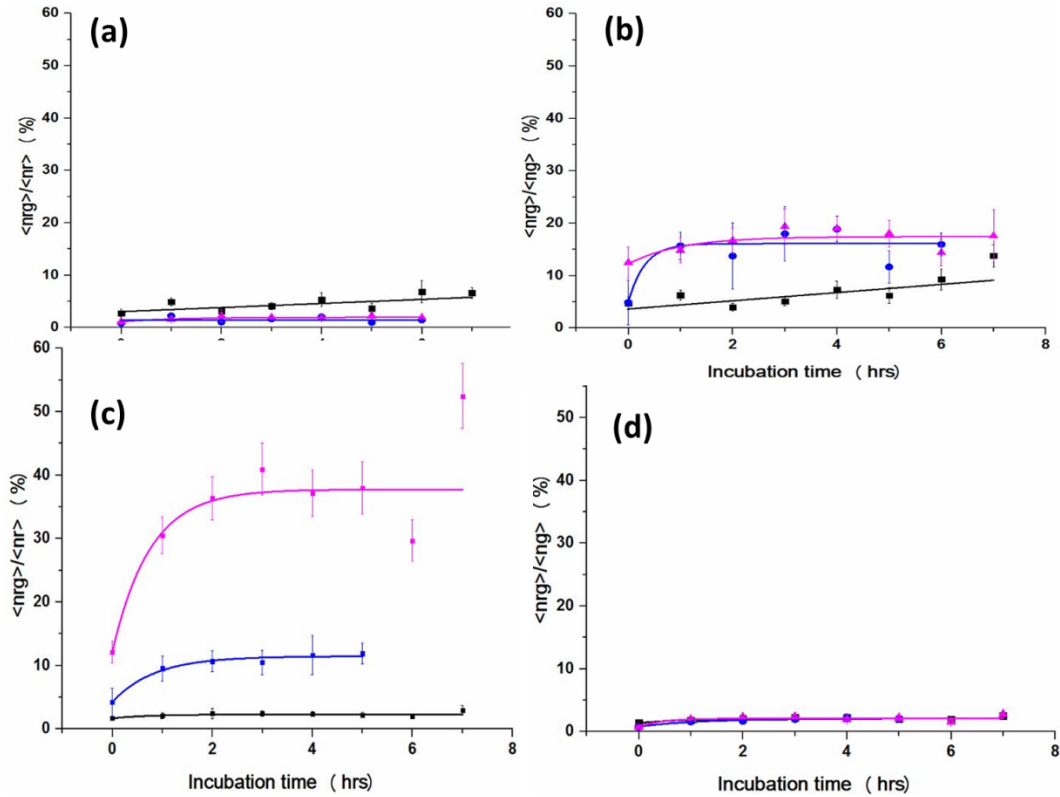


Figure 36: (a) $\frac{\langle n_{rg} \rangle}{\langle n_r \rangle}$ as a function of incubation time for FCCS 12, 14 and 18; (b) $\frac{\langle n_{rg} \rangle}{\langle n_g \rangle}$ as a function of incubation time for for FCCS 12, 14 and 18; (c) $\frac{\langle n_{rg} \rangle}{\langle n_r \rangle}$ as a function of incubation time for FCCS 21, 41 and 81; (d) $\frac{\langle n_{rg} \rangle}{\langle n_g \rangle}$ as a function of incubation time for FCCS 21, 41 and 81. Black for sample contained dimeric α -synuclein, blue for tetramers and purple for octamers.

As shown in both Figure 36 and Table 24, the engineered α -synuclein dimer, tetramer and octamer preferred to incorporate itself than monomer to the aggregation process when the same protein concentration monomer and oligomer solutions were mixed within 8 hour incubations. It concluded based on the fact that only 0.9 ~ 3% of red dye labelled monomeric α -synuclein ($\frac{\langle n_{rg} \rangle}{\langle n_r \rangle}$) of FCCS 12, 14 and 18 or Figure 36 (a)) were enrolled in the aggregation while 5-11% of green labelled oligomers ($\frac{\langle n_{rg} \rangle}{\langle n_g \rangle}$) of FCCS 12, 14 and 18 or Figure 36 (b)) were used in the

aggregation. It was further supported by the experimental data that only ~1.5% of green dye labelled monomer ($\frac{\langle n_{rg} \rangle}{\langle n_g \rangle}$ of FCCS 21, 41 and 81 or Figure 36 (d)) were contributed to the cross aggregation process (the aggregation between the monomers and oligomers), while 3~23% of red dye labelled oligomers ($\frac{\langle n_{rg} \rangle}{\langle n_r \rangle}$ of FCCS 21, 41 and 81 or Figure 36 (c)) were used for the aggregation. This result further indicated that the presence of the engineered α -synuclein oligomers does not affect the self-aggregation of the α -synuclein monomer.

Table 24: Summary of fitting amplitude of FCCS cross-aggregation tests.

	Amplitude of the fitting (%) \pm standard error					
	Codes	Test 1	Test 2	Test 3	Test 4	Average of Tests 1~4
$\frac{\langle n_{rg} \rangle}{\langle n_r \rangle}$	FCCS 12	0.7 \pm 0.5	0.9 \pm 0.1	1.0 \pm 0.2		0.9\pm0.5
	FCCS 14	2 \pm 1	1.5 \pm 0.6	2 \pm 0.4		2\pm1
	FCCS 18	3 \pm 1	3 \pm 1	1.05 \pm 0.04	2 \pm 5(\emptyset)	2\pm1
$\frac{\langle n_{rg} \rangle}{\langle n_g \rangle}$	FCCS 12	4.2 \pm 0.7	4.8 \pm 0.6	5 \pm 1		5\pm1
	FCCS 14	18 \pm 50(\emptyset)	11 \pm 4	10 \pm 4	-	11\pm6
	FCCS 18	14 \pm 90 (\emptyset)	11 \pm 2	9 \pm 20(\emptyset)	9 \pm 3	10\pm3
$\frac{\langle n_{rg} \rangle}{\langle n_r \rangle}$	FCCS 21	0.6 \pm 0.2	6 \pm 2	-	-	3\pm2
	FCCS 41	\emptyset	12 \pm 1	7.1 \pm 0.8	9 \pm 1	9\pm2
	FCCS 81	27 \pm 5	26 \pm 4	27 \pm 5	19 \pm 2	23\pm5
$\frac{\langle n_{rg} \rangle}{\langle n_g \rangle}$	FCCS 21	0.8 \pm 0.1	1.4 \pm 0.2	-	-	1.1\pm0.2
	FCCS 41	\emptyset	1.9 \pm 0.2	1.2 \pm 0.1	1.5 \pm 0.1	1.5\pm0.2
	FCCS 81	1.6 \pm 0.2	1.3 \pm 0.3	1.3 \pm 0.5	1.23 \pm 0.08	1.3\pm0.5

Table 25: Another format of summary the fitting amplitudes of all FCCS tests.

$\frac{\langle n_{rg} \rangle}{\langle n_r \rangle}$	$\frac{\langle n_{rg} \rangle}{\langle n_g \rangle}$	Snca1_Cys_ORM4 88 (536 μ M)	Snca2_Cys_ORM 488 (268 μ M)	Snca4_Cys_OR M488 (134 μ M)	Snca8_Cys_OR M488 (67 μ M)			
Snca1_Cys_TPM_Cy5 (536 μ M)	FCCS 11	FCCS 12	FCCS 14	FCCS 18				
	3\pm2	2\pm1	0.9\pm0.5	5\pm1	2\pm1	11\pm6	2\pm1	10\pm3
Snca2_Cys_TPM_Cy5 (268 μ M)	FCCS 21	FCCS 22	-	-				
	3\pm2	1.1\pm0.2	8\pm6	4\pm4				
Snca4_Cys_TPM_Cy5 (134 μ M)	FCCS 41	-	FCCS 44	-				
	9\pm2	1.5\pm0.2	13\pm4	10\pm2				
Snca8_Cys_TPM_Cy5 (67 μ M)	FCCS 81	-	-	FCCS 88				
	23\pm5	1.3\pm0.5		23\pm4	9\pm1			

Finally all average fitting amplitude in Tables 23 and 24 were rearranged into Table 25 for a better data analysis. In Table 25, digitals in red represent the fraction of red labelled α -synuclein used to form aggregates and digitals in green represent those of green labelled protein. It is apparent that the fractions of α -synuclein used in the self-aggregation were similar than those used in the cross-aggregation. For example, Experiment FCCS 11 revealed that only approximate 2-3% of red labelled or green labelled α -synuclein monomers ($\frac{\langle n_{rg} \rangle}{\langle n_r \rangle}$ and $\frac{\langle n_{rg} \rangle}{\langle n_g \rangle}$ of FCCS 11) contributed to the self-aggregation after it was incubated for 8 hours at 310.15 K. When the monomer was incubated with the oligomers, there was still 1-3% of monomers recruited in the cross-aggregation ($\frac{\langle n_{rg} \rangle}{\langle n_g \rangle}$ of FCCS 21, 41 and 81 together with $\frac{\langle n_{rg} \rangle}{\langle n_r \rangle}$ of FCCS 12, 14 and 18). Similar examples can also be found in

dimeric, tetrameric and octameric α -synuclein, such as 4% vs. 5% ($\frac{\langle n_{rg} \rangle}{\langle n_g \rangle}$ of FCCS 22 vs. 12), 10% vs. 11% ($\frac{\langle n_{rg} \rangle}{\langle n_g \rangle}$ of FCCS 44 vs. 14), 9% vs. 11% ($\frac{\langle n_{rg} \rangle}{\langle n_g \rangle}$ of FCCS 88 vs. 18), 4% vs. 3% ($\frac{\langle n_{rg} \rangle}{\langle n_r \rangle}$ of FCCS 22 vs. 21), 13% vs. 9% ($\frac{\langle n_{rg} \rangle}{\langle n_r \rangle}$ of FCCS 44 vs. 41), 23% vs. 23% ($\frac{\langle n_{rg} \rangle}{\langle n_r \rangle}$ of FCCS 88 vs. 81).

To sum up, first, the native α -synuclein monomer aggregates dramatically slower than those of engineered tetramers and octamers, and the speed of aggregation of dimer are in between. Second, the engineered oligomers prefer to incorporate itself than the native monomer into their aggregation process under the above incubation condition. Third, the fraction of α -synuclein used in the self-aggregation is similar than that used in the cross-aggregation.

Analysis of k: self-aggregation and cross aggregation. With the analysis of value A , all k values obtained in dual-color FCCS experiments after fitting are summarized in Table 26. All k values are very close to each other considering of the large standard errors. But we can still argue that labelled octameric α -synuclein takes shorter time to form aggregates, since the initial protein concentration of labelled octameric α -synuclein is much lower than that of monomers.

Table 26: Detailed information of fitting k values for all FCCS tests.

Kinetics of the fitting \pm standard error						
	Codes	Test 1	Test 2	Test 3	Test 4	Average of Tests 1~4
$\frac{\langle n_{rg} \rangle}{\langle n_r \rangle}$	FCCS 11	\emptyset	0.4 ± 0.2	0.6 ± 0.4	0.8 ± 0.9 (\emptyset)	0.5 ± 0.4
	FCCS 22	0.1 ± 0.1	0.2 ± 0.3 (\emptyset)	-	-	0.1 ± 0.1
	FCCS 44	\emptyset	0.9 ± 0.3	0.6 ± 0.3	1.0 ± 0.4	0.8 ± 0.6
	FCCS 88	0.6 ± 0.2	0.5 ± 0.2	-	-	0.6 ± 0.2
$\frac{\langle n_{rg} \rangle}{\langle n_g \rangle}$	FCCS 11	\emptyset	0.8 ± 0.5	$0.8 \pm 2(\emptyset)$	0.4 ± 0.08	0.6 ± 0.5
	FCCS 22	0.08 ± 0.1 (\emptyset)	0.2 ± 0.2	-	-	0.2 ± 0.2
	FCCS 44	\emptyset	1.2 ± 0.5	0.8 ± 0.3	1.0 ± 0.4	1.0 ± 0.7
	FCCS 88	0.6 ± 0.2	0.5 ± 0.2	-	-	0.6 ± 0.2
$\frac{\langle n_{rg} \rangle}{\langle n_r \rangle}$	FCCS 12	1.0 ± 0.6	0.9 ± 0.4	0.7 ± 0.4	-	0.8 ± 0.6
	FCCS 14	\emptyset	0.9 ± 0.9	\emptyset	-	0.9 ± 0.9
	FCCS 18	0.05 ± 0.3 (\emptyset)	\emptyset	\emptyset	\emptyset	\emptyset
$\frac{\langle n_{rg} \rangle}{\langle n_g \rangle}$	FCCS 12	1.5 ± 1.0	0.6 ± 0.2	0.3 ± 0.2	-	0.5 ± 0.3
	FCCS 14	\emptyset	$3 \pm 6(\emptyset)$	0.9 ± 0.9 (\emptyset)	-	\emptyset
	FCCS 18	0.05 ± 0.4 (\emptyset)	\emptyset	0.2 ± 0.7 (\emptyset)	0.5 ± 0.3	0.5 ± 0.3
$\frac{\langle n_{rg} \rangle}{\langle n_r \rangle}$	FCCS 21	$1.5 \pm 2(\emptyset)$	0.4 ± 0.3	-	-	0.4 ± 0.3
	FCCS 41	\emptyset	0.8 ± 0.2	1.3 ± 0.3	2 ± 1	1.4 ± 1.1
	FCCS 81	\emptyset	\emptyset	1.3 ± 0.8	1.6 ± 0.4	1.5 ± 0.9
$\frac{\langle n_{rg} \rangle}{\langle n_g \rangle}$	FCCS 21	1.0 ± 0.7	0.5 ± 0.2	-	-	0.8 ± 0.7
	FCCS 41	\emptyset	1.0 ± 0.3	0.9 ± 0.3	$3 \pm 2(\emptyset)$	1.0 ± 0.4
	FCCS 81	\emptyset	$2 \pm 3(\emptyset)$	1.0 ± 0.9	1.8 ± 0.9	1.4 ± 1.3

Effects of shaking. Figure 37 revealed the effects of continuous shaking on the aggregation process. To conclude, the continuous shaking at 250 rpm promoted

the aggregation of Cy5 tetrazine (red dye) labelled α -synucleins while inhibited the aggregations of Oregon Green 488 maleimide (green dye) labelled protein.

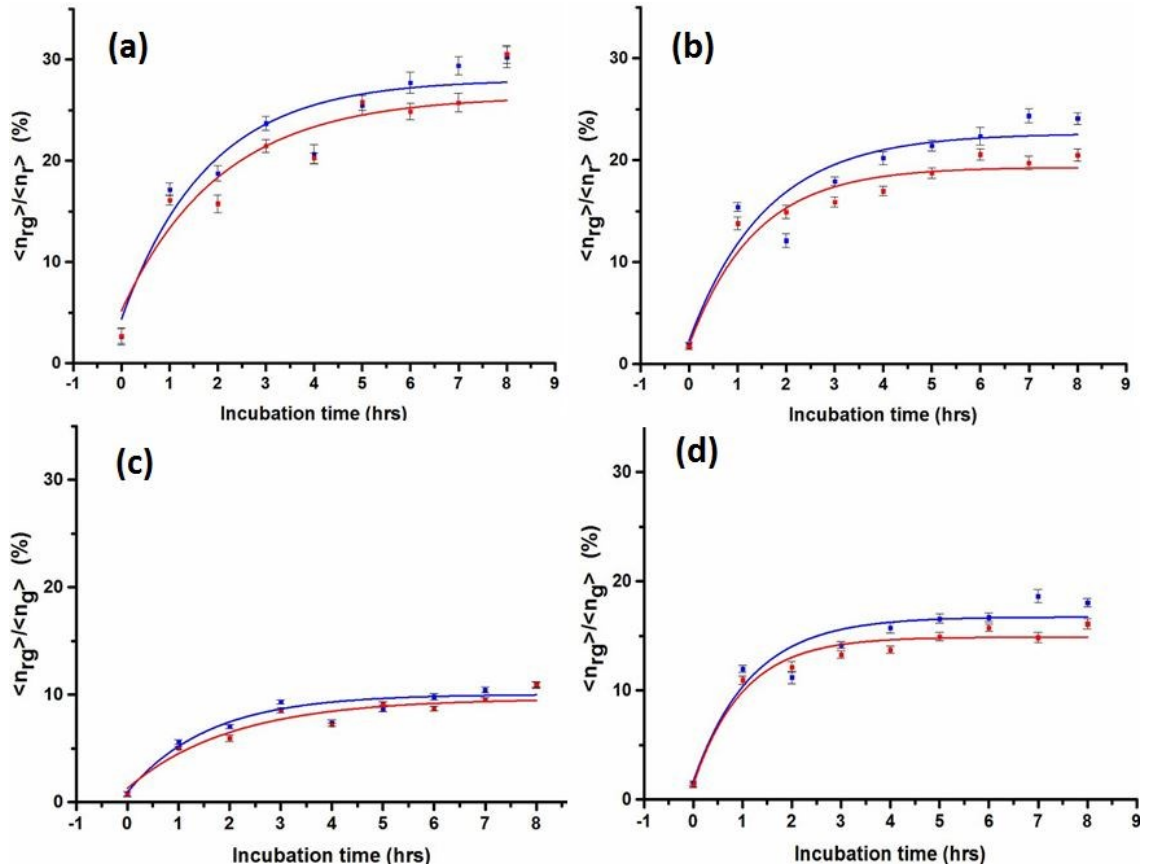


Figure 37: (a) and (b) are $\frac{\langle n_{rg} \rangle}{\langle n_r \rangle}$ as a function of incubation time for FCCS 88 with and without continuous shaking, respectively. (c) and (d) are $\frac{\langle n_{rg} \rangle}{\langle n_g \rangle}$ as a function of incubation time for FCCS 88 with and without continuous shaking, respectively.

Chapter 5: Conclusion

5.1 Research summary and contributions

α -Synucleins exist in the neurons of the human brain. It promotes the functions of neurons.⁵⁷⁻⁶¹ It is believed that specific α -synuclein oligomers play an important role of catalyzing the aggregation of normal monomeric α -synucleins, which eventually cause the irreversible damages on the neurons. Therefore, we constructed the engineered α -synuclein dimer, tetramer and octamer and studied them using a variety of analytical methods including HPLC-MS, DLS, FCS and dual-color FCCS. We measured the hydrodynamic diameters of all engineered α -synucleins using both DLS and FCS. Both experimental data agreed well. These data enable us to deduce that these engineered α -synucleins are not completely denatured, even when they bind to TPM or dyes, under the “physiological” conditions. Although, no direct evidence show that the engineered α -synuclein oligomers can act as a critical nucleus in vitro to accelerate the native monomer fibrillations at the very early stage of aggregation, my research results indicate that these engineered α -synuclein oligomers preferred to incorporate their own kinds into aggregation and aggregate faster than the native monomer.

Besides, several generic approaches are established in this research, which include: (i) a system of labelling α -synucleins in large quantities with high labelling efficiency; and (ii) an algorithm used in interpreting dual-color FCCS data in the study of protein aggregation.

To sum up, we characterized the engineered α -synuclein oligomers constructed in the lab and our study provides invaluable information for further studies of the same kind α -synuclein oligomers as discussed below. Furthermore, our results highlight the application of dual-color FCCS in the study of molecular aggregation mechanisms.

5.2 Future works

Since no experimental results demonstrate that the engineered α -synuclein oligomers accelerate the self-aggregation of the native monomer directly, several future research topics are proposed: *(i)* using a photon counting histogram (PCH) to track the brightness of the native α -synuclein monomer when it is incubated with/without the engineered α -synuclein oligomers; *(ii)* using the ThT assay to measure the incubation time needed for the native α -synuclein monomer to aggregate into a fibril when it is incubated with/without the engineered α -synuclein oligomers; and *(iii)* using single molecule Förster resonance energy transfer (smFRET) to study whether the native α -synuclein monomer conformation changes when the engineered α -synuclein oligomers bind to it.

Moreover, the same α -synuclein oligomers can also be applied to several other studies, which include but are not limited: *(i)* to study the dynamic conformation changes of these oligomeric species; *(ii)* to study the cytotoxicity of the engineered α -synuclein oligomers to the neuronal cells (whether these oligomeric species could be cleared by cell, whether they can inhibit cell growth or kill cells); and *(iii)* to discover the possible drugs that could prevent these oligomeric species from aggregating.

Bibliography

- (1) Nordhaus, W. (2008) A question of balance. *Nature* 452.
- (2) Rubinsztein, D. C. (2006) The roles of intracellular protein-degradation pathways in neurodegeneration. *Nature* 443, 780–6.
- (3) Taylor, J. P., Hardy, J., and Fischbeck, K. H. (2002) Toxic proteins in neurodegenerative disease. *Science* 296, 1991–5.
- (4) St. P. McNaught, K., Belizaire, R., Isacson, O., Jenner, P., and Olanow, C. W. (2003) Altered proteasomal function in sporadic Parkinson's disease. *Exp. Neurol.* 179, 38–46.
- (5) Seo, H., Sonntag, K.-C., and Isacson, O. (2004) Generalized brain and skin proteasome inhibition in Huntington's disease. *Ann. Neurol.* 56, 319–28.
- (6) Popiel, H. A., Burke, J. R., Strittmatter, W. J., Oishi, S., Fujii, N., Takeuchi, T., Toda, T., Wada, K., and Nagai, Y. (2011) The aggregation inhibitor peptide QBP1 as a therapeutic molecule for the polyglutamine neurodegenerative diseases. *J. Amino Acids* 2011, 265084.
- (7) Uversky, V. N., Oldfield, C. J., and Dunker, A. K. (2005) Showing your ID: intrinsic disorder as an ID for recognition, regulation and cell signaling. *J. Mol. Recognit.* 18, 343–84.
- (8) Van Rooijen, B. D., van Leijenhorst-Groener, K. A., Claessens, M. M. A. E., and Subramaniam, V. (2009) Tryptophan fluorescence reveals structural features of alpha-synuclein oligomers. *J. Mol. Biol.* 394, 826–33.
- (9) Sevcik, J., Skrabana, R., Kontsekova, E., and Novak, M. (2009) Structure solution of misfolded conformations adopted by intrinsically disordered Alzheimer's tau protein. *Protein Pept. Lett.* 16, 61–64.
- (10) Banci, L., Bertini, I., Boca, M., Calderone, V., Cantini, F., Girotto, S., and Vieru, M. (2009) Structural and dynamic aspects related to oligomerization of apo SOD1 and its mutants. *Proc. Natl. Acad. Sci. U. S. A.* 106, 6980–5.
- (11) Uversky, V. N. (2014) Introduction to intrinsically disordered proteins (IDPs). *Chem. Rev.* 114, 6557–60.
- (12) Vivekanandan, S., Brender, J. R., Lee, S. Y., and Ramamoorthy, A. (2011) A partially folded structure of amyloid-beta (1-40) in an aqueous environment. *Biochem. Biophys. Res. Commun.* 411, 312–6.

- (13) Sgourakis, N. G., Yan, Y., McCallum, S. A., Wang, C., and Garcia, A. E. (2007) The Alzheimer's peptides A β 40 and 42 adopt distinct conformations in water: a combined MD / NMR study. *J. Mol. Biol.* 368, 1448–57.
- (14) James, T. L., Liu, H., Ulyanov, N. B., Farr-Jones, S., Zhang, H., Donne, D. G., Kaneko, K., Groth, D., Mehlhorn, I., Prusiner, S. B., and Cohen, F. E. (1997) Solution structure of a 142-residue recombinant prion protein corresponding to the infectious fragment of the scrapie isoform. *Proc. Natl. Acad. Sci. U. S. A.* 94, 10086–91.
- (15) Lashuel, H. A., and Lansbury, P. T. (2006) Are amyloid diseases caused by protein aggregates that mimic bacterial pore-forming toxins? *Q. Rev. Biophys.* 39, 167–201.
- (16) Gadad, B. S., Britton, G. B., and Rao, K. S. (2011) Targeting oligomers in neurodegenerative disorders: lessons from α -synuclein, tau, and amyloid- β peptide. *J. Alzheimers. Dis.* 24 Suppl 2, 223–32.
- (17) Orr, H. T., and Zoghbi, H. Y. (2007) Trinucleotide repeat disorders. *Annu. Rev. Neurosci.* 30, 575–621.
- (18) Marks, D. S., Colwell, L. J., Sheridan, R., Hopf, T. A., Pagnani, A., Zecchina, R., and Sander, C. (2011) Protein 3D structure computed from evolutionary sequence variation. *PLoS One* 6, e28766.
- (19) Lavedan, C. (1998) The Synuclein Family. *Genome Res* 8, 871–880.
- (20) Hashimoto, M., and Takenouchi, T. (2000) The role of NAC in amyloidogenesis in Alzheimer's disease. *Am J Pathol.* 156, 734–735.
- (21) Wilkins, D., Grimshaw, S., and Receveur, V. (1999) Hydrodynamic radii of native and denatured proteins measured by pulse field gradient NMR techniques. *Biochemistry* 16424–16431.
- (22) Arzen, D., Co-advisor, R. P., and Ljubljana, D. K. (2010) Dynamic light scattering and application to proteins in solutions.
- (23) Nag, S., Sarkar, B., Bandyopadhyay, A., Sahoo, B., Sreenivasan, V. K. A., Kombrabail, M., Muralidharan, C., and Maiti, S. (2011) Nature of the amyloid-beta monomer and the monomer-oligomer equilibrium. *J. Biol. Chem.* 286, 13827–33.
- (24) Erickson, H. P. (2009) Size and shape of protein molecules at the nanometer level determined by sedimentation, gel filtration, and electron microscopy. *Biol. Proced. Online* 11, 32–51.

- (25) Greenfield, N. J. (2006) Using circular dichroism spectra to estimate protein secondary structure. *Nat. Protoc.* 1, 2876–90.
- (26) Kong, J., and Yu, S. (2007) Fourier transform infrared spectroscopic analysis of protein secondary structures. *Acta Biochim. Biophys. Sin. (Shanghai)*. 39, 549–559.
- (27) Pelton, J. T., and McLean, L. R. (2000) Spectroscopic methods for analysis of protein secondary structure. *Anal. Biochem.* 277, 167–76.
- (28) Engh, R. A., and Huber, R. (1991) Accurate bond and angle parameters for X-ray protein structure refinement. *Acta Crystallogr.* 47, 392–400.
- (29) Zweckstetter, M., and Bax, A. (2000) Prediction of sterically induced alignment in a dilute liquid crystalline phase: aid to protein structure determination by NMR. *J. Am. Chem. Soc.* 3791–3792.
- (30) Landschulz, W., Johnson, P., and McKnight, S. (1988) The leucine zipper: a hypothetical structure common to a new class of DNA binding proteins. *Science*. 240, 1759–1764.
- (31) Unwin, N., and Henderson, R. (1984) The structure of proteins in biological membranes. *Sci. Am.* 1–13.
- (32) Seshadri, I. P., and Bhushan, B. (2008) In situ tensile deformation characterization of human hair with atomic force microscopy. *Acta Mater.* 56, 774–781.
- (33) Baldwin, E. T., Weber, I. T., St Charles, R., Xuan, J. C., Appella, E., Yamada, M., Matsushima, K., Edwards, B. F., Clore, G. M., and Gronenborn, A. M. (1991) Crystal structure of interleukin 8: symbiosis of NMR and crystallography. *Proc. Natl. Acad. Sci. U. S. A.* 88, 502–6.
- (34) Clore, G. M., Appella, E., Yamada, M., Matsushima, K., and Gronenborn, A. M. (1990) Three-dimensional structure of interleukin 8 in solution. *Biochemistry* 29, 1689–96.
- (35) Kato, Y., Muto, T., Tomura, T., Tsumura, H., Watarai, H., Mikayama, T., Ishizaka, K., and Kuroki, R. (1996) The crystal structure of human glycosylation-inhibiting factor is a trimeric barrel with three 6-stranded beta-sheets. *Proc. Natl. Acad. Sci. U. S. A.* 93, 3007–10.
- (36) Selkoe, D. (1994) Alzheimer's disease: a central role for amyloid. *J. Neuropathol. Exp. Neurol.* 53, 438–447.

- (37) Gorecki, M., Votano, J. R., and Rich, a. (1980) Peptide inhibitors of sickle hemoglobin aggregation: effect of hydrophobicity. *Biochemistry* 19, 1564–8.
- (38) D’Ursi, A. M., Armenante, M. R., Guerrini, R., Salvadori, S., Sorrentino, G., and Picone, D. (2004) Solution structure of amyloid beta-peptide (25-35) in different media. *J. Med. Chem.* 47, 4231–8.
- (39) Sticht, H., Bayer, P., Willbold, D., Dames, S., Hilbich, C., Beyreuther, K., Frank, R. W., and Rosch, P. (1995) Structure of amyloid A4 (1-40) -peptide of Alzheimer ’ s disease. *Eur. J. Biochem.* 233, 293–298.
- (40) Nguyen, J., Baldwin, M. A., Cohen, F. E., and Prusiner, S. B. (1995) Prion protein peptides induce alpha-helix to beta-sheet conformational transitions. *Biochemistry* 34, 4186–92.
- (41) Pan, K., Baldwin, M., Nguyen, J., Gasset, M., Serban, A. N. A., Groth, D., Mehlhorn, I., Huang, Z., Fletterick, R. J., I, F. E. C., and Ii, S. B. P. (1993) Conversion of alpha-helices into beta-sheets features in the formation of the scrapie prion proteins. *Proc. Natl. Acad. Sci. USA* 90, 10962–10966.
- (42) Ulmer, T. S., Bax, A., Cole, N. B., and Nussbaum, R. L. (2005) Structure and dynamics of micelle-bound human alpha-synuclein. *J. Biol. Chem.* 280, 9595–603.
- (43) Davidson, W. S. (1998) Stabilization of α -synuclein secondary structure upon binding to synthetic membranes. *J. Biol. Chem.* 273, 9443–9449.
- (44) Rao, J. N., Jao, C. C., Hegde, B. G., Langen, R., and Ulmer, T. S. (2010) A combinatorial NMR and EPR approach for evaluating the structural ensemble of partially folded proteins. *J. Am. Chem. Soc.* 132, 8657–68.
- (45) Eliezer, D., Kutluay, E., Bussell, R., and Browne, G. (2001) Conformational properties of alpha-synuclein in its free and lipid-associated states. *J. Mol. Biol.* 307, 1061–73.
- (46) Nath, S., Meuvlis, J., Hendrix, J., Carl, S. A., and Engelborghs, Y. (2010) Early aggregation steps in alpha-synuclein as measured by FCS and FRET: evidence for a contagious conformational change. *Biophys. J.* 98, 1302–11.
- (47) Bacia, K., and Schwille, P. (2003) A dynamic view of cellular processes by in vivo fluorescence auto- and cross-correlation spectroscopy. *Science.* 29, 74–85.
- (48) Gregoire, S., Irwin, J., and Kwon, I. (2012) Techniques for monitoring protein misfolding and aggregation in vitro and in living cells. *Korean J. Chem. Eng.* 29, 693–702.

- (49) Harper, J. D., and Lansbury, P. T. (1997) Models of amyloid seeding in Alzheimer's disease and scrapie: mechanistic truths and physiological consequences of the time-dependent solubility of amyloid proteins. *Annu. Rev. Biochem.* 66, 385–407.
- (50) Wood, S. J. (1999) α -Synuclein fibrillogenesis is nucleation-dependent: implications for the pathogenesis of Parkinson's disease. *J. Biol. Chem.* 274, 19509–19512.
- (51) Come, J., and Jr, P. L. (1994) Predisposition of prion protein homozygotes to Creutzfeldt-Jakob disease can be explained by a nucleation-dependent polymerization mechanism. *J. Am. Chem. Soc.* 116, 4109–4110.
- (52) Kodaka, M. (2004) Interpretation of concentration-dependence in aggregation kinetics. *Biophys. Chem.* 109, 325–32.
- (53) Thyberg, P., Terenius, L., Tjernberg, L., Pramanik, A., Bjijrling, S., Thyberg, J., Nordstedt, C., Berndt, K. D., and Rigler, R. (1999) Amyloid β -peptide polymerization correlation spectroscopy studied using fluorescence. *Chem. Biol.* 6, 53–62.
- (54) Post, K., Pitschke, M., Schäfer, O., Wille, H., Appel, T. R., Kirsch, D., Mehlhorn, I., Serban, H., Prusiner, S. B., and Riesner, D. (1998) Rapid acquisition of β -sheet structure in the prion protein prior to multimer formation. *Biol. Chem.* 379, 1307–1317.
- (55) Pitschke, M., Prior, R., Haupt, M., and Riesner, D. (1998) Detection of single amyloid β -protein aggregates in the cerebrospinal fluid of Alzheimer's patients by fluorescence correlation spectroscopy. *Nat. Med.* 4, 832–834.
- (56) Uversky, V. N. (2008) α -Synuclein misfolding and neurodegenerative diseases. *Curr. Protein Pept. Sci.* 9, 507–540.
- (57) Clayton, D. F., and George, J. M. (1998) The synucleins: a family of proteins involved in synaptic function, plasticity, neurodegeneration and disease. *Trends Neurosci.* 21, 249–54.
- (58) Abeliovich, A., Schmitz, Y., Fariñas, I., Choi-Lundberg, D., Ho, W. H., Castillo, P. E., Shinsky, N., Verdugo, J. M., Armanini, M., Ryan, A., Hynes, M., Phillips, H., Sulzer, D., and Rosenthal, A. (2000) Mice lacking alpha-synuclein display functional deficits in the nigrostriatal dopamine system. *Neuron* 25, 239–52.
- (59) Chandra, S., and Fornai, F. (2004) Double-knockout mice for α - and β -synucleins: effect on synaptic functions. *PNAS* 101, 14966–14971.

- (60) Da Costa, C., Ancolio, K., and Checler, F. (2000) Wild-type but not Parkinson's disease-related A53T mutant α -synuclein protects neuronal cells from apoptotic stimuli. *J. Biol. Chem.* 275, 24065–9.
- (61) Chandra, S., Gallardo, G., Fernández-Chacón, R., Schlüter, O. M., and Südhof, T. C. (2005) α -synuclein cooperates with CSP α in preventing neurodegeneration. *Cell* 123, 383–96.
- (62) Polymeropoulos, M. H. (1997) Mutation in the α -synuclein gene identified in families with Parkinson's Disease. *Science.* 276, 2045–2047.
- (63) Breydo, L., Wu, J. W., and Uversky, V. N. (2012) α -Synuclein misfolding and Parkinson's disease. *Biochim. Biophys. Acta* 1822, 261–85.
- (64) Harada, R., Kobayashi, N., Kim, J., Nakamura, C., Han, S.-W., Ikebukuro, K., and Sode, K. (2009) The effect of amino acid substitution in the imperfect repeat sequences of α -synuclein on fibrillation. *Biochim. Biophys. Acta* 1792, 998–1003.
- (65) Kanda, S., Bishop, J. F., Eglitis, M. A., Yang, Y., and Mouradian, M. M. (2000) Enhanced vulnerability to oxidative stress by alpha-synuclein mutations and C-terminal truncation. *Neuroscience* 97, 279–84.
- (66) El-agnaf, O. M. A., Bodles, A. M., Guthrie, D. J. S., Harriott, P., and Irvine, G. B. (1998) The N-terminal region of non-A β component of Alzheimer's Disease amyloid is responsible for its tendency to assume β -sheet and aggregate to form fibrils. *EURO* 63, 157–163.
- (67) Sode, K., Ochiai, S., Kobayashi, N., and Usuzaka, E. (2007) Effect of reparation of repeat sequences in the human alpha-synuclein on fibrillation ability. *Int. J. Biol. Sci.* 3, 1–7.
- (68) Celej, M. S., Sarroukh, R., Goormaghtigh, E., Fidelio, G. D., Ruyschaert, J.-M., and Raussens, V. (2012) Toxic prefibrillar α -synuclein amyloid oligomers adopt a distinctive antiparallel β -sheet structure. *Biochem. J.* 443, 719–26.
- (69) Uversky, V. N., Li, J., and Fink, A. L. (2001) Evidence for a partially folded intermediate in alpha-synuclein fibril formation. *J. Biol. Chem.* 276, 10737–44.
- (70) Picotti, P., De Franceschi, G., Frare, E., Spolaore, B., Zamboni, M., Chiti, F., de Laureto, P. P., and Fontana, A. (2007) Amyloid fibril formation and disaggregation of fragment 1-29 of apomyoglobin: insights into the effect of pH on protein fibrillogenesis. *J. Mol. Biol.* 367, 1237–45.

- (71) Munishkina, L. A., Phelan, C., Uversky, V. N., and Fink, A. L. (2003) Conformational behavior and aggregation of α -synuclein in organic solvents: modeling the effects of membranes. *Biochemistry* 42, 2720–30.
- (72) Paik, S., Shin, H., Lee, J., Chang, C., and Kim, J. (1999) Copper (II)-induced self-oligomerization of α -synuclein. *Biochem. J* 828, 821–828.
- (73) Uversky, V. N., Li, J., and Fink, A. L. (2001) Metal-triggered structural transformations, aggregation, and fibrillation of human alpha-synuclein. A possible molecular link between Parkinson's disease and heavy metal exposure. *J. Biol. Chem.* 276, 44284–96.
- (74) Lee, H.-J., Choi, C., and Lee, S.-J. (2002) Membrane-bound alpha-synuclein has a high aggregation propensity and the ability to seed the aggregation of the cytosolic form. *J. Biol. Chem.* 277, 671–8.
- (75) Li, J., Uversky, V. N., and Fink, A. L. (2002) Conformational behavior of human α -synuclein is modulated by familial Parkinson's disease point mutations A30P and A53T. *Neurotoxicology* 23, 553–567.
- (76) Li, J., Zhu, M., Manning-Bog, A., Monte, D. Di, and Fink, A. (2004) Dopamine and L-dopa disaggregate amyloid fibrils: implications for Parkinson's and Alzheimer's disease. *FASEB J.* 22, 1–22.
- (77) Zhu, M., Rajamani, S., Kaylor, J., Han, S., Zhou, F., and Fink, A. L. (2004) The flavonoid baicalein inhibits fibrillation of alpha-synuclein and disaggregates existing fibrils. *J. Biol. Chem.* 279, 26846–57.
- (78) Cremades, N., Cohen, S. I. A., Deas, E., Abramov, A. Y., Chen, A. Y., Orte, A., Sandal, M., Clarke, R. W., Dunne, P., Aprile, F. A., Bertocini, C. W., Wood, N. W., Knowles, T. P. J., Dobson, C. M., and Klenerman, D. (2012) Direct observation of the interconversion of normal and toxic forms of α -synuclein. *Cell* 149, 1048–59.
- (79) Hoyer, W., Antony, T., Cherny, D., Heim, G., Jovin, T. M., and Subramaniam, V. (2002) Dependence of α -Synuclein Aggregate Morphology on Solution Conditions. *J. Mol. Biol.* 322, 383–393.
- (80) Uversky, V. N. (2010) Mysterious oligomerization of the amyloidogenic proteins. *FEBS J.* 277, 2940–53.
- (81) Goldberg, M. S., and Jr, P. T. L. (2000) Is there a cause-and-effect relationship between α -synuclein fibrillization and Parkinson's disease? *Nat. Cell Biol.* 2, 115–119.

- (82) Lashuel, H. A., Hartley, D., Petre, B. M., Walz, T., Jr, P. T. L., Turner, J., King, J. C., Lachlan-cope, T. A., and Jones, P. D. (2002) Amyloid pores from pathogenic mutations. *Nature* 418, 4–5.
- (83) Volles, M. J., and Lansbury, P. T. (2002) Vesicle permeabilization by protofibrillar α -Synuclein is sensitive to Parkinson's disease-linked mutations and occurs by a pore-like mechanism. *Biochemistry* 41, 4595–4602.
- (84) Lashuel, H. A., Petre, B. M., Wall, J., Simon, M., Nowak, R. J., Walz, T., and Lansbury, P. T. (2002) α -Synuclein, especially the Parkinson's disease-associated mutants, forms pore-like annular and tubular protofibrils. *J. Mol. Biol.* 322, 1089–1102.
- (85) Alves da Costa, C., Dunys, J., Brau, F., Wilk, S., Cappai, R., and Checler, F. (2006) 6-Hydroxydopamine but not 1-methyl-4-phenylpyridinium abolishes alpha-synuclein anti-apoptotic phenotype by inhibiting its proteasomal degradation and by promoting its aggregation. *J. Biol. Chem.* 281, 9824–31.
- (86) Neupane, K., Solanki, A., Sosova, I., Belov, M., and Woodside, M. T. (2014) Diverse metastable structures formed by small oligomers of α -synuclein probed by force spectroscopy. *PLoS One* 9, e86495.
- (87) De Laureto, P. P. (2014) Role of Different Regions of α -synuclein in the Interaction with the Brain Fatty Acid DHA. *J. Chromatogr.* 05.
- (88) Trexler, A. J., and Rhoades, E. (2010) Single molecule characterization of α -synuclein in aggregation-prone states. *Biophys. J.* 99, 3048–55.
- (89) Calamai, M., Canale, C., Relini, A., Stefani, M., Chiti, F., and Dobson, C. M. (2005) Reversal of protein aggregation provides evidence for multiple aggregated states. *J. Mol. Biol.* 346, 603–16.
- (90) Hong, D.-P., Fink, A. L., and Uversky, V. N. (2008) Structural characteristics of alpha-synuclein oligomers stabilized by the flavonoid baicalein. *J. Mol. Biol.* 383, 214–23.
- (91) Morris, A. M., Watzky, M. a, and Finke, R. G. (2009) Protein aggregation kinetics, mechanism, and curve-fitting: a review of the literature. *Biochim. Biophys. Acta* 1794, 375–97.
- (92) Giehm, L., Svergun, D. I., Otzen, D. E., and Vestergaard, B. (2011) Low-resolution structure of a vesicle disrupting alpha-synuclein oligomer that accumulates during fibrillation. *Proc. Natl. Acad. Sci. U. S. A.* 108, 3246–51.

- (93) Nath, S., Goodwin, J., Engelborghs, Y., and Pountney, D. L. (2011) Raised calcium promotes α -synuclein aggregate formation. *Mol. Cell. Neurosci.* 46, 516–26.
- (94) Kostka, M., Högen, T., Danzer, K. M., Levin, J., Habeck, M., Wirth, A., Wagner, R., Glabe, C. G., Finger, S., Heinzelmann, U., Garidel, P., Duan, W., Ross, C. A., Kretschmar, H., and Giese, A. (2008) Single particle characterization of iron-induced pore-forming alpha-synuclein oligomers. *J. Biol. Chem.* 283, 10992–1003.
- (95) Uversky, V. N., Yamin, G., Souillac, P. O., Goers, J., Glaser, C. B., and Fink, A. L. (2002) Methionine oxidation inhibits fibrillation of human K-synuclein in vitro. *FEBS Lett.* 517, 239–244.
- (96) Baba, M., Nakajo, S., Tu, P., Lee, V. M., Trojanowski, J. Q., and Iwatsubo, T. (1998) Short communication: aggregation of α -synuclein in lewy bodies of sporadic Parkinson's disease and dementia with lewy bodies. *Am. J. Pathol.* 152, 879–884.
- (97) Sciences, G. H. L. HiTrap desalting columns - animation.
- (98) Summary, E. (2014) Application of dynamic light scattering to protein therapeutic formulations: principles, measurements and analysis. I. Basic principles. *Malvern Instruments Tech. notes*, pp 1–7.
- (99) Dusa, A., Kaylor, J., Edridge, S., and Bodner, N. (2006) Characterization of oligomers during α -synuclein aggregation using intrinsic tryptophan fluorescence. *Biochemistry* 2752–2760.
- (100) Magde, D., Elson, E., and Webb, W. (1972) Thermodynamic fluctuations in a reacting system—measurement by fluorescence correlation spectroscopy. *Phys. Rev. Lett.* 29, 705–708.
- (101) Elson, E., and Magde, D. (1974) Fluorescence correlation spectroscopy. I. Conceptual basis and theory. *Biopolymers* 13, 1–27.
- (102) Magde, D., Elson, E., and Webb, W. (1974) Fluorescence correlation spectroscopy. II. An experimental realization. *Biopolymers* 13, 29–61.
- (103) Magde, D., Webb, W., and Elson, E. (1978) Fluorescence correlation spectroscopy. III. Uniform translation and laminar flow. *Biopolymers* 17, 361–376.
- (104) Eigen, M., and Rigler, R. (1994) Sorting single molecules: application to diagnostics and evolutionary biotechnology. *Proc. Natl. Acad. Sci. U. S. A.* 91, 5740–7.

- (105) Rigler, R., and Elson, E. (2001) Fluorescence Correlation spectroscopy. Theory and Applications. Springer Verlag, Heidelberg.
- (106) Lakowicz, J. R. (2006) Principle of fluorescence spectroscopy, p 804. Springer Science & Business Media.
- (107) Gratton, E. Lecture of FCS, autocorrelation, PCH and cross-correlation.
- (108) Haustein, E., and Schwille, P. (2007) Fluorescence correlation spectroscopy: novel variations of an established technique. *Annu. Rev. Biophys. Biomol. Struct.* 36, 151–69.
- (109) Schwille, P., Meyer-Almes, F., and Rigler, R. (1997) Dual-color fluorescence cross-correlation spectroscopy for multicomponent diffusional analysis in solution. *Biophys. J.* 72, 1878–1886.
- (110) Rayleigh, Lord. (1879) Investigation in optics, with special reference to the spectroscope. *Philos. Mag.* 8, 261–274.
- (111) Blackman, M. L., Royzen, M., and Fox, J. M. (2008) Tetrazine ligation : fast bioconjugation based on Inverse-Electron-Demand Diels - Alder Reactivity. *J. Am. Chem. Soc.* 130, 13518–13519.
- (112) Devaraj, N. K., Weissleder, R., and Hilderbrand, S. a. (2008) Tetrazine-based cycloadditions: application to pretargeted live cell imaging. *Bioconjug. Chem.* 19, 2297–9.
- (113) Invitrogen. (2005) Amine reactive probes, pp 1–11.
- (114) Invitrogen. (2006) Thiol reactive probes, pp 3–6.
- (115) Kim, Y., Ho, S. O., Gassman, N. R., Korlann, Y., Landorf, E. V, Collart, F. R., and Weiss, S. (2008) Efficient site-specific labeling of proteins via cysteines. *Bioconjug. Chem.* 19, 786–91.
- (116) Guttman, C., and Zarivach, R. FPLC standard operating procedure – AKTA system (GE).
- (117) Grishin, A. M., Cherney, M., Anderson, D. H., and Phanse, S. (2014) Supplemental information NleH defines a new family of bacterial effector kinases supplemental figures. *Structure* 22, 250–9.
- (118) Petrášek, Z., and Schwille, P. (2008) Precise measurement of diffusion coefficients using scanning fluorescence correlation spectroscopy. *Biophys. J.* 94, 1437–48.

- (119) Charles Simmonds. (1919) Alcohol, its production, properties, chemistry, and industrial applications, p 154. Macmillan and co., Limited, St. Martin's street, London.
- (120) W.M. Haynes. (2004) CRC handbook of chemistry and physics (W.M. Haynes, Ed.) 201(2014) ed., pp 6–231. Binghamton, N.Y.
- (121) Armstrong, J. K., Wenby, R. B., Meiselman, H. J., and Fisher, T. C. (2004) The hydrodynamic radii of macromolecules and their effect on red blood cell aggregation. *Biophys. J.* 87, 4259–70.
- (122) Kapusta, P., and Gmbh, P. (2010) Absolute diffusion coefficients : compilation of reference data for FCS calibration, p 1.
- (123) Milanova, D., Chambers, R. D., Bahga, S. S., and Santiago, J. G. (2011) Electrophoretic mobility measurements of fluorescent dyes using on-chip capillary electrophoresis. *Electrophoresis* 32, 3286–94.
- (124) Becker, M. (2014) Hydrodynamic diameters of alpha-synulceins by DLS.